

Design and development of an external cavity diode laser for laser cooling and spectroscopy applications

Gibson Peter Nyamuda

Thesis presented in partial fulfilment of the requirements



Stellenbosch University

Supervisors:

Dr C.M. Steenkamp

Dr E.G. Rohwer

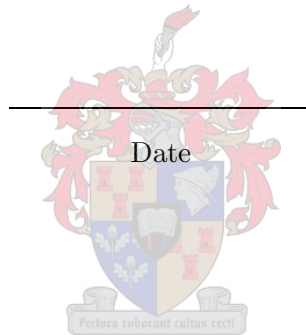
December 2006

Declaration

I, the undersigned, hereby declare that the work contained in this thesis is my own original work and that I have not previously in its entirety or in part submitted it at any university for a degree.

Signature

Date



Abstract

External cavity diode lasers are used increasingly as sources of light in applications ranging from industrial photonic systems to basic laboratory research on the interaction of light and atoms. External cavity diode lasers offer more stable output frequency and narrow spectral bandwidth than the typical free-running diode lasers. These characteristics are achieved by exploiting the sensitivity of diode lasers to external optical feedback. In this study the design and development of an external cavity diode laser system for future applications in spectroscopy and laser cooling of rubidium atoms is presented. The external cavity diode laser including mechanical components and control electronics of the system is developed from basic components. The system uses frequency selective optical feedback from a diffraction grating in a Littrow configuration to provide collimated, narrow-band, frequency tunable light near 780 nm. The external cavity diode laser is designed to increase the mode-hop-free frequency tuning range, and allow accurate frequency tuning and stabilisation. A low-noise current source and a temperature controller for thermal stability were developed as part of the system since the output frequency changes with temperature and current. The temperature controller is optimised experimentally for the thermal characteristics of the external cavity. An electronic sidelock servo circuit for frequency locking of the external cavity diode laser to an external reference for long term frequency stabilisation is proposed and discussed. The servo circuit electrically controls the grating tilt and the current through the diode laser in order to lock the frequency of the diode laser. The external cavity diode laser is optimised and characterised near 780 nm. Results obtained in this study indicate that the external cavity diode laser is suitable for future applications in spectroscopy and laser cooling of neutral rubidium atoms.

Opsomming

Eksterne resonator diodelasers word toenemend as ligbronne gebruik in 'n wye verskeidenheid toepassings van industriële fotoniese sisteme tot basiese navorsing op die interaksie tussen lig en atome. 'n Eksterne resonator diodelaser bied 'n stabielere uitsetfrequentie en smaller spektrale bandwydte as die tipiese diodelaser wat sonder 'n eksterne resonator bedryf word. Hierdie eienskappe word verkry deur die diodelaser se sensitiwiteit vir eksterne optiese terugvoer te benut. In hierdie studie word die ontwerp en ontwikkeling van 'n eksterne resonator diodelaser sisteem vir toekomstige toepassings in spektroskopie en laser afkoeling van rubidium atome voorgedra. Die eksterne resonator diodelaser, insluitend die meganiese komponente en die elektroniese beheerselsels van die sisteem, is ontwikkel vanaf basiese komponente. Die sisteem benut die frekwensieselektiewe optiese terugvoer vanaf 'n diffraksierooster in 'n Littrow konfigurasie om gekollimeerde, frekwensie-afstembare lig met 'n smal spektrale bandwydte naby 780 nm te lewer. Die eksterne resonator diodelaser is ontwerp om die frekwensie gebied waarvoor geskander kan word sonder modus spronge te vergroot en om akkurate frekwensie afstemming en frekwensie stabilisering toe te laat. 'n Stroombron met lae ruisvlakke en 'n temperatuurbeheerder vir termiese stabiliteit is ontwikkel as deel van die sisteem aangesien die uitsetfrequentie verander met temperatuur en stroom. Die temperatuurbeheerder is eksperimenteel geoptimeer vir die termiese eienskappe van die eksterne resonator. 'n Elektroniese servo stroombaan, wat dit moontlik maak om die uitsetfrequentie van die eksterne resonator diodelaser op 'n eksterne verwysingsfrequentie te sluit vir stabilisasie oor lang periodes, is voorgestel en bespreek. Die servo stroombaan oefen elektriese beheer uit oor die oriëntasie van die diffraksierooster en die stroom deur die diodelaser om die frekwensie van die diodelaser te sluit. Die eksterne resonator diodelaser is geoptimeer en gekarakteriseer naby 780 nm. Die resultate wat in hierdie studie verkry is dui aan dat die eksterne resonator diodelaser geskik is vir toekomstige toepassings in spektroskopie en laser afkoeling van neutrale rubidium atome.

Acknowledgements

I would like to express my sincere gratitude to the following people who contributed significantly to this project

- Dr C.M. Steenkamp for her tremendous supervision, patience, guidance and numerous discussions which have contributed to the success of this project.
- Dr E.G. Rohwer for his supervision and support throughout this study.
- Prof P.E. Walters for useful discussions on experimental work. Prof Carl. E. Wieman of JILA, University of Colorado in Boulder, Colorado, USA for kind help and advice.
- Mr Timo Stehmann for building the electronic components of this project. Mr U.G.K. Deutschländer and Mr J.M. Germishuizen for their availability for technical matters. Mr A.S. Botha and the workshop team for their assistance in manufacturing some of the mechanical parts used in this project.
- All members of the Laser Research Institute; special mention goes to the Lasertech group, Pieter, Gurthwin, Saturnin, Eckhard and Anton, for the useful weekly discussions, their enthusiasm and assistance.
- My parents for their love and support that has carried me through thick and thin over the past years.

Above all I thank the Almighty Lord.

My studies were partially funded by the African Institute for Mathematical Sciences (AIMS), the Faculty of Natural Sciences of the University of Stellenbosch, the African Laser Centre (ALC) and the National Research Foundation (NRF).

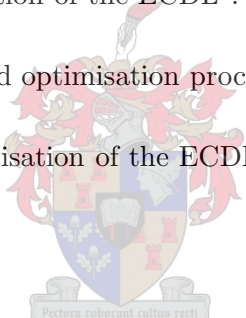
Contents

Abstract	i
Opsomming	i
Acknowledgements	ii
List of Figures	x
List of Tables	xi
1 Introduction	1
1.1 Motivation and background	1
1.2 Aim	3
1.3 Outline of thesis	3
2 Literature review of semiconductor diode lasers	5
2.1 Introduction	5
2.2 Density of states and occupation probability	7
2.3 Doping of semiconductor material	10

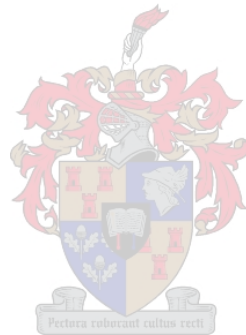


2.4	Electron-hole recombination	11
2.5	Gain and threshold in semiconductor diode lasers	13
2.6	Semiconductor diode laser structures	16
2.7	Beam spatial characteristics	18
2.8	Effects of temperature and current	20
2.8.1	Mode-hopping in diode lasers	24
2.9	Theory of external cavity diode laser	26
2.9.1	Three-mirror system	28
2.9.2	External cavity diode laser modes	30
2.9.3	External cavity diode laser linewidth	31
2.9.4	Effects of antireflection (AR) coatings	32
2.10	Basic ECDL configurations	33
2.10.1	Littrow configuration	33
2.10.2	Littman-Metcalf configuration	36
3	Experimental setup and methods	38
3.1	Setup for the characterisation of a free-running diode laser	38
3.2	Mechanical design and development of ECDL	39
3.2.1	Choice of geometry	40
3.2.2	Choice of grating and polarisation	40
3.2.3	Choice of diode laser	42
3.2.4	Beam collimation	42

3.2.5	Grating and piezo mount	44
3.2.6	Assembly	45
3.2.7	Base plate and enclosure	47
3.3	Electronic system of the ECDL	49
3.3.1	Diode laser current source	49
3.3.2	Laser diode protection circuit	52
3.3.3	Temperature controller	53
3.3.4	Frequency stabilisation of the ECDL	59
3.4	Optimisation and characterisation of the ECDL	62
3.4.1	Feedback alignment and optimisation procedure	62
3.4.2	Experimental characterisation of the ECDL	63
4	Results and discussion	65
4.1	Free-running diode laser	65
4.1.1	Turn-on characteristics	65
4.1.2	Tuning characteristics	68
4.2	Characterisation of the grating	70
4.3	Optimisation of temperature controller	75
4.4	Alignment of feedback	76
4.5	Characterisation of the ECDL	78
4.5.1	Comparison of the turn-on curves for a diode laser and ECDL	81
5	Summary and conclusions	83

A watermark of a university crest is centered on the page. The crest features a shield with various symbols, including a cross and a book, topped with a crown and a banner. Below the shield is a motto scroll with the Latin text "Pectora roburant cultus recti".

Appendices	86
A Diode laser (GaAlAs) mode spacing	87
B Derivation of equations 2.25 and 2.31	89
C PID controller	91
Bibliography	94



List of Figures

2.1	(a) A plot of energy E against density of states $\rho(E)$ in the conduction band and valence band, as depicted by equations 2.1 and 2.2. (b) The plot of energy E against the probability function $f(E)$ in each band during the quasi-equilibrium state, as indicated by equations 2.5 and 2.6. (c) The product of the two graphs (a) and (b) to give the density of holes in the valence band and the density of electrons in the conduction band. The plots are derived from equations 2.7 and 2.8.	8
2.2	(a) Energy band diagram showing the position of donor levels in a n -type semiconductor. (b) Concentrations of mobile electrons and holes $n(E)$ and $p(E)$ respectively in a n -type semiconductor. The shifted Fermi level is shown by E_f	10
2.3	(a) Energy band diagram showing the position of acceptor levels in a p -type semiconductor. (b) A sketch diagram showing the concentrations of mobile electrons and holes $n(E)$ and $p(E)$ respectively in a p -type semiconductor.	10
2.4	Schematic representation of the relative energy levels for valence bands, conduction bands, and Fermi levels of a $p - n$ junction for: (a) separated materials, (b) p and n materials in contact, and (c) p and n materials in contact with an applied forward bias [13].	12
2.5	An illustration of (a) direct and (b) indirect band gap semiconductors, showing positions of energy, E , and momentum wavevector k	16

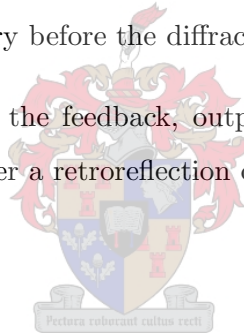
2.6	A heterojunction diode laser [15] structure, showing a GaAs active layer sandwiched by AlGaAs semiconductor material. The diode laser output propagates in the x-direction.	17
2.7	Schematic representation of the far-field radiation pattern of a laser diode illustrating the TM and TE modes in an elliptical beam output.	19
2.8	Schematic view of cavity modes and gain spectrum of a diode laser.	21
2.9	Schematic representation showing how the gain profile and longitudinal modes shift as the temperature changes.	26
2.10	The three-mirror model of an external cavity diode laser with its effective cavity [1].	29
2.11	Schematic representation of the gain spectrum, feedback spectrum and longitudinal modes of an ECDL.	30
2.12	The Littrow ECDL configuration.	34
2.13	The general Littrow oscillator to prove that synchronous scanning is possible by rotating the back facet of the diode laser and grating at pivot point, P.	35
2.14	The Littman-Metcalf configuration.	36
3.1	A schematic illustration of the experimental setup used for the characterisation of a free-running diode laser.	39
3.2	A sketch diagram showing how the diode laser and collimation lens are mounted together in a collimation tube to provide a collimated beam [37].	43
3.3	Schematic representation showing how the mechanical components of the ECDL were assembled in a Littrow cavity. The diagram is not to scale.	46
3.4	A photograph showing the top view of the mechanical setup of the ECDL developed.	48
3.5	A circuit diagram for the current source used to drive the Hitachi HL7851G diode laser [38]. <i>Circuit reproduced with permission.</i>	50

3.6	The protection circuit used for the diode laser.	52
3.7	A schematic illustration of the complete temperature regulating system of the ECDL.	53
3.8	The circuit diagram of a temperature circuit used for temperature regulation of the ECDL system [39]. <i>Circuit reproduced with permission.</i>	55
3.9	An illustration of how temperature is regulated using a PID system, thermistor and Peltier cooler.	56
3.10	A schematic arrangement of the setup used to optimise the temperature controller. .	57
3.11	A layout of the experimental setup for locking the diode laser frequency using a sidelock servo.	59
3.12	The circuit diagram for the sidelock servo for locking the frequency of the diode laser [40]. <i>Circuit reproduced with permission.</i>	61
3.13	The experimental setup used for the characterisation of the ECDL.	64
4.1	Graphical results of the turn-on characteristics of a free-running diode laser (Hitachi HL7851G) at different temperatures.	66
4.2	Graphical illustration of the temperature dependence of output power at fixed currents.	66
4.3	Illustration of the temperature dependence of threshold current derived from the turn-on curve, Figure 4.1.	67
4.4	Graphical representation of temperature dependence of slope efficiency derived from Figure 4.1.	68
4.5	Graph showing the variation of wavelength with temperature at a fixed current of 122 mA. The arrows show regions of mode-hops.	69
4.6	Graph showing the variation of wavelength with current at two fixed temperatures. Mode hops are indicated by small arrows.	70

4.7	Characterisation of the grating for incident light polarised perpendicular (p-polarisation) to the grating rulings. The dashed line shows the Littrow angle, and a typical angle for the Littman-Metcalf angle is shown by the dotted line.	72
4.8	Characterisation of the grating for incident light polarised parallel (s-polarisation) to the grating rulings. The dashed line shows the Littrow angle, and a typical angle for the Littman-Metcalf angle is shown by the dotted line.	72
4.9	(a) The Littrow configuration showing the first-order diffraction (D) and zeroth-order diffraction (R) components with losses (L) at grating. (b) A sketch of Littman-Metcalf geometry before the diffracted light is reflected back by the mirror. (c) Littman-Metcalf configuration after mirror reflection.	73
4.10	Results of the optimisation of the temperature controller indicating the region where the error signal is zero. The proportional current through the Peltier cooler is shown.	76
4.11	The ECDL output spectrum exhibiting multimode emission during the alignment process.	77
4.12	Captured spectrum results showing good and bad alignment, taken at a temperature of 14 °C and operating current of 80 mA.	78
4.13	The turn-on characteristics of the ECDL at certain wavelengths within the tuning range.	79
4.14	The ECDL's power versus wavelength at fixed currents based on results of Figure 4.13.	80
4.15	Results of the approximate tuning range showing the change in wavelength as the grating is manually rotated at a fixed current of 80 mA.	80
4.16	A comparison of the turn-on curves for the free-running diode laser and the ECDL at room temperature.	81
C.1	A sketch diagram showing a control loop using PID control function [44]	91

List of Tables

4.1	A summary of the feedback, output and losses for a Littrow cavity at a Littrow angle of 45° for the two polarisation orientations.	73
4.2	Typical percentage values for the first order power, output power and losses at 70° for a Littman-Metcalf geometry before the diffracted beam is reflected by the mirror.	74
4.3	Typical percentage values for the feedback, output power and losses at 70° for a Littman-Metcalf geometry after a retroreflection of the beam by the mirror.	75



Chapter 1

Introduction

1.1 Motivation and background

The invention of the first laser in 1960 by Maiman, using a ruby crystal, motivated many scientists to carry out research into new lasers, particularly new lasing materials. A year later the idea of using semiconductors as lasing materials was proposed by Basov et al. according to Ye [1]. They suggested that stimulated emission of radiation could occur in semiconductors by the recombination of charge carriers injected across a p-n junction. The first homojunction semiconductor diode laser¹ appeared in 1962. Progress was subsequently slow due to several reasons, the main one being the problem of high threshold currents which limited laser operation to short pulses at cryogenic temperatures. The problems attracted further research in this area, until double heterostructures were designed. This was a major breakthrough in device design and was made possible by new fabrication technologies. This has allowed the operation of diode lasers at low threshold currents and simultaneously improved the quality of the output beam.

Since their advent, semiconductor diode lasers have revolutionised many fields of research, ranging from basic laboratory research on the interaction of light and atoms to industrial photonic systems. To date, semiconductor diode lasers have found many applications such as in atomic and molecular spectroscopy, laser cooling of neutral atoms and ions, wavelength division multiplexing in optical telecommunications, and in optical data storage just to mention a few.

¹In this thesis the words semiconductor diode laser, laser diode and diode laser are used interchangeably

Lasers that can be tuned to a particular atomic transition are important in order to understand the interaction of light and atoms, especially in laser cooling and spectroscopy. Traditionally this was accomplished by using tunable dye lasers. Although the spectral properties of dye lasers are known to be excellent there are other limitations to their use such as high production cost, compatibility and the fact that they are difficult to use because of their complexity. It has been proved that semiconductor diode lasers can overcome some of these limitations due to their low cost because of mass production, high reliability, small and compact size, ease of operation, they are easily tunable by modulating the injection current and temperature, and have a longer lifetime, whilst providing stable output. Semiconductor diode lasers can also be easily controlled electronically and incorporated into integrated systems, can operate in single mode and have output powers as high as 100 mW. Therefore semiconductor diode lasers are gradually substituting expensive dye lasers [2] in many fields of research and applications.

The frequency tuning characteristics of an “off the shelf” laser diode is far from ideal and this greatly limits its utility [3] in laser cooling and spectroscopy applications. Most free-running diode lasers are not single mode, they operate in multimode and exhibit broad linewidth [4]. Although they can be tuned by varying the temperature and current, the small tuning range cannot meet many applications. Furthermore, the output from such diode lasers does not tune synchronously with either current or temperature. The tuning is characterised by mode-hops as the laser output switches from one longitudinal mode to the next, which is a major drawback of using diode lasers in spectroscopy.

However, soon after the successful operation of the diode lasers research scientists addressed some of the shortcomings of free-running diode lasers by exploiting their sensitivity to optical feedback. The idea is implemented in external cavity diode lasers (ECDLs) in which a wavelength selective element is used to select a certain spectral component of the diode laser output and return it to the diode laser. To date ECDLs can provide a single mode, collimated beam, increase the stability of the output and increase the mode-hop-free tuning range whilst reducing the laser linewidth. External cavity diode lasers have therefore emerged as attractive light sources for application in laser cooling and spectroscopy due to their narrow linewidth and broad tuning range [4]. High resolution spectroscopy can be achieved due to their narrow linewidth.

In each experimental development of the ECDL it is essential to design an appropriate mechanical

geometry that provides sufficient thermal damping, increases the mode-hop-free tuning range and is rigid to overcome mechanical vibrations. The ECDL system also require control electronics such as a low-noise current source to drive the diode laser, a temperature controller for thermal stability and a sidelock servo circuit to stabilise the output frequency.

1.2 Aim

The main aim of the experimental work documented in this thesis is to develop an ECDL system for future applications in laser cooling and atomic laser spectroscopy of rubidium. The theoretical background on semiconductor diode lasers presented in Chapter 2 serves to motivate the experimental study documented. The ECDL and control electronics are to be developed from basic components instead of using a commercial ECDL and commercial control electronics. The practical aim is to have a hands on approach, providing the author with more experience and a better technical understanding of ECDL technology, and also to determine whether this is a feasible approach within a limited budget for obtaining a tunable narrow-band laser source for research and educational purposes. The chosen diode laser and the developed ECDL system is to be characterised for use in laser cooling and spectroscopy of rubidium atoms. The requirements are that the output laser beam should be continuous wave and the wavelength emission should be near 780 nm, and power output of at least 5 mW, according to Wiemann et al. [5] and also supported by Harvey and Myatt [6]. The ECDL should operate on a single mode and have a mode-hop-free tuning range of at least 3 GHz [5]. The ECDL system should be thermally stable, free from mechanical vibrations and transient voltages in order to provide stable output power and frequency.

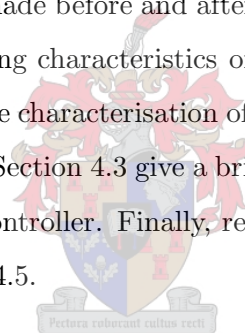
1.3 Outline of thesis

A literature review of semiconductor diode lasers is presented in Chapter 2. A distinction is made between solitary diode lasers and ECDL. A general background to semiconductor materials is described in Sections 2.2 and 2.3. The physics of semiconductor diode lasers is introduced and explored in Sections 2.4 to 2.7 in which the electron-hole recombination process, gain and threshold, typical diode laser structures and the output radiation characteristics for semiconductor diode lasers are illustrated and explained. The effects of external variables such as current and temperature on

the diode laser output frequency are explained in Section 2.8. The principle and theory of ECDL is described in Section 2.9 and the two basic configurations of ECDL are described in Section 2.10.

Chapter 3 is dedicated to the experimental setup and methods used during the design and development of the ECDL. As part of the preliminary study, the experimental setup to investigate the characteristics of a free-running diode laser is presented in Section 3.1. The mechanical design of the ECDL is explored in Section 3.2, where the design considerations and mechanical assembling are outlined and discussed. Section 3.3 describes the electronic systems of the ECDL, i.e. the current controller, temperature controller for temperature stabilisation, and the sidelock servo circuit for frequency stabilisation. The circuits are presented and discussed. The final section, Section 3.4 describes the testing, optimisation and characterisation of the developed ECDL system.

The results of the experimental study documented in Chapter 3 are presented, analysed and discussed in Chapter 4. A distinction is made before and after the diode laser was incorporated in the external cavity. The turn-on and tuning characteristics of a free-running diode laser are given in Section 4.1. Results obtained during the characterisation of the grating before being incorporated in the ECDL are outlined in Section 4.2. Section 4.3 give a brief account of the results obtained during the optimisation of the temperature controller. Finally, results obtained from the characterisation of the ECDL are discussed in Section 4.5.




Chapter 5 presents a summary of and conclusion to the results of the experimental work carried out. Proposals for future work and suggestions for improvements are given.

Chapter 2

Literature review of semiconductor diode lasers

2.1 Introduction

The image shows a faint watermark of a university crest in the center of the page. The crest features a shield with various symbols, topped with a crown and a banner. The Latin motto 'Pectus sobrietas cultus recti' is visible at the bottom of the crest.

This study relies heavily on exploiting the characteristics of semiconductor diode lasers. These characteristics are mainly due to the unique properties of the semiconducting material that make up the diode laser. This chapter describes the basic properties of semiconductor materials that makes them suitable for laser design and the physics of semiconductor diode lasers. Section 2.2 introduces the concepts of density of states and occupation probability of charge carriers in a semiconductor material. Section 2.3 illustrates the effect of doping, since most materials used for laser design are extrinsic semiconductors. It is necessary to examine the mechanism by which radiation is emitted by the diode lasers through electron-hole recombination when a forward bias voltage is applied, and this is discussed in Section 2.4. The physics of semiconductor diode lasers, including gain and threshold, diode laser structures, and the beam's spatial characteristics, are each described in Section 2.5, 2.6 and 2.7, respectively. The effects of temperature and current on diode laser performance is explored in Section 2.8. The theory of external cavity diode lasers is explained in Section 2.9. Section 2.10 illustrates two most common configurations of external cavity diode lasers.

A semiconductor is a crystalline or amorphous solid whose electrical conductivity is intermediate

between that of a metal and an insulator and can be changed by altering the temperature or the impurity content of the material, or by illumination with light [7]. The atoms in semiconductors cannot be treated as isolated entities with discrete energy levels because of their strong interaction with other atoms in the material. Energy levels of the semiconductor take the form of bands with finely separated discrete energy levels, which can be approximated as continuum. The formation of bands is a result of the Pauli exclusion principle which states that no electrons can occupy the same quantum state. The lower valence band and the upper conduction band are separated by a “forbidden” energy gap, E_g , which is crucial in determining the electrical and optical properties of the material. In conductors the valence and conduction bands overlap. In insulators such as diamond the bandgap is typically 5.4 eV. In semiconductors the bandgap has intermediate values, for example 1.1 eV for silicon [8].

In the absence of any thermal excitation (that is at $T = 0$ K), the valence band of an ideal semiconductor is completely filled with electrons while the conduction band is empty. As the temperature increases some electrons are thermally excited into the empty conduction band where there are many unoccupied states, leaving an empty state in the valence band, called a hole. Other excitation mechanisms can be optical or electrical pumping. An electron can decay from the conduction band into the valence band to fill an empty state by means of a process called electron-hole recombination. When this occurs, the electrons can either radiate the energy or give it up via interactions or collisions with the semiconductor lattice, which induce a form of lattice vibration or phonon relaxation in the material.

Semiconductors are classified into two distinct types, namely intrinsic and extrinsic. Intrinsic semiconductors such as germanium and silicon are pure and do not have any impurities, whilst extrinsic semiconductors contain additional impurities called dopants to alter the electrical properties of semiconductors. Efforts to improve the electrical and other properties of semiconductor materials for specific applications have led to the fabrication of semiconductors made of two or more elements such as GaAs, InP or $\text{Al}_x\text{Ga}_{1-x}\text{As}$, where x refers to the aluminium content of the material.

2.2 Density of states and occupation probability

The presence of a finite energy gap, E_g , between a valence and conduction band has a profound effect on carrier density and the transport properties of the semiconductor. The carrier density, which is a measure of holes and electrons, determines how a semiconductor laser diode operates. In this section the density of states and the occupation probability of the charge carrier under equilibrium conditions in the bands are discussed.

In order to determine the concentration of charge carriers as a function of energy in each band it is important to have knowledge of the density of allowed energy levels and the probability that each level is occupied. The quantum state of an electron in a semiconductor is characterised by its energy E , its wave vector k and its spin [9]. An electron near the conduction band edge can be approximated as a particle of mass m_c confined to a three-dimensional infinite rectangular potential well. According to Saleh et al. [7] the density of states function near the edge of a conduction band, $\rho_c(E)$, and a valence band, $\rho_v(E)$, are given by the following equations respectively:

$$\rho_c(E) = \frac{(2m_c)^{3/2}}{2\pi^2\hbar^3} (E - E_c)^{1/2}, \quad E \geq E_c \quad (2.1)$$

$$\rho_v(E) = \frac{(2m_v)^{3/2}}{2\pi^2\hbar^3} (|E - E_v|)^{1/2}, \quad E \leq E_v \quad (2.2)$$

where the constants m_c and m_v are the effective masses of the holes and electrons in the conduction and valence bands respectively, E_c is the energy at the bottom of the conduction band, and E_v is the energy at the top of the valence band. The dependence of the density of states on energy for both the conduction and valence bands can be approximated by Figure 2.1(a). The shaded regions indicate possible states that can be filled. No states are available in the band gap. The curvature of the curves in Figure 2.1 depends on the effective masses of the holes and electrons, where their effective masses depend on the type of the material and crystal orientation [10].

At a finite temperature T , a number of electrons from the valence band are thermally excited to the conduction band. The occupancy probability that a given available electron energy state E will be occupied if it exists is given by the Fermi-Dirac distribution function [11]

$$f(E) = \frac{1}{e^{(E-E_f)/kT} + 1} \quad (2.3)$$

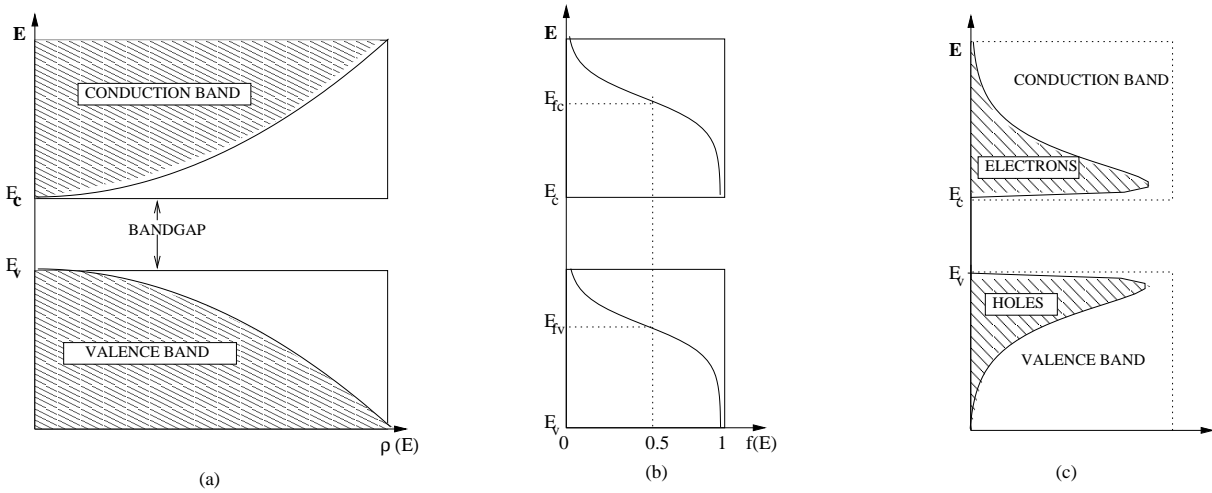


Figure 2.1: (a) A plot of energy E against density of states $\rho(E)$ in the conduction band and valence band, as depicted by equations 2.1 and 2.2. (b) The plot of energy E against the probability function $f(E)$ in each band during the quasi-equilibrium state, as indicated by equations 2.5 and 2.6. (c) The product of the two graphs (a) and (b) to give the density of holes in the valence band and the density of electrons in the conduction band. The plots are derived from equations 2.7 and 2.8.

where E_f is a constant known as the Fermi energy or Fermi level and k is the Boltzmann constant. Whatever the value of T is, $f(E_f) = 1/2$, the Fermi level is that energy level for which the probability of occupancy is 1/2 if there was an allowed state there [7]. At a temperature of absolute zero ($T = 0\text{K}$) all electrons occupy the lowest available energy states, therefore the valence band is completely filled with electrons, whilst the conduction band is empty. The significance of E_f is the division between the occupied and unoccupied energy levels at $T = 0\text{K}$.

If the Fermi level is in the forbidden gap, $E_v < E_f < E_c$, and if the difference $(E - E_f) \gg kT$, then the Fermi-Dirac distribution function can be approximated by the Boltzmann function [12], and the probability of an electron state being occupied at an energy E above E_f is given by

$$f(E) \approx e^{-[(E-E_f)/kT]} \quad (2.4)$$

The occupation probability described so far is applicable only for a semiconductor in thermal equilibrium. There are situations in which the conduction-band electrons are in thermal equilibrium among themselves, as are the valence-band holes, but the electrons and holes are not in mutual thermal equilibrium. This can occur, for example, when an external electric field or photon flux

induces band-to-band transition at too high a rate for interband equilibrium to be achieved. The bands are treated separately and use the concept of the quasi-Fermi level E_{fc} to describe the probability of a state being filled in the conduction band and the quasi-Fermi level E_{fv} to describe the probability that a state in the valence band is filled. This is based on the fact that intraband relaxation occurs on a much shorter time scale than the interband recombination rate. Therefore, according to Verdeyen [11], the probability of an occupied state in the conduction band as from equation 2.3 is given by

$$f_c(E) = \frac{1}{e^{(E-E_{fc})/kT} + 1} \quad (2.5)$$

and the probability of an occupied state in the valence band is

$$f_v(E) = \frac{1}{e^{(E-E_{fv})/kT} + 1} \quad (2.6)$$

A plot of functions $f_c(E)$ and $f_v(E)$ in each band is shown in Figure 2.1(b). For the energy interval dE , the density of electrons in the conduction band is obtained by multiplying the density of states from equation 2.1 by the Fermi-Dirac function 2.5 to obtain

$$n_c(E)dE = \rho_c(E)f_c(E)dE = \frac{(2m_c)^{3/2}}{2\pi^2\hbar^3} \frac{(E - E_c)^{1/2}}{e^{[(E-E_{fc})/kT]} + 1} dE \quad E > E_c \quad (2.7)$$

The density of holes in the valence band in the energy interval dE , below E_v , is determined by using the density of states for the valence band and multiplying by $1 - f_v(E)$, which is the probability that the state is empty, thus

$$p_v(E)dE = \rho_v(E)(1 - f_v(E))dE = \frac{(2m_v)^{3/2}}{2\pi^2\hbar^3} \frac{(E_v - E)^{1/2}}{e^{[(E_{fv}-E)/kT]} + 1} dE \quad E < E_v \quad (2.8)$$

where the inequalities show that there are no states to be filled or emptied for $E_v < E < E_c$, which is true for intrinsic semiconductors containing no impurities or doping [11].

The population of the charge carriers is obtained by integrating equations 2.7 and 2.8. A plot of equations 2.7 and 2.8 is shown in Figure 2.1(c). The shaded area shows the population of the holes and electrons in the valence and conduction bands respectively. This is true at a finite temperature, where both the density of states and the Fermi function have finite values in the bands.

2.3 Doping of semiconductor material

The electrical and optical properties of semiconductors can be substantially altered by adding small controlled amounts of specially chosen “impurities” or dopants which alter the concentration of mobile charge carriers by many orders of magnitude. Pure intrinsic semiconductor materials have relatively low conductivity. Mixing small amounts of “impurity” atoms with the semiconductor material provides additional free electrons and holes that increase the conductivity and thereby allow current to flow more easily [13]. Electrical current flow in semiconductor laser materials is essential in order to provide excitation energy to the laser levels. The alteration will affect the Fermi energy level and the density of charge carriers in the two bands of the semiconductor.

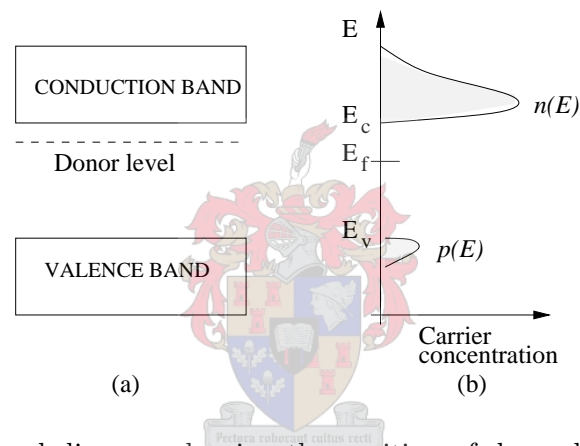


Figure 2.2: (a) Energy band diagram showing the position of donor levels in a n -type semiconductor. (b) Concentrations of mobile electrons and holes $n(E)$ and $p(E)$ respectively in a n -type semiconductor. The shifted Fermi level is shown by E_f .

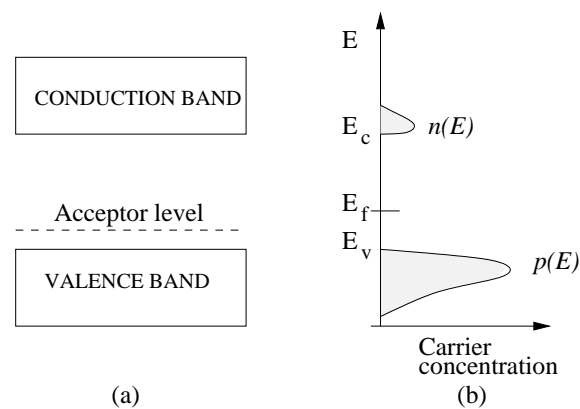


Figure 2.3: (a) Energy band diagram showing the position of acceptor levels in a p -type semiconductor. (b) A sketch diagram showing the concentrations of mobile electrons and holes $n(E)$ and $p(E)$ respectively in a p -type semiconductor.

Dopants with excess valence electrons (donors) can be used to replace a small proportion of the normal atoms in the crystal lattice thereby creating a predominance of electrons. The material is said to be a *n*-type semiconductor e.g. atoms in group V replacing some of the group IV atoms. Similarly, a *p*-type material can be made by using dopants with a deficiency of valence electrons (acceptors) giving a predominance of holes e.g. group IV atoms replaced with some group III atoms. Therefore the concentration of mobile electrons in an *n*-type semiconductor is greater than the concentration of holes that is $n \gg p$, as shown in Figure 2.2. Holes are majority carriers in a *p*-type semiconductor and $p \gg n$, as shown in Figure 2.3.

The net effect of doping is to produce either an excess number of electrons, which begin filling the conduction band, or an excess number of holes, which leave a region vacant of electrons in the valence band [13]. Donor electrons in a *n*-type semiconductor occupy an energy slightly below the conduction-band edge, as indicated in Figure 2.2(a). At room temperature most donor electrons will be thermally excited into the conduction band, creating a higher electron carrier concentration in the lower part of the conduction band. For a *p*-type semiconductor, the acceptor energy level lies at an energy slightly above the valence-band edge, as shown in Figure 2.3(b). At room temperature electrons from upper valence levels are excited into acceptor levels leaving holes in upper part of the valence band. In both cases there is a shift in the Fermi energy level. For *n*-type doping the Fermi level shifts upward towards or into the conduction band, since there are excess electrons, which therefore moves the entire distribution upwards, as shown in Figure 2.2(b). For *p*-type doping the Fermi level shifts downward towards the valence band, as in Figure 2.3(b).

2.4 Electron-hole recombination

The emission of radiation in a semiconductor laser requires the creation of electron-hole pairs in the active region of the semiconductor material. Therefore it is desirable to cause the excess electrons of a heavily doped *n*-type material to come into contact with the excess holes of the heavily doped *p*-type material. This is achieved by using separate samples of *p*-type material and *n*-type material with distinctly different Fermi energy levels, as shown in Figure 2.4(a).

When the *p*-type and the *n*-type semiconductor regions are brought in contact, electrons will diffuse away from the *n*-region into the *p*-region, leaving behind positively charged ionised donor atoms

[7]. In the p -region the electrons recombine with the abundant holes. Similarly, holes diffuse away from the p -region to recombine with the abundant mobile electrons leaving behind negatively charged ionised acceptor atoms under thermal equilibrium conditions. The diffusion stops when the resulting build up of electric field due to charged ions can counteract the diffusion process. This field is formed in the depletion region and is known as the depletion electric field, qV_o , and acts as an energy barrier.

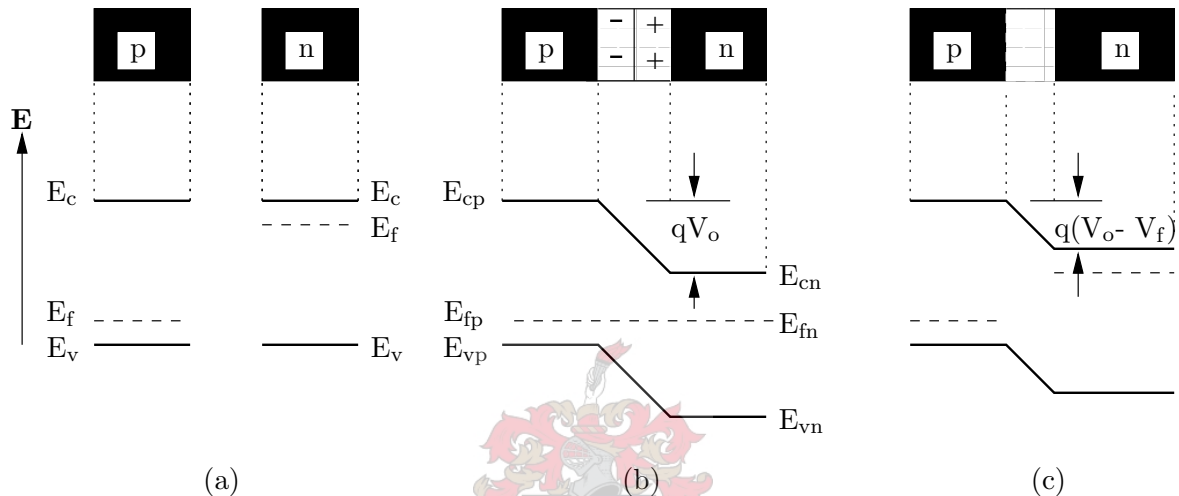


Figure 2.4: Schematic representation of the relative energy levels for valence bands, conduction bands, and Fermi levels of a $p - n$ junction for: (a) separated materials, (b) p and n materials in contact, and (c) p and n materials in contact with an applied forward bias [13].

When the initial flow occurs, the electrons and holes produce the minimal amount of recombination radiation. This ceases as soon as the space charge stabilises the junction region and the Fermi energy levels align, as shown in Figure 2.4(b), to produce equilibrium. The $p - n$ junction effectively shifts the valence and conduction bands of the p -type material to a higher value relative to the n -type material, as shown in Figure 2.4(b) [13].

The recombination described above does not last for a long time and the radiation is small. By applying an external forward voltage V_f that creates an electric field qV_f which opposes the depletion electric field qV_o , to a heavily doped $p - n$ junction, the energy barrier between the two materials is reduced significantly, as shown in Figure 2.4(c). The reduction in the potential hill, $q(V_o - V_f)$, allows current to readily flow through the junction of the two materials. The presence of an external bias voltage causes a switch from equilibrium and a misalignment of the Fermi levels in the p - and n -regions, as shown in Figure 2.4(c). Because of the positions of the Fermi energy levels,

these carrier movements will create a very narrow region in which there are both electrons in the higher energy conduction band and holes in the valence band [14], a situation which is impossible for an ordinary $p-n$ junction described above. This condition corresponds to population inversion and makes direct recombination transitions possible.

Since in the depletion region or junction there are vacant electron sites in the valence band, it is possible for an electron from the highly populated conduction band to recombine with a hole in the valence band, thereby emitting a photon. Large quantities of electrons then flow through the junction region and the recombination radiation is proportional to current flow. Non-radiative recombination also occurs, producing heat that limits the amount of current flow in the material.

2.5 Gain and threshold in semiconductor diode lasers

A semiconductor diode laser can be modelled as a two-level laser system where the upper state is the conduction band and the lower state is the valence band. A population is said to be inverted if at a finite energy the valence band is empty down to an energy E_{fv} and the conduction band is filled up to an energy E_{fc} , with more electrons near the conduction band edge than near the valence band edge on the p -side of the junction [1]. This population inversion is directly proportional to optical gain of the laser.

Gain is central to an understanding of any laser regardless of the physical or chemical processes by which it is established. In conventional lasers gain is established in the active material if the population of the upper state exceeds that of the lower state. In semiconductors the existence of gain can be represented as a region containing filled electron states at higher energy than empty electron states (or holes). According to Verdeyen [11], the gain coefficient of any laser, gas, solid state, or semiconductor, is always proportional to the population inversion multiplied by the line shape function, that is, how that inversion is distributed out among the various energy states.

From [15], the gain coefficient, $g(\nu)$, of most lasers can be approximated by the following equation, which holds for a so-called two-level laser

$$g(\nu) = \frac{\lambda^2 A}{8\pi n^2} \left(N_2 - \frac{g_2}{g_1} N_1 \right) S(\nu) \quad (2.9)$$

where

A is the Einstein coefficient for spontaneous emission

N_1 and N_2 are the densities of electrons near the valence-band edge and conduction-band edge respectively in the active region of the semiconductor laser

n is the refractive index at wavelength λ .

g_1 and g_2 are the degeneracies of lower and upper levels respectively

$S(\nu)$ is the lineshape function, as a function of ν .

At population inversion $N_2 \gg \frac{g_2}{g_1} N_1$, it can be assumed that $N_1 \approx 0$, implying that the density of electrons in the lower level is small enough that any excitation of an electron from the lower to the upper band is negligible. Assuming homogeneous broadening, $S(\nu)$ can be replaced by the Lorentzian lineshape $\delta\nu_o$, and equation 2.9 becomes

$$g(\nu_o) = \frac{\lambda^2 A}{8\pi n^2 \delta\nu_o} N_2 \quad (2.10)$$

where N_2 is the conduction band density of electrons injected by forward biasing into the active region from the conduction band of the n -type material of a semiconductor laser.

The threshold gain g_{th} , of semiconductor lasers is determined by unit round trip condition [1]

$$r_1 r_2 \exp[2(\Gamma g_{th} - \alpha_m)l] = 1 \quad (2.11)$$

where r_1 and r_2 are the end facet reflectance, l is the cavity length between the end facets, Γ is the confinement factor, which is a measure of the fraction of the oscillating field distribution that experiences gain within the active layer [12], and α_m represents losses in the cavity and at the end facets of the diode laser. Diode lasers do not employ mirrors for feedback because the refractive index of the semiconductor material is large enough to give considerable reflections at the semiconductor air interface.

From equation 2.11

$$g_{th} = \frac{1}{\Gamma} \left(\alpha_m - \frac{1}{2l} \ln r_1 r_2 \right) \quad (2.12)$$

Using the threshold condition

$$g(\nu_o) = g_{th}$$

gives $(N_2)_{th}$ the threshold value of the upper level population as

$$(N_2)_{th} = \frac{8\pi^2 n^2 \delta\nu_o}{\lambda^2 \Gamma A} \left(\alpha_m - \frac{1}{2l} \ln r_1 r_2 \right) \quad (2.13)$$

It is useful to express $(N_2)_{th}$ in terms of current density through the diode laser. The current density J is the flow of charge per unit area per unit time. The average current density is equal to I/A where I is the injection current and A is the cross sectional area of the active region of the diode laser. The rate per unit volume at which electrons are injected into the active region is J/ed , where d is the distance travelled by a conduction electron going from the n -doped region to the p -doped region before it recombines with a hole, and e is the charge of the electron. During steady-state conditions the injection rate is equal to the loss rate (R_e) of conduction electrons due to both radiative and non-radiative recombination processes [12], thus

$$J/ed = R_e N_2$$

Then the threshold current density is given by

$$J_{th} = edR_e(N_2)_{th} \quad (2.14)$$

Substituting for $(N_2)_{th}$ in equation 2.14 gives the threshold current density as

$$J_{th} = \frac{8\pi^2 n^2 \delta\nu_o}{\lambda^2} (ed)\Gamma^{-1}\eta_i^{-1} \left(\alpha_m - \frac{1}{2l} \ln r_1 r_2 \right) \quad (2.15)$$

where $\eta_i = A/R_e$ is the internal quantum efficiency. The threshold current density, J_{th} , is a key parameter in designing semiconductor laser materials. For a homojunction, the confinement factor Γ is very small and d is very large. This gives a high threshold gain, therefore lasing is achieved at high threshold currents. This causes heating of the diode laser, which in turn decreases its efficiency. J_{th} is minimised by using materials with high internal quantum efficiency η_i , minimising the resonator length or volume losses coefficient α , and reducing the diffusion length d .

2.6 Semiconductor diode laser structures

The commonly used semiconductor laser materials are the direct band gap materials whose energy $E(k)$ variation with wave vector k is shown in Figure 2.5(a). The minimum energy of the conduction band lies directly above the maximum energy of the valence band at the same value of momentum vector k [11]. Recombinations in such materials can conserve energy and momentum, therefore they are efficient semiconductor laser materials, for example gallium arsenide. For indirect band gap semiconductors the maximum energy of the valence band does not lie exactly on the minimum of the conduction band at the same wave number k [11], as shown in Figure 2.5(b). Such semiconductors are associated with the creation of a phonon in order to conserve momentum. The phonon carries away the excess momentum. Recombinations in the two-particle process in indirect band gap semiconductors usually occur by thermal or collisional processes which are inefficient.

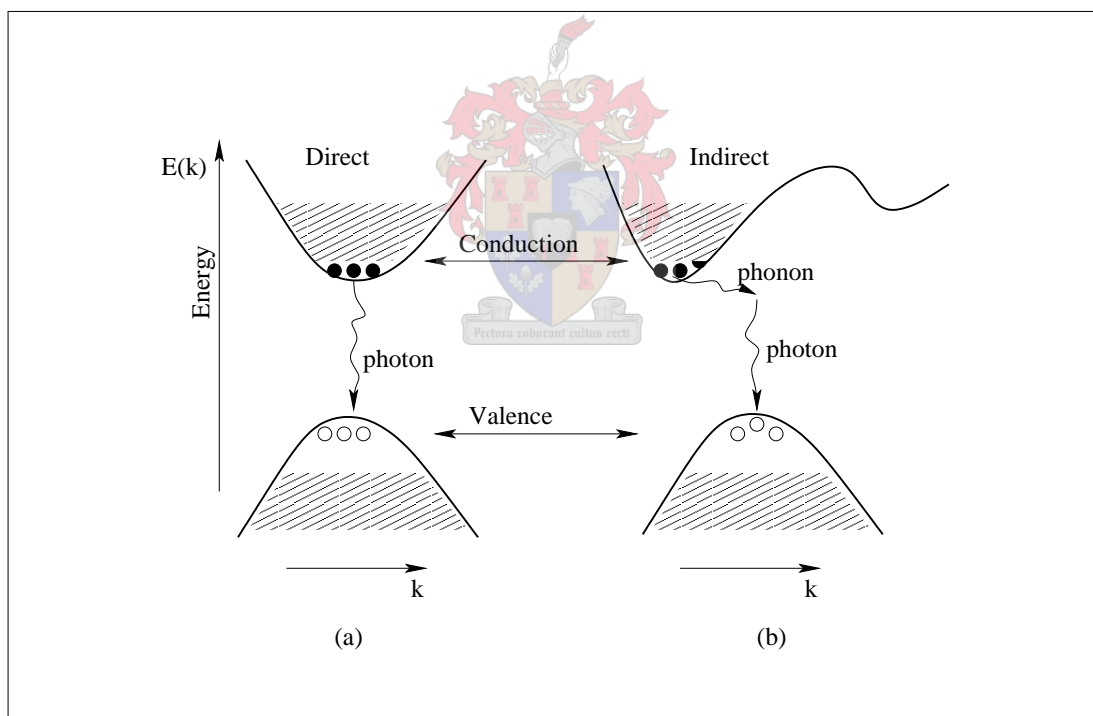


Figure 2.5: An illustration of (a) direct and (b) indirect band gap semiconductors, showing positions of energy, E , and momentum wavevector k .

The emission wavelength range, output powers and efficiency of semiconductor lasers can be improved by using doped semiconductor materials and using different diode laser geometries. Most semiconductors consist of elements of group III and group V of the periodic table, for example GaAs

(gallium arsenide). Modern semiconductor lasers contain three or four elements from the periodic table to increase the electrical conductivity of the materials. These alloys are called ternary or quaternary compound semiconductors, e.g. $\text{Al}_{1-x}\text{Ga}_x\text{As}$ (aluminium gallium arsenide), a ternary compound and $\text{In}_{1-x}\text{Ga}_x\text{As}_{1-y}\text{P}_y$ (indium gallium arsenide phosphate), a quaternary compound. In this notation x and y are composition parameters which take on values of between 0 and 1.

The problem of high threshold currents in homojunctions was solved by the development of heterojunctions, where a junction is made up of different semiconducting materials. A simple heterostructure shown in Figure 2.6 confines light and charge carriers to a well defined active region in the laser diode, limiting the thickness of the active region in the z -direction. The concept of the double heterostructure is to form potential barriers on both sides of the $p-n$ junction to provide a potential well that limits the distance over which minority carriers diffuse in the z -direction of Figure 2.6. Double heterojunctions do not only employ $n-p$ type GaAs layers, but also n - and p -type layers of an AlAs-GaAs alloy such as AlGaAs, as shown in Figure 2.6.

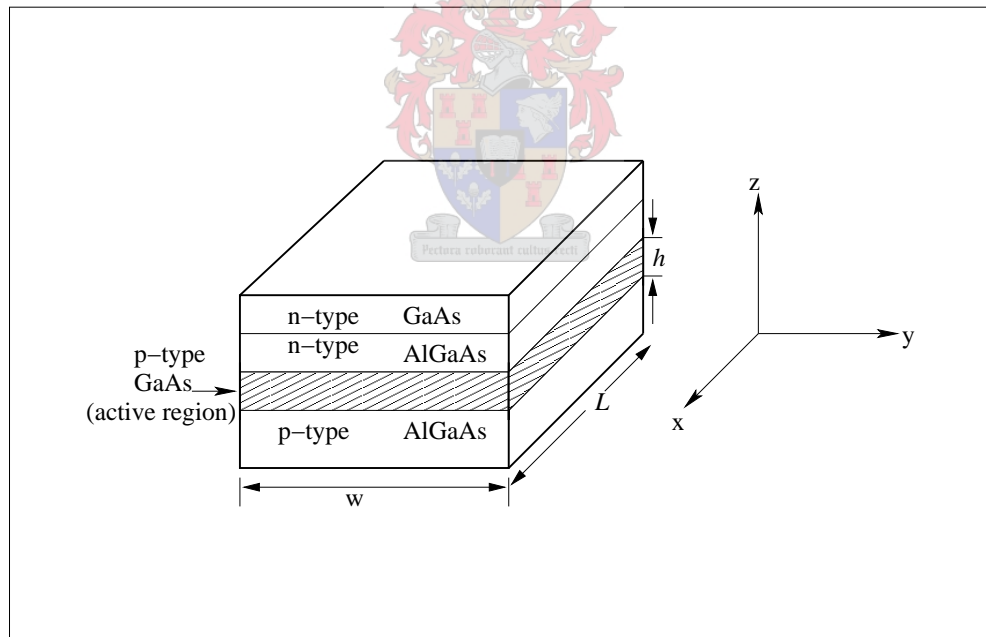


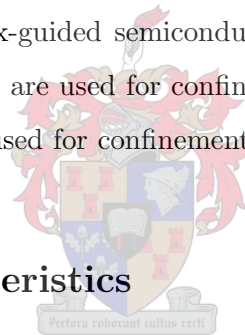
Figure 2.6: A heterojunction diode laser [15] structure, showing a GaAs active layer sandwiched by AlGaAs semiconductor material. The diode laser output propagates in the x -direction.

The AlGaAs material has a larger energy band gap than GaAs, and also a smaller refractive index [15]. Due to the bandgap differences at the two GaAs-AlGaAs junctions, there is greater confinement of electrons and holes in the active region. The bandgap acts as the potential barrier for electrons and holes preventing them from diffusing out of the active p -type GaAs layer into

which they are injected by forward biasing. Loss of light within the active region will be smaller than in homojunctions because the radiation moving into the AlGaAs layers will find itself in a non-resonant, non absorbing medium because of the large band gap compared with the radiation frequency. In Figure 2.6, most of the light is confined within the active layer because of the higher refractive index inside the layer than that of the outer AlGaAs layers. Light can be reflected back by total internal reflection at large angles into the active medium, thus reducing the width d in equation 2.15. Thinner confinements of approximately $0.01 \mu\text{m}$ can be achieved with quantum well lasers [9].

Mechanisms have been developed to confine the charge carriers in the y -direction of the junction plane by, for example, confining the injection current to a narrow stripe therefore reducing the width w of the active region. This can be done by building high-resistance regions into the diode. The cross-sectional area of the output beam is also reduced by using stripe geometry. Other common mechanisms are gain-guided and index-guided semiconductor diode lasers. In gain-guided diode lasers the lateral variations of the gain are used for confinement and in the index-guided type the lateral refractive index variations are used for confinement.

2.7 Beam spatial characteristics



For most applications the spatial characteristics of the output beam are important. In most lasers the laser beam lies totally within the active medium so that the spatial distribution of the different modes is determined by the shapes of the mirrors and their separation [7]. The situation is different in semiconductor lasers since the beam extends outside the active layer, so that the geometry of the active layer and surrounding structures influences the beam profile.

The transverse modes of the diode laser can be determined by considering a rectangular waveguide whose cross-section dimensions are h and w [11]: h is the width and w is the length of the cross-section of the active layer, see Figure 2.7. The transverse mode is divided into a transverse magnetic mode (TM) which is polarised perpendicular to the active layer, and a transverse electric mode (TE) which is polarised parallel to the active layer, as shown in Figure 2.7.

If h/λ_o , where λ_o is the wavelength of light propagating in the dielectric waveguide, is sufficiently small the waveguide will only admit a single mode in the transverse direction perpendicular (TM

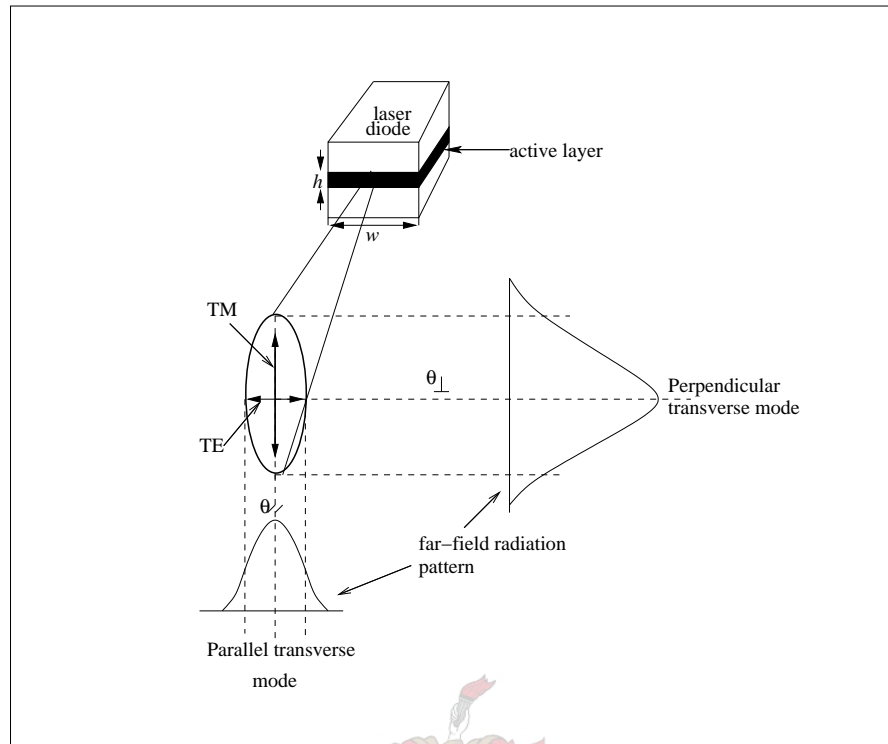


Figure 2.7: Schematic representation of the far-field radiation pattern of a laser diode illustrating the TM and TE modes in an elliptical beam output.

mode) to the junction. The divergence of the laser beam depends on the thickness of the active layer compared to the wavelength of light propagating within the layer. The TM mode has a far-field angular divergence of approximately λ_o/h radians [7]. Since h is less than w , the TE mode has a smaller divergence, λ_o/w radians, compared to the TM mode. The far-field radiation pattern has therefore an elliptical shape as shown in Figure 2.7.

Usually w/λ_o is large and therefore the waveguide will support several modes in the direction parallel (TE mode) to the plane of junction [7]. The higher order modes in the direction parallel to the junction have a wider spatial spread, they are less confined; their loss coefficient is therefore higher than that of lower order modes. Some of the highest order modes will fail to satisfy the oscillation conditions, while others will oscillate at a lower power than the fundamental modes, therefore they will die out.

Typical dimensions of the active region are a length L of 400 μm , a thickness h of about 1 μm and a width w of about 3 μm [16]. The spatial distribution of the far-field light within the radiation cone depends on the number of the transverse modes and on their optical powers. The rectangular

shape of the active region gives the output an elliptical shape, as illustrated in Figure 2.7. A typical output beam will have a divergence angle of 30° in the direction perpendicular to the junction and 10° in the plane parallel to the junction [17]. The beam's far field radiation pattern can be easily corrected by using cylindrical lenses.

2.8 Effects of temperature and current

In this section the microscopic effects of temperature and current on the semiconductor active medium are discussed. These include their effects on the bandgap of the material, charge carrier density and the overall expansion of the active material.

Compared to other conventional lasers the diode laser has a very small cavity length, typically of the order of microns. Under laser oscillation a light standing wave is created with its wavefront parallel to the end facets while light is travelling back and forth within the small laser cavity. This standing wave consists of longitudinal and transverse modes. The longitudinal modes satisfy the condition of the standing wave confined in the cavity. The frequency, ν_m , of a longitudinal mode of fixed mode number m is determined by the optical round trip length of the cavity which is given by the product of its geometrical length L and the index of refraction $n(\nu_m)$ as well as the phase change φ that the light undergoes at reflection at the cavity mirrors. The expression for ν_m is

$$\nu_m = \frac{mc}{2n(\nu_m)L + \varphi/2\pi\nu_m} \quad (2.16)$$

where c is the speed of light in a vacuum [18].

The frequency spacing or the free spectral range (FSR) for GaAlAs diode laser with $L = 400 \mu\text{m}$ and $n = 3.6$ is approximately 99 GHz². The lasing wavelength corresponds to the longitudinal mode which has maximum gain, thus the one closest to the gain peak. The laser will operate at that cavity mode as shown in Figure 2.8.

The frequency of the gain curve maximum ν_{gain} is determined by the bandgap of the semiconductor which is influenced by the injection current I , and temperature T of the junction. The temperature

²The calculation of this value is shown in Appendix A

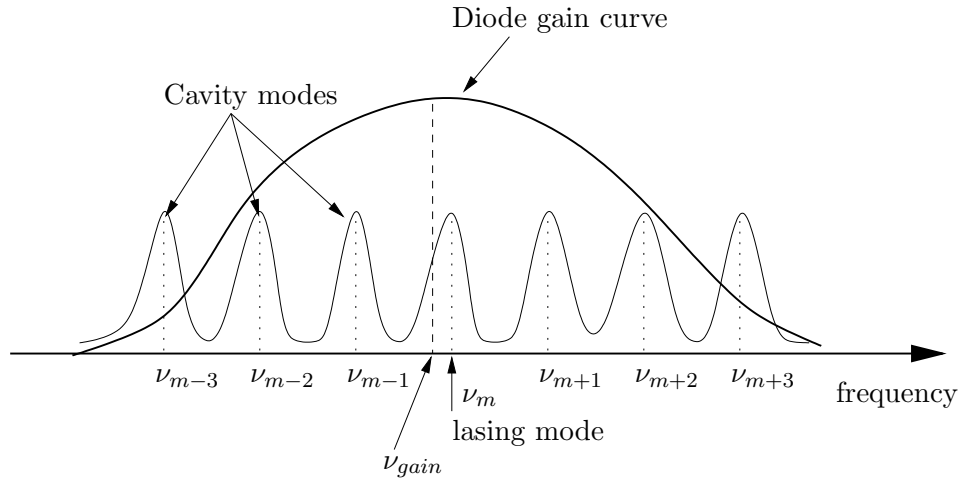


Figure 2.8: Schematic view of cavity modes and gain spectrum of a diode laser.

coefficient giving the shift in the gain curve per Kelvin (K), [18] is given by

$$\Delta\nu_{gain} = \phi_{gain}\Delta T \quad \text{where} \quad \phi_{gain} = \frac{\partial\nu_{gain}}{\partial T} \quad (2.17)$$

The injection current affects the gain curve shift in two ways:

- (i) the density N of free charge carriers changes, which has a direct influence on the bandgap

$$\Delta\nu_{gain} = \phi'_{gain}\Delta I \quad \text{where} \quad \phi'_{gain} = \frac{\partial\nu_{gain}}{\partial N} \frac{\partial N}{\partial I} \quad (2.18)$$

- (ii) the increase in current causes Joule heating, which in turn changes the temperature of the laser diode

$$\Delta\nu_{gain} = \phi_{gain} \frac{\partial T}{\partial I} \Delta I \quad (2.19)$$

Equation 2.16 shows that the emission frequency depends on some parameters which are temperature dependent and these are the geometrical length L (dependent on temperature) and refractive index n (dependent on mode frequency, temperature, and charge carrier density).

The linear expansion of the geometrical length L of the cavity due to temperature is given by

$$\Delta L = \beta_1 L \Delta T \quad \Rightarrow \quad \beta_1 = \frac{1}{L} \frac{dL}{dT} \quad (2.20)$$

where β_1 is the coefficient of linear expansion due to changes in temperature. The temperature

effects on the refractive index [18] can be written as

$$\Delta n = \beta_2 n \Delta T \quad \Rightarrow \quad \beta_2 = \frac{1}{n} \frac{\partial n}{\partial T} \quad (2.21)$$

Moreover, n depends on the density N of free carriers

$$\Delta n = \beta_3 n \Delta N \quad \Rightarrow \quad \beta_3 = \frac{1}{n} \frac{\partial n}{\partial N} \quad (2.22)$$

which itself is temperature dependent:

$$\beta_4 \equiv \frac{\partial N}{\partial T} \quad (2.23)$$

Therefore the change in refractive index due to temperature is given by

$$\Delta n = \beta_3 \beta_4 n \Delta T \quad \Rightarrow \quad \beta_3 \beta_4 = \frac{1}{n} \frac{\partial n}{\partial N} \frac{\partial N}{\partial T} \quad (2.24)$$

The combinations of these coefficients is given by ³

$$\phi_{mode} = (\beta_1 + \beta_2 + \beta_3 \beta_4) \nu / 2 \quad (2.25)$$

ϕ_{mode} can be understood as the sensitivity of the longitudinal mode frequency to variations of the heat sink temperature. The differential change in the emission frequency due to the shift of the longitudinal mode frequencies with temperature ΔT is given by

$$\Delta \nu_{mode} = \phi_{mode} \Delta T \quad (2.26)$$

As ϕ_{mode} is negative, an increase in temperature causes a redshift in frequency. In addition to the environmental temperature effect, the laser diode temperature can be modified by varying Joule heating, that is, by changing the injection current. The total thermal effects will give a differential change $\Delta \nu_{mode}$ of the emission frequency as

$$\Delta \nu_{mode} = \phi_{mode} \Delta T + H_{\nu,th} \Delta I \quad (2.27)$$

³The full derivation of this equation is shown in Appendix B

where $H_{\nu,th}$ denotes the thermal component of the current-frequency conversion factor

$$H_{\nu,th} = \phi_{mode} \frac{\partial T}{\partial I}$$

Equation 2.27 becomes

$$\Delta\nu_{mode} = \phi_{mode} \left(\Delta T + \frac{\partial T}{\partial I} \Delta I \right) \quad (2.28)$$

The sign of ϕ_{mode} is negative whereas that of $\partial T/\partial I$ is positive [18]. Hence an increase of the injection current leads to a red shift of the emission frequency.

Let α be the coefficient representing changes due to current. The effects of current can be summarised as follows:

- (i) the current affects the density of charge carriers N which in turn changes the refractive index n such that

$$\Delta n = \beta_3 \alpha_1 n \Delta I \quad \beta_3 = \frac{1}{n} \frac{\partial n}{\partial N} \quad \text{and} \quad \alpha_1 = \frac{\partial N}{\partial I} \quad (2.29)$$

- (ii) the temperature changes due to Joule heating as the current changes. As explained above, the temperature dependent variables changes, namely the geometrical length, the refractive index and the density of charge carriers. If $\alpha_2 = \partial T/\partial I$ is the coefficient representing Joule heating then the current effect on the mode frequency is given by

$$\Delta\nu_{mode} = \phi_{mode} \frac{\partial T}{\partial I} \Delta I = \phi_{mode} \alpha_2 \Delta I \quad (2.30)$$

Combining the Joule heating and the carrier density effect on the mode frequency yields the following ⁴

$$\Delta\nu_{mode} = \left(\phi_{mode} \alpha_2 + \frac{\nu}{2L} \beta_3 \alpha_1 \right) \Delta I \quad (2.31)$$

The fluctuations in the index of refraction affects the α -parameter of the diode laser which is the linewidth enhancement factor. The α -parameter is defined as the ratio of the changes in the real to the imaginary parts of refractive index with charge carrier density [19]. Effects due to changes in temperature can be summarised as follows

- The bandgap changes due to temperature changes and this causes the gain curve to shift

⁴This equation is shown in Appendix B

towards the red with an increase in temperature according to equations 2.17 and 2.18.

- The change in temperature of the active medium, according to equation 2.20, implies a change in the cavity length L , therefore the longitudinal modes shift according to equation 2.26.
- The sensitivity of the refractive index to changes in temperature (equation 2.21) and the temperature dependence of carrier density (equation 2.22) affects the optical path length of the light in the active region, therefore the longitudinal modes shift according to equation 2.26.

Effects due to changes in current are

- A change in current affects the density of charge carriers in the active region. As the current increases so the carrier density increases and the bandgap changes, therefore the gain curve shifts according to equation 2.18. The refractive index also changes and has an effect on the mode frequency as shown in equations 2.29 and 2.31. The refractive index also influences the α - parameter.
- As the current increases the temperature of the active substrate increases as a result of Joule heating. The temperature of the laser diode increases and this implies a shift in longitudinal modes according to equation 2.30, but on a shorter time scale than environmental temperature changes. This temperature increase also have a small effect on the gain curve as given by equation 2.28.

Generally, the emission frequency of semiconductor diode lasers is strongly dependent on temperature and the injection current. The variation in temperature and current sometimes causes the diode laser to exhibit poor frequency stability [20].

2.8.1 Mode-hopping in diode lasers

The emission frequency of a diode laser is determined on a coarse scale by the maximum of its gain curve ν_{gain} and on a fine scale by the frequency positions ν_{cav} of the longitudinal resonances of its cavity. The shift in the gain curve and longitudinal modes due to temperature and current

changes described in Section 2.8 cause mode-hopping since they shift differently. The gain curve shifts faster than the longitudinal modes.

Mode-hops can be explained as regions of discontinuity or jumps in the diode laser wavelength or frequency output as either the injection current or temperature of the diode laser is changed continuously. These occur as the laser diode switches from one longitudinal lasing mode to the next. Not all of the longitudinal modes are supported within the laser cavity but those with sufficient gain exist with only a single longitudinal mode, with the highest gain lasing at a time. This implies that the diode laser operates in a single mode when the cavity mode is on the peak of the gain curve. The cavity modes do not form a continuum but are equally spaced by approximately 0.228 nm^5 for a typical GaAlAs active layer.

The gain curve distribution of diode lasers is given by band to band transitions between the conduction and the valence band of the semiconducting material giving a broadband spectrum. The changes in temperature affect the band gap causing the gain curve to shift by about $+0.25 \text{ nm/K}$ for GaAlAs semiconducting material. The cavity modes shift by about $+0.06 \text{ nm/K}$ [17], therefore the gain curve and the longitudinal modes shift differently as the temperature changes.

Suppose that at a temperature T the longitudinal mode is at the peak of the gain curve the diode laser is said to be operating on a single mode, as shown in Figure 2.9. A drift to higher temperatures, say $T + \Delta T$, causes both the gain curve and the cavity modes to shift differently. As described in Section 2.8, as the temperature of the diode laser increases the gain curve shifts faster than the longitudinal modes and therefore the gain curve peak overtakes the once lasing mode approaching the next longitudinal mode. When the gain curve peak is between the cavity modes the diode laser switches to the next longitudinal mode, as shown in Figure 2.9. This is true as soon as the maximum of the gain curve reaches the next resonator mode, the gain for this mode becomes larger than that of the oscillating one and the laser frequency jumps to this mode. When this occurs it is referred to as mode-hopping. A further increase in temperature to about $T + 2\Delta T$, the next cavity mode, will be at the gain curve peak and the diode laser operates in a single mode.

It is possible that the diode laser can switch to another longitudinal mode by jumping two or more cavity modes thereby increasing the gap of mode-hopping. Mode-hopping does not occur at a definite temperature or current, making predictions difficult. Mode-hopping also depends on the

⁵The mathematical calculation of this value is given in Appendix A

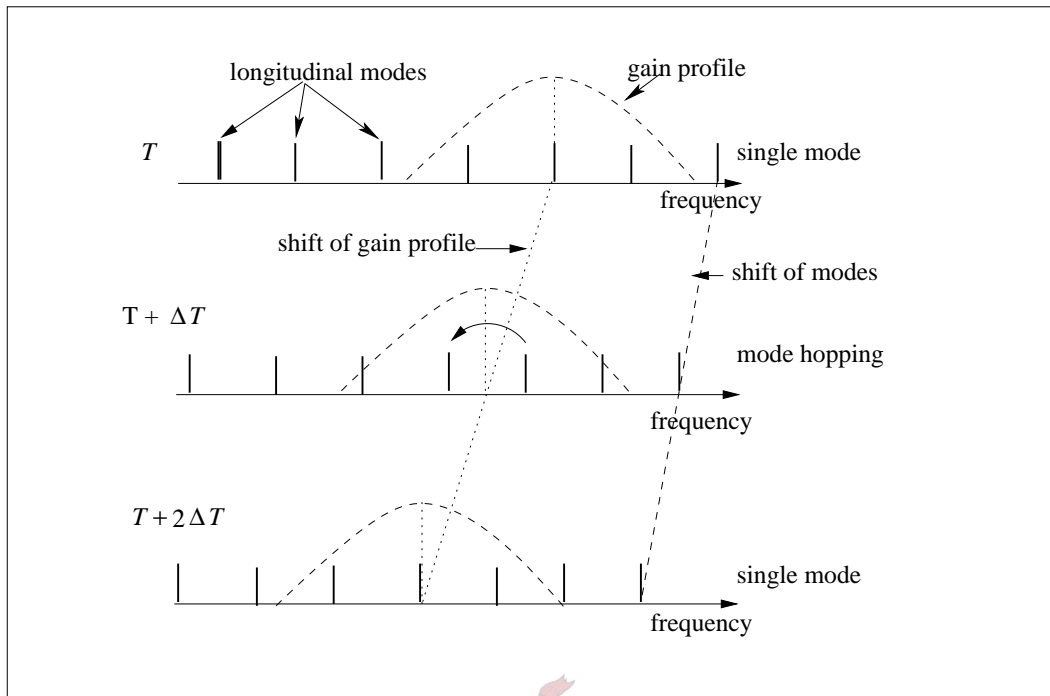


Figure 2.9: Schematic representation showing how the gain profile and longitudinal modes shift as the temperature changes.

ageing of the diode laser. Under some circumstances mode-hops can occur in an erratic manner, with the laser switching back and forth rapidly between wavelengths [21]. During mode-hopping the laser's output intensity fluctuates slightly, resulting in an increase in relative intensity noise [21]. Therefore the output wavelength from a diode laser does not tune continuously with temperature or current, it is subject to mode-hops as the laser diode switches from one longitudinal lasing mode to the next.

2.9 Theory of external cavity diode laser

The wavelength of a diode laser is tunable over a small fraction of the gain profile by either current or temperature variation [22]. Diode lasers do not always operate in a single longitudinal mode or at the appropriate wavelength of interest [23]. Continuous wavelength tuning can be obtained only in a limited spectral range due to mode-hops from one longitudinal mode to another. The mode-hops create gaps in the spectral tuning curve which are typically 0.3 nm wide [22], creating spectral features which are undesirable for experimental applications. Although diode lasers can

be used for many applications, for some applications, e.g. spectroscopy where linewidth is of major concern, they are unsuitable [22]. The linewidth is quite large due to the small resonator length, the low cavity finesse and gain dependent fluctuations of the refractive index [22].

Diode lasers are known to be highly susceptible to optical feedback induced by parasitic reflections from outside the laser cavity according to Lang and Kobayashi [24] in Genty et al. [25]. Under proper circumstances this undesirable effect can however also be used as an advantage [25]. The spectral properties of semiconductor lasers can be improved by using optical feedback in various external resonator configurations. The static, dynamic and spectral properties of the laser are affected by coupling a portion of the diode laser output back into the laser cavity in a controlled fashion [26]. The dynamic properties of diode lasers are significantly affected by external feedback, depending on the interference conditions between the laser field and the delayed field returning from the external cavity [1].

The purpose of the optical cavity is to increase the quality factor of the laser resonator, thereby narrowing the linewidth and stabilising the laser's output. It has been demonstrated that the optical feedback in an external cavity diode laser (ECDL) can reduce the laser linewidth to about 100 kHz [27], which is sufficient for spectroscopy applications. Furthermore, continuous mode-hop-free wavelength tuning over ranges as large as 40 nm have been achieved by Wandt et al. [22] based on the Littman-Metcalf configuration. Certain configurations were shown to reduce the multimode emission to a single longitudinal mode [1].

Common configurations of ECDL use a selective diffractive optical element such as a grating, which spatially separates the spectral components of the diode laser. The selected spectral wavelength is fed back to the diode laser cavity, forcing it to operate at the wavelength of the optical feedback [23]. The selected component of the optical feedback is amplified by extracting more gain from the diode laser active medium therefore the selected spectral component becomes the dominant mode. The diffracted longitudinal mode forces the diode to emit at this mode even if this mode is not close to the peak of the gain curve [28].

2.9.1 Three-mirror system

The ECDL can be modelled as a three-mirror system [19]. In conventional commercial diode laser the diode facets serve as two mirrors, the back reflector and the output coupler. The output coupler is partially reflective due to an antireflective coating and the transmitted beam serves as the output. The back reflector is highly reflective to ensure that almost all light is reflected back into the active medium for further amplification.

In the case of an ECDL the third optical element is placed a small distance, $L \approx 10$ mm, from the output facet thereby increasing the cavity length to about 10 – 20 mm. In this case the laser diode is represented by a short optical cavity (internal cavity $\approx 400 \mu\text{m}$) with plane mirrors M_1 and M_2 coupled to a much longer external cavity having a frequency selective and tunable end reflector M_3 , as shown in Figure 2.10.

The third optical element, M_3 , has a characteristic feature of returning part of the selected output back to the diode laser for further amplification and part is coupled out as diode laser output for diagnostic and experimental purposes. Therefore in the model the third optical element can be regarded as a mirror which transmits part of the diode laser output and reflects some of the output from the laser, as shown in Figure 2.10. The two mirrors M_1 and M_2 are d distance apart, M_2 and M_3 are L distance apart, where $L \gg d$.

If the diode laser front facet (M_2) is coated with a highly effective antireflection (AR) coating then the resonator treatment is the same as in conventional lasers with the rear facet of the diode laser and the diffractive element, M_3 , forming the cavity, and the threshold gain is given by equation 2.12 in Section 2.5. In the absence of a very good AR coating the ECDL is modelled as a three-mirror system as shown in Figure 2.10, where distances d and L play a crucial role in the phase accrual of feedback. The reflection from the external mirror M_3 can be treated by combining it with the reflection of the laser end facet M_2 , ending up with reflectance R_{2eff} , as shown in Figure 2.10.

By considering the reflected components at mirror M_3 , according to Ye [1], the threshold condition can be written as

$$\sqrt{R_1 R_{2eff}} e^{2(\Gamma g - \alpha_i)d} e^{-j(\phi + \phi_L)} = 1 \quad (2.32)$$

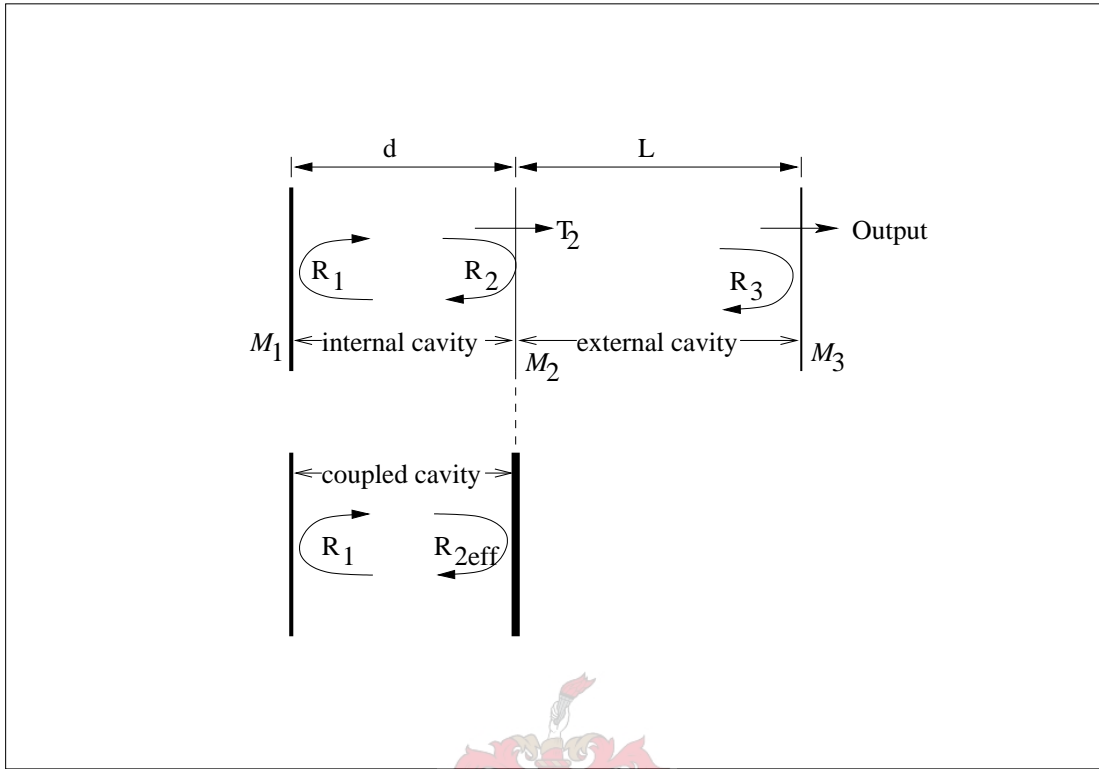


Figure 2.10: The three-mirror model of an external cavity diode laser with its effective cavity [1].

therefore

$$\Gamma g = \alpha_i + \frac{1}{2d} \ln \frac{1}{\sqrt{R_1 R_{2eff}}} \quad (2.33)$$

where Γ is the confinement factor, g is the threshold gain of the external cavity diode laser, $\phi_L = \omega\tau_L$, ω is the angular frequency of the diode laser, and τ_L is the round trip delay in the external cavity given by $\tau_L = 2L/c$, where c is the speed of light in a vacuum and α_i are losses in the internal cavity. Losses incurred in the external mirror are included in R_{2eff} .

The total phase accrual ϕ is given by

$$\phi = 2\pi q - \phi_L \quad (2.34)$$

where q is a positive integer and ϕ_L is the phase change due to the external cavity. In the absence of feedback $\phi = 2\pi q$. In the presence of feedback the mode of the three-mirror system must satisfy equation 2.34. Generally the phase condition has multiple solutions for a certain combination of the external cavity length L and the external reflection coefficient R_3 . If R_3 is less than some value, then $\phi(\lambda)$ will decrease monotonically and the laser will remain single mode regardless of the phase of the feedback [1]. For large feedback values, $\phi(\lambda)$ is no longer monotonically decreasing and the

laser will exhibit multiple external cavity modes for at least some range of feedback.

2.9.2 External cavity diode laser modes

Figure 2.8 shows the gain curve and the cavity modes for a diode laser. Compared to the gain spectrum of a diode laser shown in Figure 2.8 for an ECDL there is a third curve due to the optical feedback from the third optical element which forms part of the cavity. The spacings between cavity modes in an ECDL are smaller compared to a solitary diode laser since the cavity length is now large, $d + L$. In most common ECDL arrangements M_3 is usually a diffraction grating in which the first-order diffraction is the optical feedback and the zeroth-order diffraction is the output. The broad gain bandwidth of diode lasers allows another spectrum of feedback from the

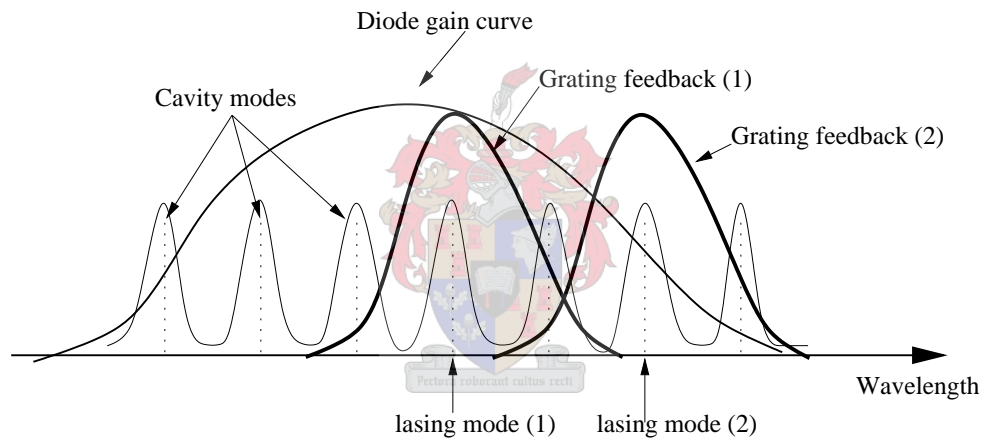


Figure 2.11: Schematic representation of the gain spectrum, feedback spectrum and longitudinal modes of an ECDL.

grating to exist within its gain spectrum. An ECDL usually operates at a single longitudinal mode when the lasing mode is exactly at the peak of the feedback spectrum. The feedback curve peak is not necessarily at the gain curve peak and can be shifted by adjusting the spectral response of M_3 . Lasing occurs at the feedback spectrum peak as illustrated by Figure 2.11. Mode-hops described in Section 2.8.1 can still occur in ECDL if the shift in feedback spectrum and cavity modes does not occur synchronously. The feedback spectrum is shifted by changing the angle of incidence, that is, by rotating the diffractive element M_3 as illustrated by two feedback curves in Figure 2.11. The cavity modes shift by changing the length L of the cavity, that is, by translation of the diffractive element, and as a result of the effect of temperature and current. The temperature and current can be kept constant and the rotation and translation can be done synchronously to avoid mode-hops.

A scenario where the longitudinal lasing mode close to the peak of the feedback spectrum is not necessarily the output of the ECDL can exist. In this case the lasing mode will be at the peak of the gain spectrum whilst the feedback strength is almost negligible. This is common when the optical feedback is not well coupled to the diode laser as a result of misalignment.

2.9.3 External cavity diode laser linewidth

One of the remarkable features of a stable ECDL is its linewidth. Compared to solitary diode lasers the linewidth of an external cavity diode laser is very narrow. This allows its application to high resolution spectroscopy. For a diode laser the cavity bandwidth is given by [1],

$$\Delta\nu_{\text{sd}} = \frac{\Delta\nu}{F} \quad (2.35)$$

where $\Delta\nu = c/2nd$ is the intermode spacing and F is the finesse of the cavity given by $F = \pi\sqrt{R}/(1-R)$, d is the cavity length and R is the effective reflectance of the cavity mirrors. τ_p is the photon lifetime in the cavity, n is the refractive index of the medium. In an external cavity diode laser the photon lifetime is longer due to loss-free propagation over a distance $L \gg nd$ [1]. The photon lifetime modifies the threshold gain, threshold carrier density and the threshold current of the laser [19]. The cavity bandwidth of ECDL is given by

$$\Delta\nu_{\text{ec}} = \frac{c}{2\pi(nd + L)} \quad (2.36)$$

Expressing the above in terms of the linewidth of a diode without feedback $\Delta\nu_{\text{sd}}$ for a given mode the linewidth of ECDL is given by

$$\Delta\nu_{\text{ec}} = \frac{\Delta\nu_{\text{sd}}}{(1 + \gamma)} \quad (2.37)$$

where $\gamma = L/nd$. Two conclusions can be drawn from equation 2.37:

- $\gamma \gg 1$ since $L \gg nd$ hence the linewidth of ECDL is less than that of a diode laser, and
- the fact that $L \gg nd$ implies that the refractive index effect on the resonant laser frequency is negligible for an external cavity laser whilst it contributes significantly to the linewidth of a diode laser.

The above expressions for linewidth are for an open cavity since gain of the medium is not taken into account. In the presence of gain the photon lifetime increases and the linewidth decreases. The α - parameter defined in Section 2.8 increases the linewidth of diode lasers [19].

2.9.4 Effects of antireflection (AR) coatings

The application of high quality AR coatings to a laser diode that should be incorporated in an ECDL is important. This allows the efficient operation of the ECDL as the external cavity dominates the internal cavity in controlling and determining the lasing longitudinal modes. The generated light in the diode laser cavity should be transmitted practically completely through the diode output coupler to the third optical element by applying effective AR coatings on its surface. Without effective AR coatings the non-wavelength specific optical feedback of the reflection from the front facet causes the free-running diode laser to lase. In the three-mirror model shown in Figure 2.10, the reflectivity of the mirrors can be represented as $M_2 \ll M_3$.

A diode laser with an output facet with AR coatings reflectivity estimated between 2% and 10% with the back facet high-reflection coating of approximately 97% reflectivity works well in an ECDL [6]. The internal cavity modes of the diode laser will therefore be strongly coupled to the external cavity. The quality of the AR coatings and the interaction of the laser diode with the optical feedback influences the physical properties of the ECDL.

One of the effects of AR coatings on laser diodes is the effect on the threshold current and quantum efficiency [29]. Below threshold the increase in injection current causes an increase in carrier density within the active layer. Above threshold the carrier density remains constant so that any further increase in injection current will cause an increase in the optical power. This effect is known as gain saturation. AR coatings cause a shift of threshold current to high current values [16]. This results in a larger carrier density at the threshold for AR coated laser diodes compared with uncoated laser diodes. This is described by the splitting of the Fermi level into quasi-Fermi levels⁶ that describe the distribution of electrons and holes. Higher values of the carrier density cause an increase of the energy splitting of the quasi-Fermi levels, which results in the violet shift of the spontaneous-emission spectrum of a laser diode [29]. ECDLs benefit from this effect, in particular the tuning range is enlarged at the low-wavelength side of the total tuning range in comparison

⁶Refer to the description of quasi-Fermi levels in Section 2.2

with a non-AR-coated diode laser.

AR coatings strongly enhance the mode-hop-free tuning range of laser diodes in an external cavity [29]. AR coatings also reduce the probability of multimode operation [16] of the ECDL. Multimode operation is practically eliminated by AR coatings having a reflectivity below 0.005%. A reflectivity range of 30% - 0.5% has a high probability of multimode operation in some parts of its tuning range. When incorporated in ECDL a diode laser with AR coatings on its front facet is more suitable. Diode lasers with front facet reflectivity of 0.05% and 0.005% are optimal for the Littrow and Littman-Metcalf cavities respectively [16]. With such reflectivities an excellent coupling of the laser diode output to the external cavity is guaranteed.

2.10 Basic ECDL configurations

In this section a discussion of the two most common ECDL configurations is presented, namely the Littrow and Littman-Metcalf geometries.



2.10.1 Littrow configuration

The Littrow configuration [30] is shown in Figure 2.12. The main components of the Littrow cavity are the diode laser chip, the lens and the diffraction grating. The diffraction grating is positioned a small distance away from the front facet of the diode laser with the lens positioned at the correct distance between the diode laser and the grating to provide a collimated beam. Light from the diode laser is incident on the diffraction grating which separates the spectral components of the laser diode output spatially. The first-order diffraction is reflected back into the diode laser as external optical feedback. The zeroth-order diffraction from the grating is coupled out as the output for use in experiments as shown in Figure 2.12. The output wavelength is tuned by rotating the grating and thereby changing the wavelength of the optical feedback. The cavity length is extended compared to a solitary diode laser and the length is from the back facet of the diode laser chip to the diffraction grating. In the Littrow cavity, for maximum performance of the ECDL, the diode laser with AR coatings on its front facet is used to reduce non-wavelength-selective optical feedback. The main advantages of the Littrow cavity are that:

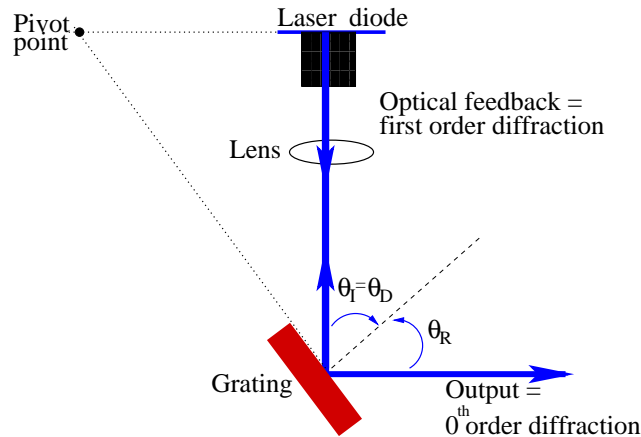


Figure 2.12: The Littrow ECDL configuration.

- it is simple and has a small cavity length,
- it has fewer optical elements than most of the configurations, making alignment easy, and
- it has high output power due to low losses in the cavity.

The main disadvantage of the Littrow cavity is that the output beam direction is wavelength dependent therefore the output beam steers as the grating is rotated in order to tune the output wavelength. This makes regular alignment of the beam necessary in experiments where wavelength tuning is required. In the Littrow cavity, the mode-hop-free tuning range is increased by synchronously rotating and translating the grating to ensure that the feedback curve shifts at the same rate as the longitudinal lasing mode. This is achieved by changing the grating angle θ and the cavity length L simultaneously. Therefore the following equation must be satisfied

$$\frac{d\lambda_{feedback}}{d\theta} \Delta\theta = \frac{d\lambda_{mode}}{dL} \Delta L = \frac{d\lambda_{mode}}{dL} \frac{dL}{d\theta} \Delta\theta \quad (2.38)$$

It is well documented by McNicholl and Metcalf [30] that synchronous tuning is possible when the rotation axis is at the intersection of the plane of back facet of the diode and the plane of the grating surface marked as pivot point in Figure 2.12.

Figure 2.13 shows a Littrow oscillator, where A denotes the axis of rotation. Using a mathematical proof from [30] it can be shown that synchronous tuning is possible in Littrow cavity. The cavity consists of a diode back facet and a grating at the Littrow angle Φ to the mirror. The feedback

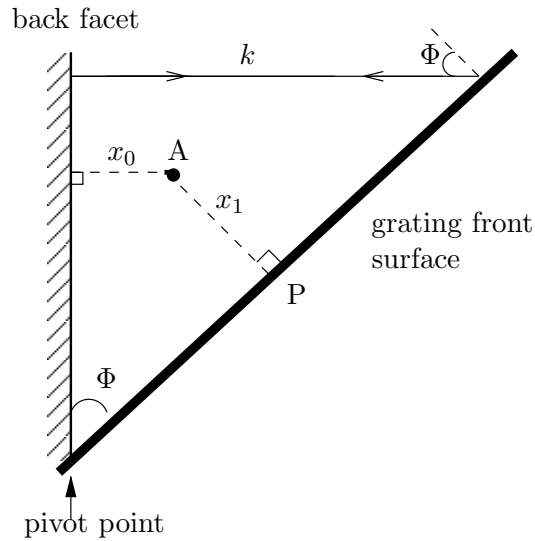


Figure 2.13: The general Littrow oscillator to prove that synchronous scanning is possible by rotating the back facet of the diode laser and grating at pivot point, P.

wavelength is related to the Littrow angle by

$$2 \sin \Phi = mg/k \quad (2.39)$$

where $k = 2\pi/\lambda$, $g = 2\pi/d$, and d is the grating spacing. The position of A is given by the perpendicular distances x_0 and x_1 to the mirror and grating surfaces respectively.

The round trip phase accrual φ is calculated by first propagating the wave front from the end mirror to the plane intersecting the grating at P and yields a phase factor

$$\exp[ik(x_0 + x_1 \cos \Phi)] \quad (2.40)$$

The effect of round trip on the wave front is represented as

$$G_m(P) \exp[2ik(x_0 + x_1 \cos \Phi)] \quad (2.41)$$

$G_m(P)$ is a diffraction factor off the grating back to the same plane P. The total phase is given by

$$\varphi = 2k(x_0 + x_1 \cos \Phi) \quad (2.42)$$

From equation 2.42, when the centre of rotation of the grating is chosen to be at the intersection of the mirror and the grating (at pivot), that is, $x_0 = x_1 = 0$, the round trip phase is independent of Φ hence independent of the feedback wavelength. Therefore synchronous tuning is possible at this point since the returned wave maintains a constant phase relative to the incident wave.

2.10.2 Littman-Metcalf configuration

The geometry of the Littman-Metcalf [31] is shown in Figure 2.14. In this geometry a mirror is added. The grating is usually positioned at a grazing incidence with the output from the diode laser. The first-order diffraction beam goes to the mirror, which then reflects it back to the grating [23]. At the grating the reflected component is diffracted again and the first-order diffraction is sent to the diode laser as optical feedback. The zeroth-order diffraction of the output from the diode laser serves as the output. The zeroth-order diffraction from the light returning from the mirror is lost.

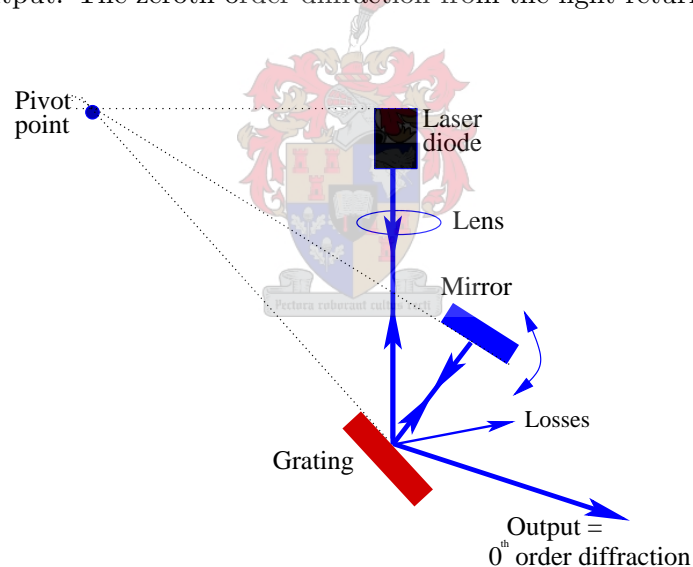


Figure 2.14: The Littman-Metcalf configuration.

The cavity length is from the diode laser chip to the mirror. Tuning of the Littman-Metcalf geometry is accomplished by mechanically varying the mirror angle instead of the grating angle, allowing the grating and thus the zeroth-order diffraction output beam to remain fixed as the wavelength is changed [32]. This configuration has more losses than the Littrow cavity since light passes twice at the diffraction grating where major losses are experienced and zeroth-order diffraction of light returning from mirror is lost. Therefore the output power is lower than a comparable Littrow

cavity.

The main advantage of this geometry over the Littrow cavity is that the beam direction remains unchanged when the mirror is rotated. The Littman-Metcalf geometry can be designed to increase the wavelength range in which continuous mode-hop-free tuning is possible. This is achieved when the feedback gain curve is tuned synchronously with the cavity modes. The shift in feedback gain curve corresponds to the rotation of the mirror and a change in cavity modes is the result of the translational movement of the mirror. The two rates are equal when the plane of back facet, plane of grating surface and plane of mirror intersect at a pivot which acts as the rotational axis, as shown in Figure 2.14.



Chapter 3

Experimental setup and methods

In this chapter the experimental setup and methods implemented in the design and development of the ECDL are discussed. Section 3.1 describes the preliminary study of the characterisation of a free-running commercial Hitachi HL7851G diode laser before incorporation in an ECDL. In Section 3.2 the mechanical design and development of the ECDL is presented. This section describes some of the design considerations and the general assembling of the mechanical components of the ECDL. The electronic system of the ECDL is discussed in Section 3.3. The circuits for the temperature controller, the current controller and the sidelock servo are presented and discussed, giving details of their functions. Finally, in Section 3.4 the experimental optimisation and characterisation of the ECDL are discussed.

3.1 Setup for the characterisation of a free-running diode laser

The setup used for the characterisation of the diode laser is shown in Figure 3.1. The diode laser is powered by a commercial ILX lightwave ultra low-noise current source (LDX -3620) which supplies maximum current of 500 mA. The diode laser is placed in an aluminium housing which is thermally controlled by an ILX lightwave temperature controller (LDT-5412). The temperature of the diode laser is controlled by a set of thermoelectric coolers placed close to the diode laser chip.

The output from the diode laser chip is collimated by a lens on an adjustable mount outside the housing. A Schlumberger monochromator fitted with a CCD array on its focal plane and an Ocean

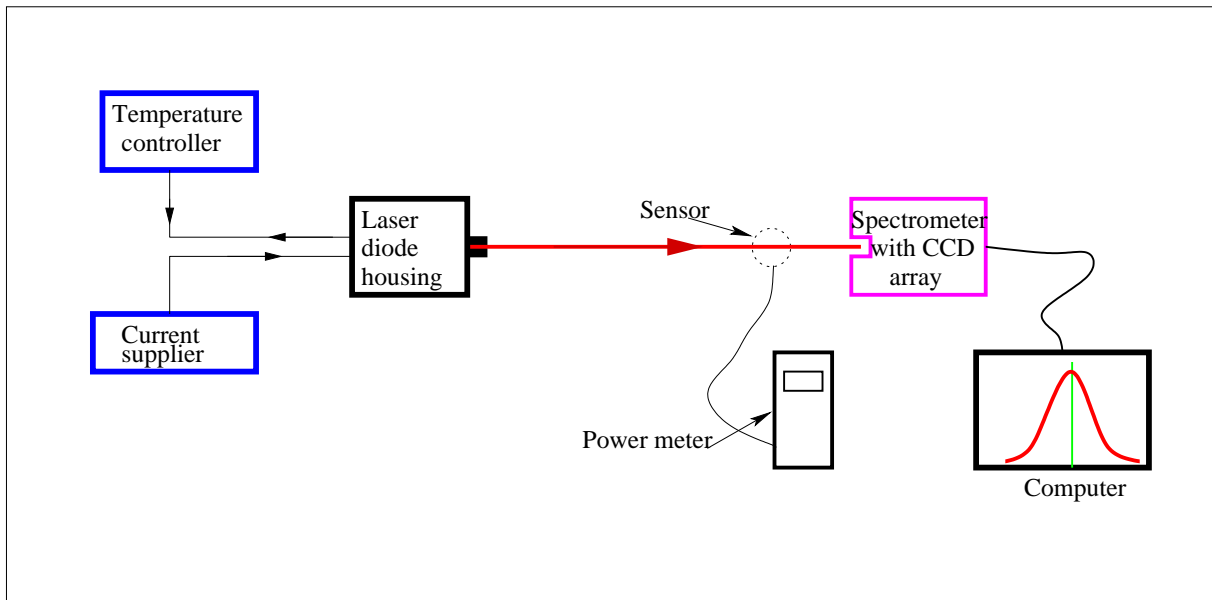


Figure 3.1: A schematic illustration of the experimental setup used for the characterisation of a free-running diode laser.

Optics readout to a computer is used to measure the intensity of the diode laser output versus its wavelength. The output power is measured using a power meter (Coherent MIL-STD-45662-A), where the sensor (LM-2 VIS) is placed between the diode laser and monochromator.

The turn-on characteristics (power versus current) at different temperatures were investigated. The injection current through the diode laser was varied at fixed temperatures while the power output was recorded. Experiments on the tuning characteristics, wavelength versus temperature at fixed currents and wavelength versus current at a fixed temperature were carried out.

3.2 Mechanical design and development of ECDL

The experimental design and development of the external cavity diode laser is organised in the following systematic way:

- Design considerations. This first part includes a discussion of the choice of configuration, either Littrow or Littman-Metcalf geometry, the choice of the grating and diode laser to be used in the ECDL, modifications, and construction of the auxiliary components.
- Assembling of the various components of the ECDL. These include a Peltier cooler (Melcor,

CP1.4-127-06L), thermistor (GE Infrastructure Sensing, DKF303N10S427 from RS components), grating (Thorlabs GH1318V), piezoelectric transducer (Thorlabs AE0203D08), collimation tube (Thorlabs L230P-B), collimation lens (Thorlabs C230TM) and the diode laser (Hitachi HL7851G).

3.2.1 Choice of geometry

In the laboratory the Littrow cavity was chosen and implemented rather than the Littman-Metcalf geometry because of its simplicity and high output powers.

3.2.2 Choice of grating and polarisation

Considerations in the choice of the grating included a target wavelength close to 780 nm, and to have a Littrow configuration with an angle of incidence of approximately 45° so that the reflected beam exits at a convenient angle of 90° to the incident beam, as shown in Figure 3.3. At an angle of incidence α to the grating normal, one obtains constructive interference for those directions β of the reflected light for which the path difference is an integer multiple m (the diffraction order) of the wavelength λ [33]. This gives the grating equation

$$d(\sin\alpha + \sin\beta) = m\lambda \quad (3.1)$$

In the Littrow configuration the diffracted beam is reflected back in the same path as the incident beam, therefore $\alpha = \beta$. In such an arrangement the grating equation 3.1 reduces to

$$2 d \sin\alpha = m\lambda \quad (3.2)$$

Maximum diffraction of light occurs in the first order ($m = 1$). For $\lambda \approx 780$ nm therefore

$$\begin{aligned} \frac{1}{d} &= \frac{2 \sin 45^\circ}{780 \times 10^{-6}} \text{ mm}^{-1} \\ &\approx 1800 \text{ grooves/mm} \end{aligned}$$

Therefore, a grating with 1800 lines per mm is suitable for this application. Among other factors, the grating efficiency depends on the polarisation of light incident on it. The diffraction efficiency into the first order is high if the light polarisation of the diode laser is oriented perpendicular to the grating rulings [34]. If the polarisation is parallel to the grating rulings then the grating is less efficient, less light is diffracted in the first order, and instead there will be more light output in the zeroth-order diffraction. The two different polarisation orientations will be investigated experimentally during the optimisation of the ECDL in order to find the most suitable one.

In order to reduce losses due to scattering of light at the grating-light interface a holographic grating is highly preferred. Holographic gratings are free from “grating ghosts”, which are unwanted maxima, which occur for a given angle of incidence α into wrong directions β , caused by minute deviations of the distance d between adjacent grooves as a consequence of inaccuracies during the ruling process. A holographic grating (6 mm x 12.7 mm x 12.7 mm), distributed by Thorlabs (GH13-18V), was used. The grating surface (12.7 mm x 12.7 mm) will allow sufficient angle tuning without clipping the beam at the edges of the grating.

Characterisation of the grating



The grating was characterised before being incorporated in the ECDL, using a free-running diode laser. The wavelength of the free-running diode laser was set at 780 nm by adjusting the injection current and the temperature of the diode laser. Visual alignment was done to ensure that the output falls on the centre of the grating surface. The grating was positioned on a rotation stage in such a way that the angle of incidence of the beam to the grating normal is known and can be easily changed.

The power of the incident beam was measured, and kept constant throughout the experiment by fixing the injection current and temperature. The power of the first-order diffraction and the zeroth-order diffraction were measured at each angle of incidence. The grating was rotated to change the angle of incidence. The experiment was repeated for both the vertical and horizontal orientation of the dominant polarisation of the incident beam. To select a certain orientation the diode laser was rotated in order to have the dominant polarisation, which is parallel to the main axis of the elliptical beam profile, oriented horizontally or vertically. The laser beam consists of 99% of the dominant polarisation when tested with a linear polariser.

3.2.3 Choice of diode laser

The diode laser, Hitachi HL7851G, has a maximum power output of 50 mW and operates on a single mode with continuous wave (CW) output at a central wavelength of 785 nm at room temperature. The typical operating current is 140 mA, a threshold current of 45 mA and a typical slope efficiency of 55 mW/mA. The operating temperature ranges from $-10\text{ }^{\circ}\text{C}$ to $+60\text{ }^{\circ}\text{C}$ according to the specification sheet [35]. These specifications were chosen based on the work of Wieman et al., [5] and [17], where a tunable narrow bandwidth, CW diode laser which produce at least 5 mW of power, is suitable for atomic physics experiments such as laser cooling and atomic spectroscopy. The maximum output power of 50 mW will allow considerable power losses when incorporated in ECDL but still provide sufficient power for laser cooling and spectroscopy applications.

The wavelength is tuned to the desired wavelength of 780 nm by decreasing the temperature, which causes a blue shift in wavelength. Cooling is done to just below room temperature, while above dew-point temperatures to avoid the formation of water droplets on the diode laser setup as a result of condensation. Cooling is advantageous over heating as the latter decreases the efficiency of the diode laser. Periodic subjection of diode lasers to high temperatures can cause microcracks of the semiconductor material forming the active medium, and this decreases the lifetime of the device [36]. According to Wieman and Hollberg [17], for fixed injection current, the laser's output increases rapidly as the temperature is lowered. The AR coatings of the front facet of the diode laser used in this study is not specified by the manufacturer but it is believed to be not more than a few percent, approximately 3%. According to the specification sheet [35] the beam divergence of the diode laser is 9.5° parallel and 23° perpendicular to the active layer. The diode laser polarisation is dominant in the TM mode.

3.2.4 Beam collimation

The diode laser beam spatial extent is divergent in the far-field as described in Section 2.7. This suggests that the output cannot be used for any experimental work without proper collimation. Figure 3.2 shows how the diode laser and the collimation lens with $f = 4.5\text{ mm}$ are mounted together in a collimation tube which is about 19 mm long. The centre of the lens is approximately 4.3 mm from the front facet of the diode laser. The lens can be adjusted back or forward by about 0.41 mm

by means of a fine screw to achieve collimation of the beam. The adjustable retaining ring is used to mechanically anchor the diode laser inside the collimation tube. The rigid mechanical mount of the lens close to the diode laser is important. The reason is that there is always optical feedback from the reflections from lens, and if this optical feedback changes due to mechanical movement of the lens relative to the diode laser it will affect the output power and frequency of diode laser. The collimation lens was adjusted back and forth while observing the output in the far-field. The

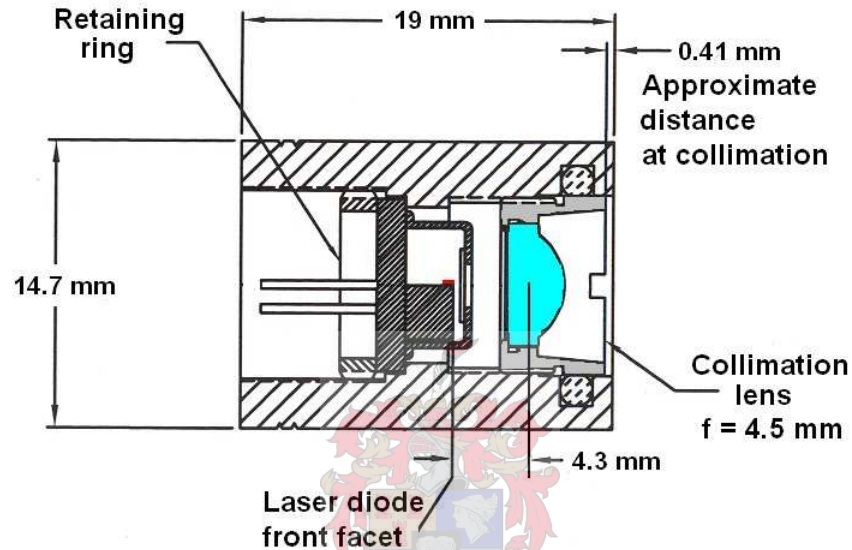


Figure 3.2: A sketch diagram showing how the diode laser and collimation lens are mounted together in a collimation tube to provide a collimated beam [37].

various beam shapes were monitored at each adjustment of the lens. The output was collimated for a distance of approximately two metres, providing a relatively good beam quality. The shorter and longer diagonals of the elliptical output were approximately 1 mm and 2.5 mm respectively around an injection current of 100 mA.

The collimation tube as illustrated in Figure 3.2 was housed in an aluminium holder whose dimensions are 6.5 mm x 19 mm x 48 mm, in a circular hole with diameter 14 mm at its centre. To ensure mechanical stability, the holder is screwed to the base plate using plastic screws, by clamping the Peltier cooler between the holder and the base plate. The plastic collimation tube is the most severe barrier in the thermal conductance between the diode laser and the aluminium housing.

3.2.5 Grating and piezo mount

The grating is anchored on an adjustable mount as shown in Figure 3.3. The mount is designed in such a way that:

- the grating is tilted around a horizontal axis
- the grating is rotated around the correct pivot point to maximise mode-hop-free tuning range
- the grating is mechanically stable as far as possible with respect to vibrations, and
- the grating holder assembly has a minimal mass to maximise the mechanical resonance frequency, which limits the frequency at which the sidelock servo system controls the piezo.

The grating and piezo holder consists of three adjustable screws, two of the screws allow manual rough translational and angle tuning of the grating while one can be fixed and act as a pivot point around which the grating is rotated, as shown in Figure 3.3. A piezo is inserted under the grating in a hole (2 mm x 3 mm x 10 mm) on the grating arm bar (see Figure 3.3). The piezo changes electrical signals to mechanical movement by expanding when a voltage is applied across it. The expansion changes the position of grating in rotation and translation thereby electrically fine tuning the grating. The piezo is directly on top of a screwball and covered with a small metal brass cover. This will ensure that the piezo is always under pressure from the screw held by the spring, and as a result the piezo will be stable and expand homogeneously. The holder is rigidly fixed to the base plate using slots at both ends. Unscrewing the slots will allow the movement of the holder back and forth in order to change the external cavity length and to position the grating relative to the diode laser output.

To ensure that the piezo's load will not exceed the recommended value, the force exerted onto the piezo by the springs holding the screws was investigated. According to the specification sheet of the piezo the recommended preload should be less than 100 N. The spring constant (k) was measured and using Hooke's law, $F = -kx$, the spring constant of each was found to be 2100 N/m. A rough estimate of the spring extension was done by adjusting the holder screws halfway. The extension was used to calculate the force exerted by the two springs as

$$F_s = 2 kx \approx 21 \text{ N}$$

If the force is evenly distributed on the three screws then one supporting screw carries $1/3F_s$, which is 7 N. This value is less than the recommended maximum preload of 100 N, therefore the piezo will not break.

The piezo's specified mechanical resonance frequency is 138×10^3 Hz without any extra mass attached to it. The mass (m) of the holder's arm driven by the piezo was measured, since this contributes to the mechanical resonance of the system. Using the formula

$$\nu = \frac{1}{2\pi} \sqrt{\frac{k}{m}}$$

where ν is the frequency. Using the value of $k = 2100$ N/m and the mass $m = 22,28$ g, the value of the resonance frequency was found to be lower than the specified value. In order to maximise the frequency the arm with a lower mass is preferred and an aluminium metal with an approximate mass of 10 g was used.

3.2.6 Assembly

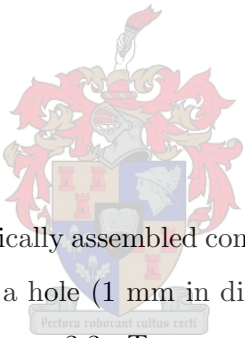


Figure 3.4 shows the top view of mechanically assembled components of the ECDL on the aluminium base plate. A thermistor is inserted in a hole (1 mm in diameter) on the collimation holder close to the laser diode chip, as shown in Figure 3.3. To ensure good thermal contact at the interface of thermistor and holder, thermal paste is applied between the interfaces. The diode holder is clamped on top of a Peltier cooler whose surface is larger than the base of the diode holder and thermal paste was applied on its interfaces. The diode holder is positioned in such a way that the output from the diode laser hits the centre of the grating.

The geometry is arranged such that a line from the back facet of the diode meets a line from the surface of the grating at the pivot point represented by screw A. The grating and piezo holder are fixed in such a way that the three adjustable screws (A,B and C) shown in Figure 3.4 are easily accessible from one side of the housing using Allan keys. Screws B and C are used in rough tuning of the grating during alignment. Screw B is used for horizontal translation of the grating and screw C allows the vertical tilting of the grating. The slots on the holder shown in Figure 3.4 are used to fix the holder to the base plate and also allow the holder to be moved back and forth, in order to have a maximum cavity length of approximately 30 mm. The output from the ECDL is obtained

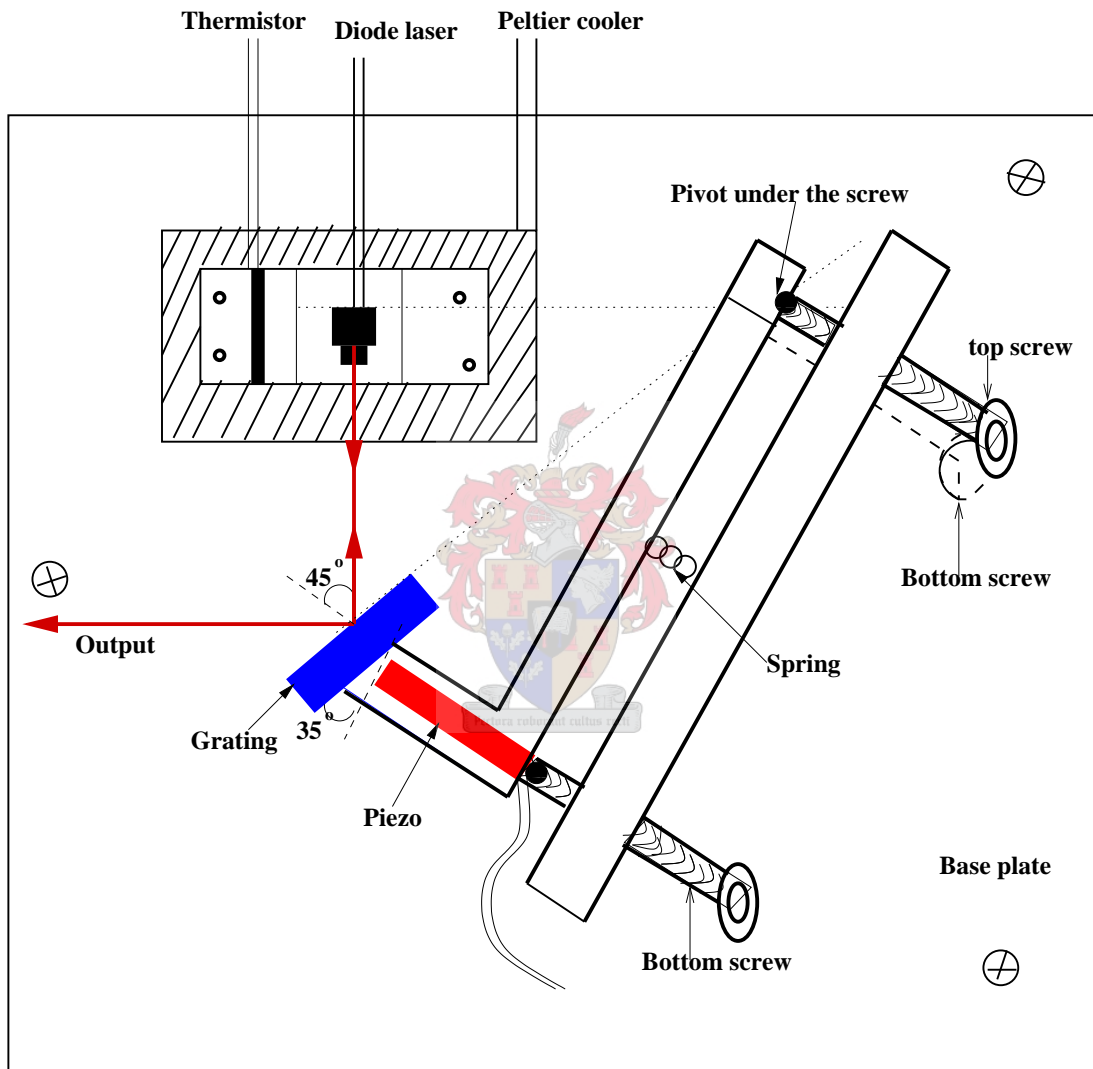


Figure 3.3: Schematic representation showing how the mechanical components of the ECDL were assembled in a Littrow cavity. The diagram is not to scale.

from one side indicated by an arrow showing the output from grating in Figures 3.3 and 3.4.

3.2.7 Base plate and enclosure

The base plate is made of aluminium, with a thickness of about 25 mm and a base surface of 135 mm x 150 mm. Both the collimation tube holder and the grating holder are firmly fixed to the base plate using the tapped holes. Besides mechanical anchoring of the system the base plate is the heat sink to ensure thermal stability of the system. Heat is extracted from the diode holder by a Peltier cooler and is dissipated into the large sink baseplate. The baseplate used has a fairly large thermal mass. In order to ensure that the laser is as stable as the optical table, the base plate is anchored on the table by three aluminium bars (diameter 36 mm), and height 125 mm from the optical table. The three aluminium bars will raise the diode laser to a workable height making it easier to align the spectrometer and other optical elements.

Without enclosure the ECDL is prone to air currents which cause rapid thermal drifts. The grating should be protected from dust falling on to it, therefore the geometry was housed using aluminium plates. The rectangular aluminium plates (1 mm thick) were screwed to the base plate. One side of the housing is made of perspex to isolate the electrical connections. A transparent removable perspex lid was placed on top of the ECDL to easily monitor the laser output and the position of the grating inside the housing during operation and to allow frequent access to the diode laser and the grating with minimum disruption. Frequent access is necessary during alignment and collimation of the laser beam. Moisture absorbers can be placed inside the housing to prevent formation of water droplets as a result of condensation during the cooling process.

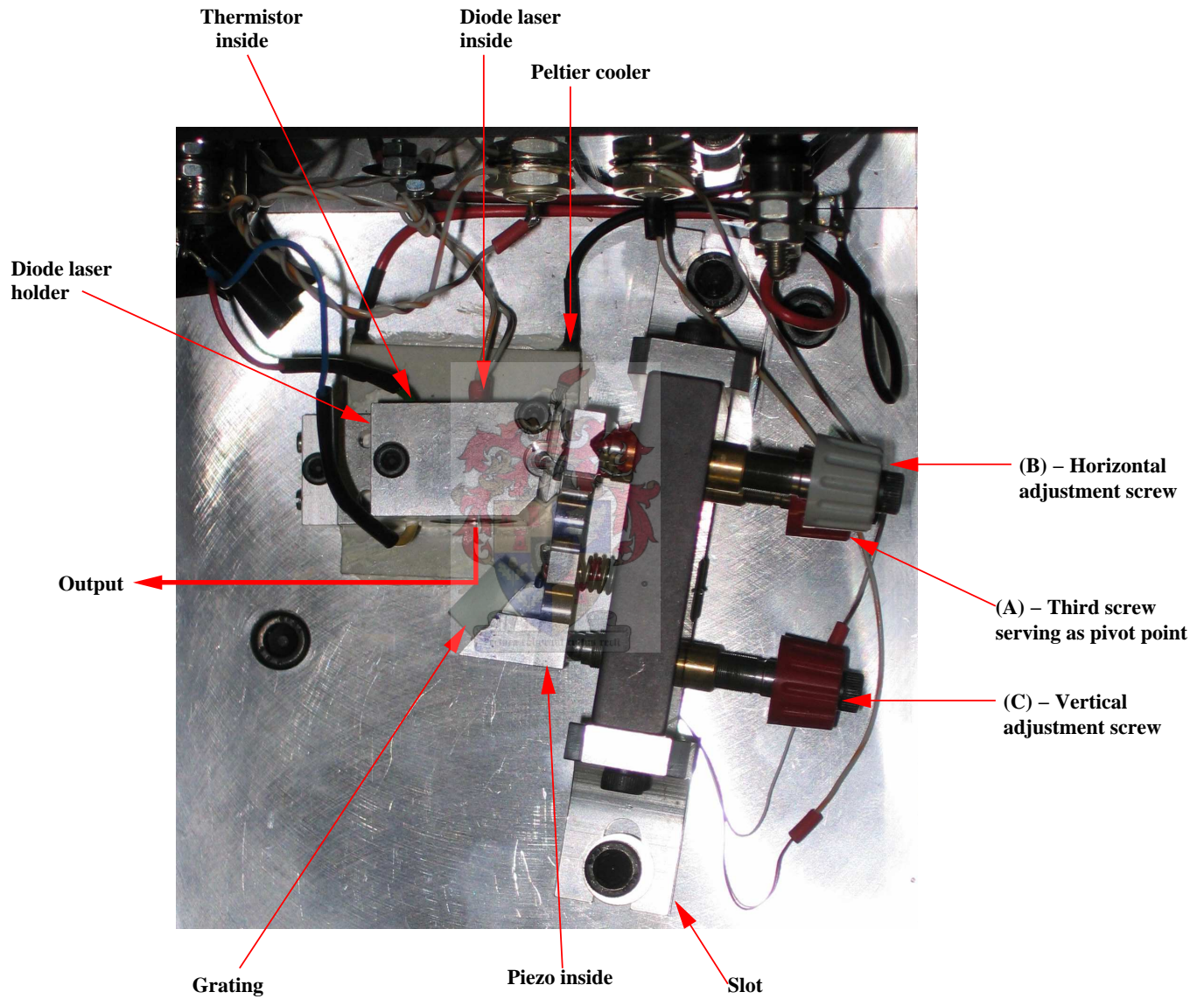


Figure 3.4: A photograph showing the top view of the mechanical setup of the ECDL developed.

3.3 Electronic system of the ECDL

The following electronic systems are required for the operation of the ECDL. These systems were developed from basic components using layouts based on designs originating from the electronics workshop of JILA, University of Colorado, USA.

- (i) A low noise current source to drive the diode laser.
- (ii) A protection circuit to protect the diode laser from any voltage spikes and reverse current.
- (iii) The temperature controller to stabilise temperature in the desired region of 14 - 25 °C.
- (iv) A servo circuit used to lock the frequency of the laser by controlling the piezo and the injection current through the diode laser.

3.3.1 Diode laser current source

Figure 3.5 shows a circuit diagram [38] for the diode laser current source or controller. The current controller should be a stable low-noise current source [3]. The main component of the current controller shown on the circuit diagram is the transistor Q10 (2N6660) since it acts as the current source for the laser diode. The laser diode is connected across J2 and draws current from the drain (D) of the transistor Q10. The circuit branch connected to the gate (G) of Q10 offers a drive voltage which sets a voltage (V_{ref}) at the gate. The voltage is derived from a precision voltage source U20 LM399H clamped at 6.95 V by a diode. The variable resistor R23 is used to adjust the reference voltage and therefore to adjust the current to the diode laser coarsely. A combination of resistors, capacitors and amplifier U10 (AD797AN) in this circuit reduce electrical noise in the gate signal and provide the correct voltage at the gate of Q10. To reduce electrical noise in the power supplied to each amplifier, a 100 nF capacitor is connected to each amplifier.

The circuit connected to the source (S) of Q10 consists of a feedback loop and a source loop. The feedback loop consists of a branch with resistor R14 and capacitor C11. The source (S) reads the output of the transistor and adjusts the output through the feedback loop so that the output remains constant. Resistor R16 sets the maximum current through the laser diode. The circuit connected to a branch with resistor R16 and transistor Q30 (TIP127) stabilise the ground. Inductors L10

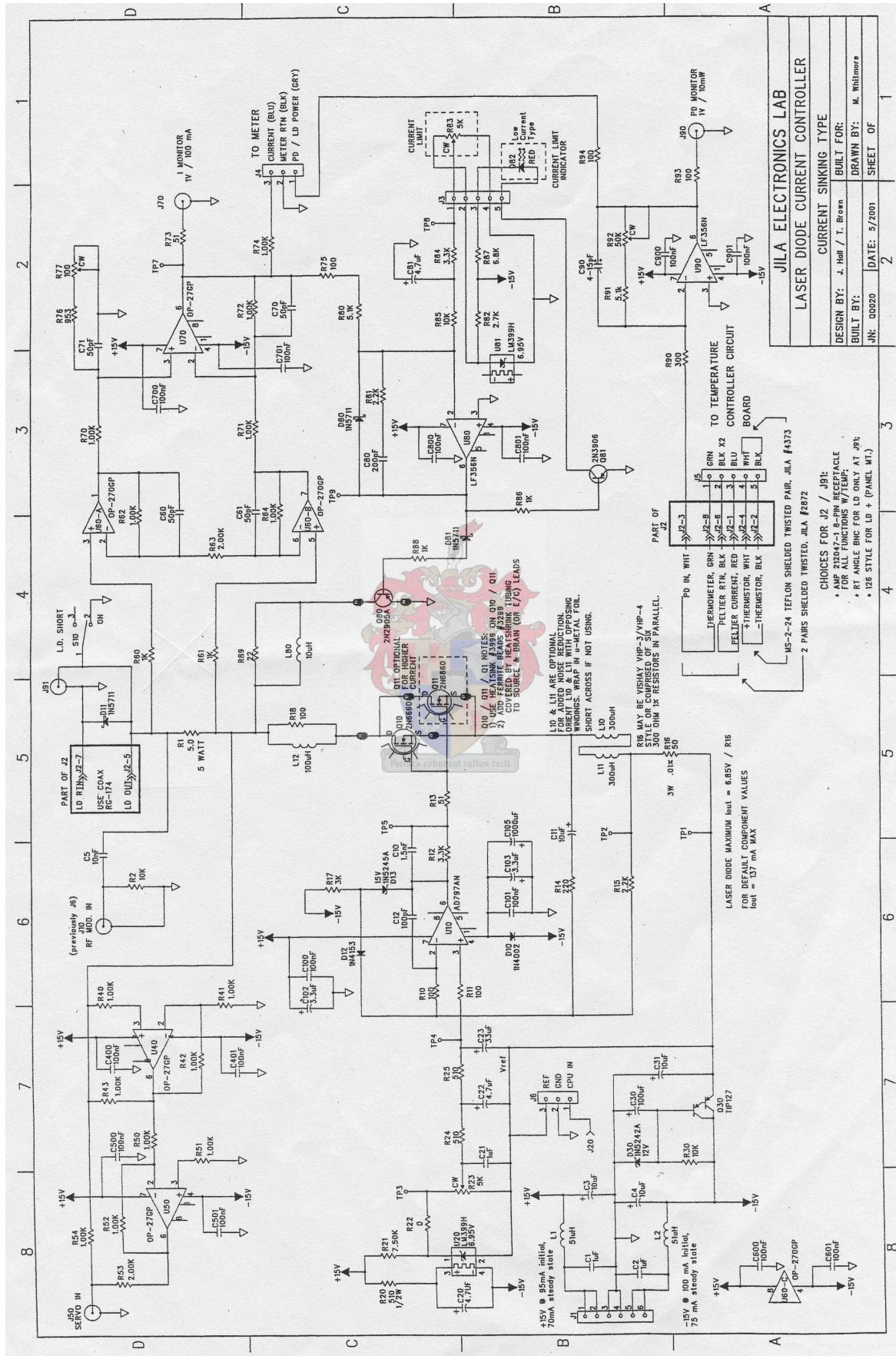


Figure 3.5: A circuit diagram for the current source used to drive the Hitachi HL7851G diode laser [38]. Circuit reproduced with permission.

and L11 are included for noise reduction in the feedback signal to the gate of Q10. Q11 (2N660) is an optional transistor that is used when high currents through the diode laser are required. The signal coming out through the drain (D) of the transistor Q10 is further processed by inductor L12 and resistor R18 which is a low-pass filter. The inductive low-pass filter, filters out the AC ripples created when an AC signal is converted to DC. Only pure DC component will pass through to the diode laser. Resistor R1 protects the diode laser from transient spikes in the current signal.

The circuit branch with resistors R60 and R61 across R1 measures the voltage across R1 through the difference amplifier U70 (OP-27GP) in order to measure the current through the diode laser at the port marked J70. Amplifiers U60-A(OP-270GP) and U60-B (OP-270GP) isolate the output signal from input signal and the gain of each amplifier is controlled by one resistor R63 to increase accuracy of measurement. The circuit branch with transistor Q80 (2N2905A) works the same way as that of transistor Q10 but it is a low current source and is used for fine tuning the current through the diode laser while that of Q10 is for rough current tuning. The current limit of the diode laser is set through the circuit branch with transistor Q80 using a variable resistor R83. J50 is a port that receives signals from the servo circuit in order to change the current through the diode laser. The signals pass through buffers U40 (OP-27GP) and U50 (OP-27GP), and then passes through resistor R1, which perform the function of smoothing the signals from transient spikes.

In order to change the wavelength of the diode laser output rapidly, the current source output can be modulated by sending a ramp signal from a signal generator through port J10. Since the current source is not a commercial one the first step is to test it using a resistor in place of the diode laser or light-emitting diode. A $50\ \Omega$ resistor was used in place of the diode laser. The primary concern is to avoid damaging the diode laser with unwanted current or voltage spikes. A calibration of the current supplier was done to check whether the exact current passing through the laser is the same as displayed on the digital panel meter. A check was also done to see whether there are no significant transients when turning the diode laser on or off. To avoid accidental damage when switching off the diode laser the current is first lowered to zero. Switching off the laser while it is operating can easily damage the diode laser due to the sudden change in voltage.

3.3.2 Laser diode protection circuit

A laser diode is very sensitive to static charges, sparks, and a sudden change in voltage or current, which can permanently destroy the laser diode or decrease its lifetime. Therefore careful handling and protection circuits against electrical surges are required. A protection circuit is connected across the laser pins between the current supplier and laser diode as close as possible to the laser diode. Figure 3.6 shows the protection circuit used. This protects the laser diode against voltage spikes which may exceed the 2.7 V forward and 2 V back bias that the diode laser can tolerate.

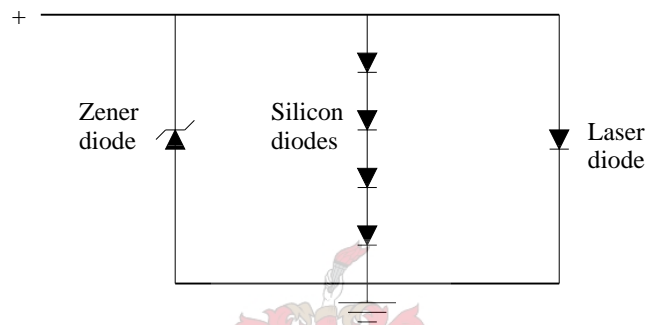


Figure 3.6: The protection circuit used for the diode laser.

The protection circuit consists of four silicon diodes which are connected in series across the laser diode, as shown in Figure 3.6. The silicon diodes with a total switch on voltage of 2.4 V are connected across the laser diode. A Zener diode with a reverse breakdown zener voltage of 2.7 V is connected across the silicon diodes and the laser diode. The Zener diode has similar conduction properties for forward voltage as the laser diode. It is connected to conduct in the reverse direction.

From the specification sheet [35], the laser diode conducts from a minimum of 2.3 V to a maximum of 2.7 V and an absolute maximum reverse voltage of 2 V is specified. Under normal operation the turn-on voltage of the laser diode is lower than that of the four silicon diodes and the Zener breakdown voltage so the current passes through the laser diode. In the presence of a voltage spike greater than 2.4 V the silicon diodes switch on, allowing current to flow through them to earth instead of passing through the laser diode, and the voltage difference remains 2.4 V. The laser diode will only see the clamped 2.4 V by the diodes and conduct normally. The Zener diode will allow reverse current to pass through it if there is a reverse connection at the source by accident, or if there is a spike on the earth, and limits the reverse voltage to 2 V.

3.3.3 Temperature controller

Any thermal drift in the operation of the ECDL has drastic effects on the diode laser output power and wavelength, as described in Section 2.8. Active temperature regulation to stabilise the temperature for long periods is required for the efficient operation of the ECDL.

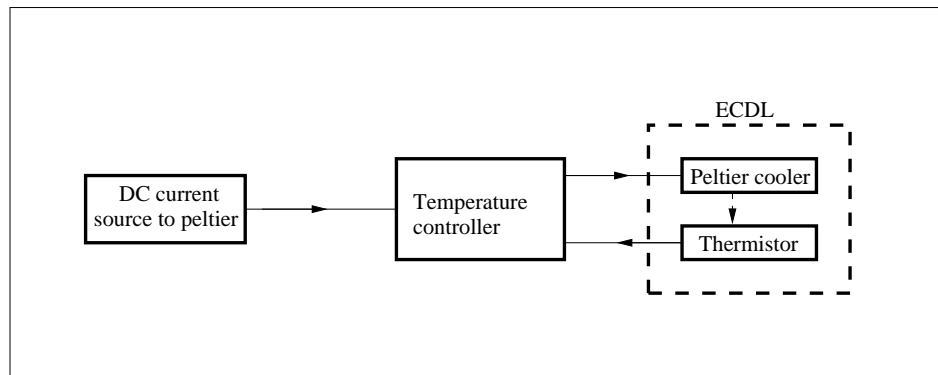


Figure 3.7: A schematic illustration of the complete temperature regulating system of the ECDL.

The complete temperature controller system is illustrated in Figure 3.7. The system consists of a Peltier cooler, a thermistor and a DC current source (DF1731SB), all connected to the temperature controller. The Peltier cooler and the thermistor are part of the ECDL. The temperature controller performs a central role of regulating the current through the Peltier cooler from a DC current source, depending on the temperature of the ECDL of which the thermistor voltage provides a measure. The current drawn by the Peltier cooler from a current source drives a transfer of heat by the Peltier cooler from one junction (diode laser holder) to the heat sink (aluminium base plate) thereby cooling the diode laser. Due to the low thermal load of the ECDL a current of about 1.5 A, which is much lower than the rated value of 6 A for the Peltier, was sufficient to cool and maintain the system at stable temperatures. The circuit diagram [39] of the temperature controller built for the ECDL is shown in Figure 3.8. The circuit was not adopted as it is; some components on the design circuit were omitted to provide a simple, cost-effective, but reliable source of temperature control. The components that were omitted are shown by crosses on the circuit diagram in Figure 3.8. A summary of the major components omitted is given below:

- Resistor R21 which fixes the temperature was removed and the coarse temperature control was enabled using the rotary switch in order to vary the set temperature.

- No active heating is required for the ECDL system since the diode laser is operated below room temperature, therefore the heater was removed. The Darlington transistor Q1 (TIP127) to the heater was removed. The emitter of the Darlington transistor Q2 (TIP122) was connected to the ground.
- The temperature sensor circuit to display the temperature of the ECDL was not necessary and therefore it was removed.

Some parts or components useful to describe the circuit are summarised below

- The thermistor is connected across J5 in a bridge circuit where the thermistor voltage proportional to the temperature in the ECDL is compared with a set voltage by amplifier U3-D (AD704JN).
- The set voltage is adjusted manually using the coarse temperature adjustment knob on a rotary switch marked on the circuit diagram. A rotary switch has resistors that allow coarse set temperatures from 2 °C up to 35 °C, with step temperature increment of 3 °C.
- An error signal is generated by comparing the thermistor voltage and the reference voltage. The error signal is brought to zero by proportional-integral-derivative (PID) controller ⁷, by controlling the current through the Peltier cooler. When the Peltier cooler is active, its cooling directly affects the voltage of the thermistor shown by the dashed arrow in Figure 3.7.
- The current to the Peltier cooler is controlled by the circuit after the point marked VLF on the circuit diagram with resistors R7, R8, ..., amplifiers U3-B (AD704JN) and U4-A (AD706JN), capacitors and a Darlington transistor Q2 (TIP122). V_2 is the DC current source to the Peltier.

PID system of the temperature controller

The temperature controller works on the principles of PID system. Figure 3.9 is a diagrammatic illustration of how the voltage equivalent of the set temperature is compared with the thermistor

⁷A full description of the PID system is given in Appendix C

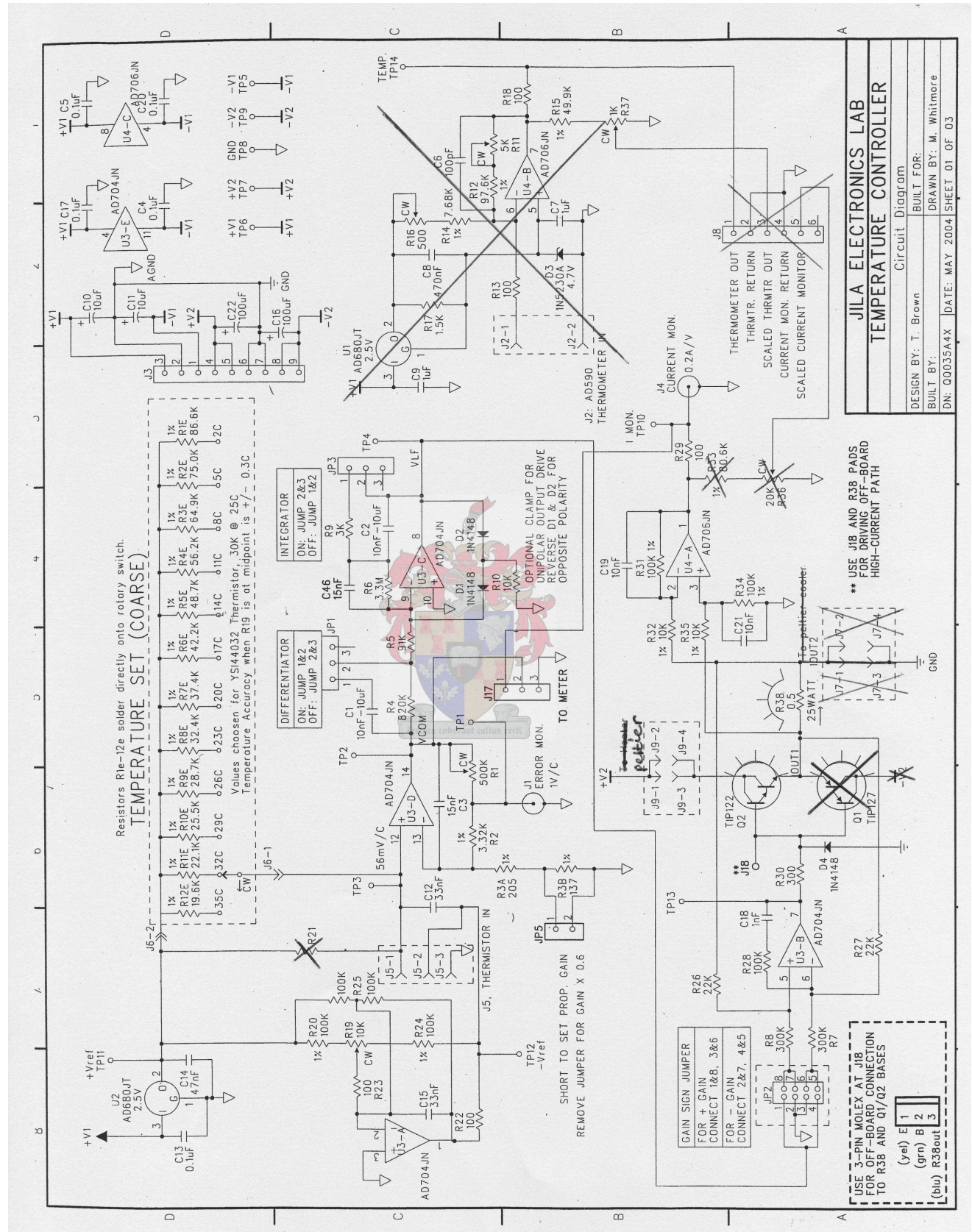


Figure 3.8: The circuit diagram of a temperature circuit used for temperature regulation of the ECDL system [39]. *Circuit reproduced with permission.*

voltage to produce an error signal (E). The error signal is modified by the electronics which provide gain and some compensation (PID controller) and the result is feedback, which drives current through the Peltier to alter the thermistor value towards the desired set temperature of the ECDL. This feedback is negative, and with this feedback the error signal decreases to a value of $E_f = E/\text{gain}$ in the limit of $\text{gain} \gg 1$ [41], where E_f is the error with feedback. The gain should be large in order to push the error signal as close to zero as possible, which is equivalent of forcing the thermistor voltage to be close to reference voltage, that is, $V_c \equiv V_t$. The gain is regulated by the proportional part of the PID controller, whose gain is given by

$$\text{Gain} = 1 + \frac{R_F}{R_A} \quad (3.3)$$

where $R_F = R1 + R2$ and $R_A = R3A + R3B$. The gain is adjusted by changing R1 since the other resistors are fixed in order to obtain stable operation as discussed in Appendix C.

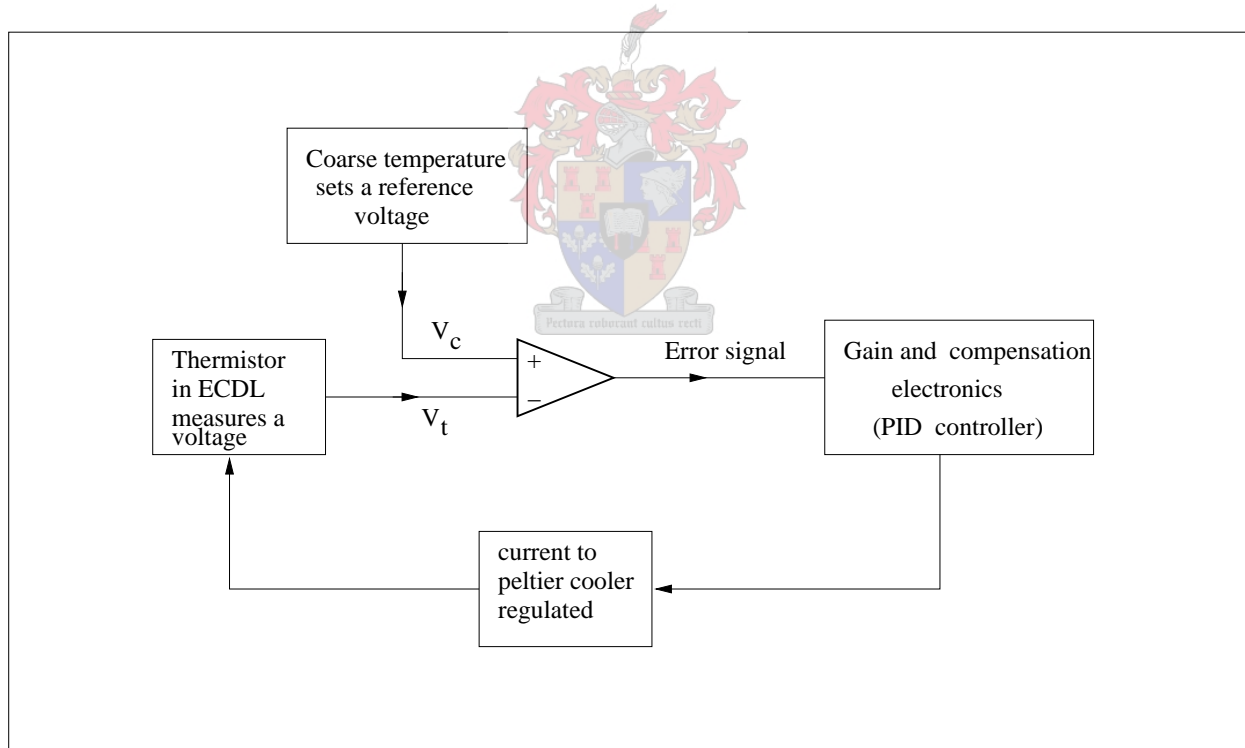


Figure 3.9: An illustration of how temperature is regulated using a PID system, thermistor and Peltier cooler.

Temperature stabilisation

The gain of the PID system was optimised by setting the time constants of the differentiator and the integrator. The time constants were set by determining the appropriate values of the capacitors C_1 and C_2 in the range 10 nF - 10 μ F as indicated in Figure 3.8. The experimental setup to optimise the system is shown in Figure 3.10. The optimisation was carried out in the absence of a working laser since the laser has little effect on the thermal dynamics of the setup. The temperature of the temperature controller box was set at 17 °C. The error and current signals were monitored on a Tektronix oscilloscope (TDS1012).

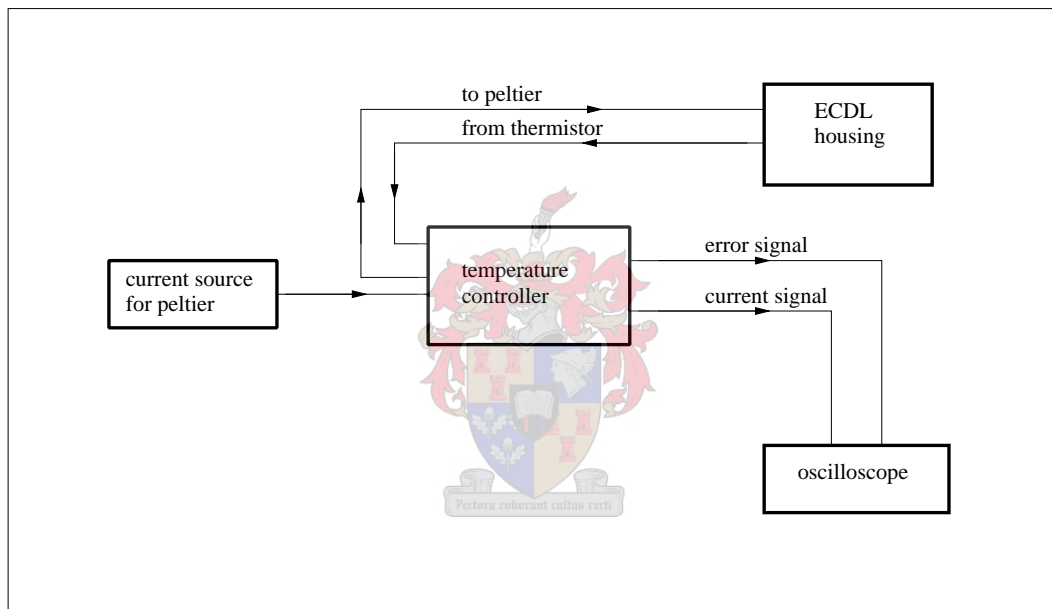
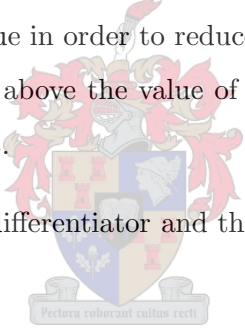


Figure 3.10: A schematic arrangement of the setup used to optimise the temperature controller.

- Resistors R26 and R27 were each replaced by a 220 k Ω resistor to allow more current through the Peltier cooler. This ensures that the Peltier cooler is working efficiently. A current of 1.5 A through the Peltier cooler was sufficient to offer good thermal damping of the setup due to the low thermal load of the ECDL.
- The resistor R3B was replaced by a large 47 k Ω resistor to decrease the gain of the proportional part of the PID controller.

The Ziegler-Nichols tuning procedure [42], for optimisation of the gain and setting of the time constant of the PID, was carried out as follows.

- The resistor R1 on the temperature control circuit board was set to zero to minimise the gain of the proportional part: counterclockwise - smaller value and clockwise - larger value.
- The differentiator and integrator were turned off by jumping 2 and 3, and by jumping 1 and 2, respectively.
- The gain of the system was increased by increasing the value of R1 until the error signal showed stable oscillations on the oscilloscope.
- The value of R1 at which stable oscillations appeared was measured across TP1 and TP2 on the circuit board. The period τ of the oscillations was recorded.
- The value of R1 at which stable oscillations appear shows that the gain has been set to maximum, as evidenced by undamped oscillations. Operating the system at this value of R1 will easily cause overshoots or ringing. As a rule of thumb the gain is reduced by setting the new value of R1 to 60% of its value in order to reduce the proportional gain by 40%. Due to change of resistor R3B described above the value of R1 was set to 70% of its original value in order to reduce the gain to 40%.
- To set the time constants of the differentiator and the integrator, C_1 and C_2 were calculated as follows



$$\tau_i = \tau_{integrator} = \tau/2 \quad \text{and} \quad \tau_d = \tau_{differentiator} = \tau/8$$

where τ is the oscillation period measured to be 38 seconds. Therefore

$$C_1 \equiv C_d \equiv \frac{\tau/8}{R1} \equiv \frac{\tau/8}{820 \text{ k}\Omega} \quad (3.4)$$

and

$$C_2 \equiv C_i \equiv \frac{\tau/2}{R6} \equiv \frac{\tau/2}{3.3 \text{ M}\Omega} \quad (3.5)$$

- The capacitors $C_1 \equiv C_2 \equiv 5.8 \mu\text{F}$ were inserted on the circuit board and the integrator and the differentiator were switched on. The error signal on the oscilloscope quickly damped to zero at various set temperatures over the desired region of temperature stability.

3.3.4 Frequency stabilisation of the ECDL

Frequency stabilisation of ECDLs is essential, since over a long period of time the frequency drifts with fluctuations in injection current, temperature and mechanical movements. The laser frequency can be stabilised by locking it to an external reference. Figure 3.11 shows the general layout of the experimental setup required to lock the laser frequency to a rubidium absorption line as an external reference for frequency stabilisation. The ECDL is temperature stabilised using the temperature

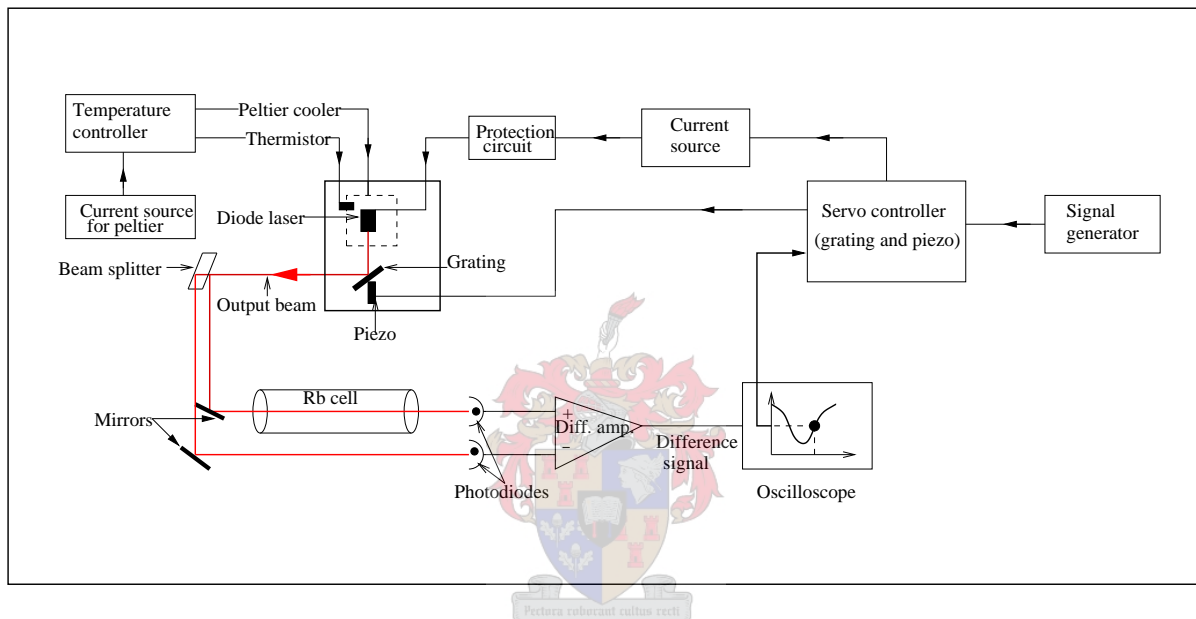


Figure 3.11: A layout of the experimental setup for locking the diode laser frequency using a sidelock servo.

controller system, Peltier cooler and thermistor. In order to detect the absorption lines of rubidium (Rb), the laser frequency is scanned by sending a ramp signal from the signal generator through the servo sidelock circuit to modulate the piezo voltage. The output beam is sent to a beam splitter, where one beam passes through the Rb cell and the other one acts as a reference beam. The two beams are detected by two photodiodes and electronically compared simultaneously by the differential amplifier to give a difference signal which represents the absorption signal and is displayed on an oscilloscope. The detector signal is displayed as volts versus time, where time is proportional to frequency. The laser is locked using the voltage value at a frequency on the positive slope of the absorption signal, as shown in Figure 3.11. The frequency scanning is switched off and the absorption signal is sent to the servo circuit where PID electronics controls the diode laser frequency by adjusting the grating position and changing the current through the diode laser,

depending on the magnitude of the error.

The sidelock servo circuit diagram [40] is shown in Figure 3.12. The absorption signal enters through J9 (SAT IN section 7D) and is compared to a specific set point values. One of the set points SP1 to SP4 is shorted to the ground to select a particular set point. When connected to the ground this is equivalent to logic 0 which switches the device on through DG201ACJ. The error signal is generated by comparing the set point value and the reference signal from the absorption line. Amplifier U2-B (TL074CN) isolates the input from the output. The set point monitor can be used to display the difference between the set point voltage V_{ref} and the photodiodes voltage V_D on an oscilloscope.

The circuit consists of two PID systems, one for controlling the piezo and the other for controlling the current. The signal branches towards the two systems after the switch U3-A (DG200ACJ). The generated error signal is electrically manipulated and used as feedback to change the frequency of the diode laser through the control variables, that is injection current (port J15) and piezo (port J11). Depending on the feedback frequency, the current controller receives fast signals for fine tuning the frequency. The piezo is for rough frequency changes and receives slow signals. The error signal $V_{err} = V_{ref} - V_D$ serves as the error signal for both the piezo loop and the current loop. For the piezo loop, switching of the polarity (S2) is done manually on the servo box. Negative polarity enables a unit gain buffer which inverts the signal and allows to lock on the left side slope of the signal while positive polarity can be used to lock the right side of the absorption signal. In the piezo loop amplifier U2-C (TL074CN), capacitor C15 and resistor R11 form an integrator that acts like a low-pass filter with a cut-off frequency of 15 Hz. Amplifier U5-A (TL074CN) and variable resistor R10 is used to vary the gain of the feedback; a maximum gain of 50 can be attained. A ramp from the signal generator can be sent through port J12 to the piezo and the PZT BIAS sets the DC voltage difference across the piezo.

The current loop consists of a capacitor C19 for decoupling of direct current and a low-pass filter consisting of U7 (OP-27GP), R22, R25 and C18 with a cut-off frequency of about 720 Hz. Resistors R39 - R42 and amplifier U8(OP-27GP) sets the gain of the feedback of the current loop. Each amplifier is connected to a power input of 15 V and has a decoupling capacitor of 100 nF that protects the amplifier from spikes in the power supply due to switching.

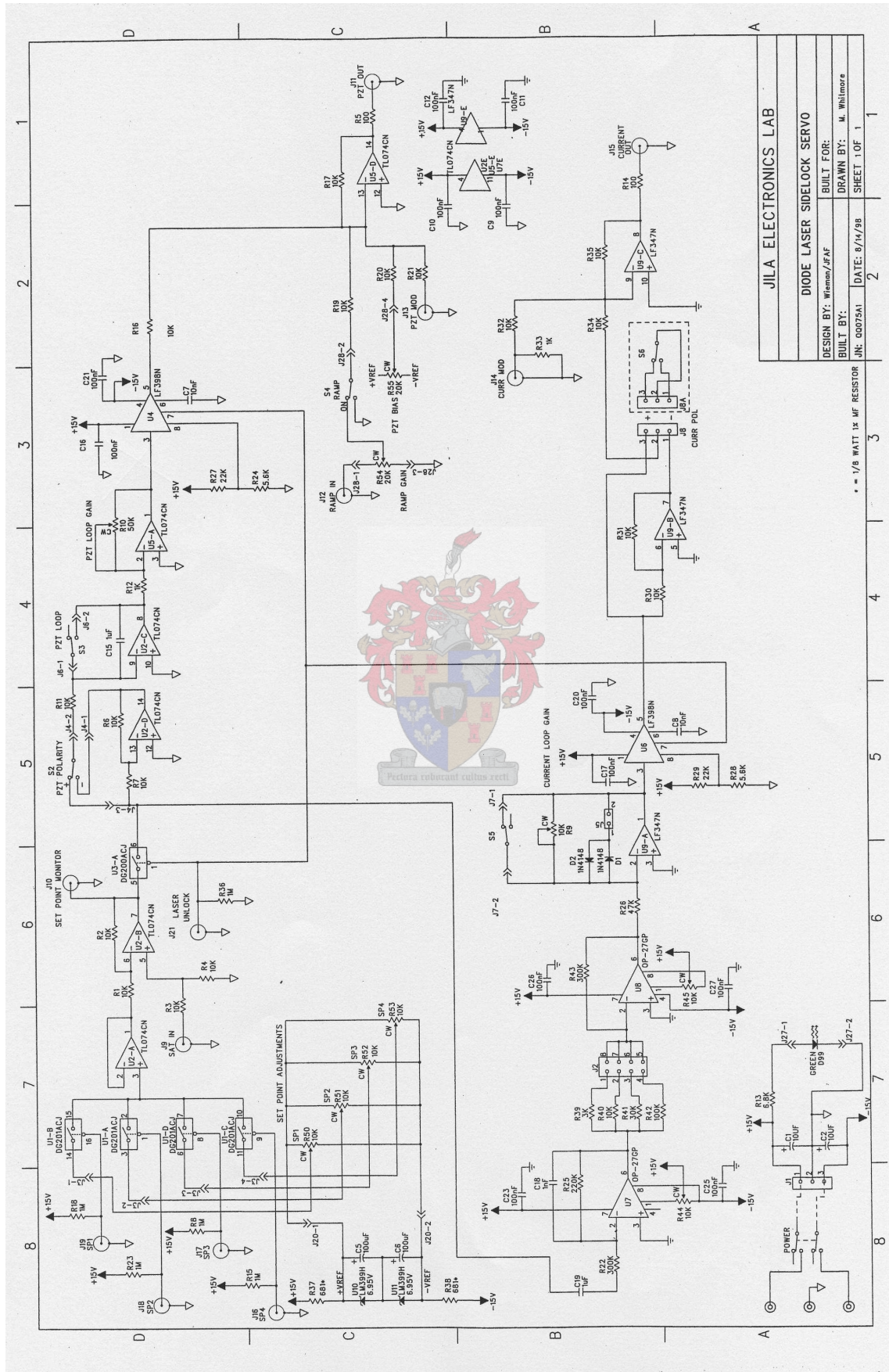


Figure 3.12: The circuit diagram for the sidelock servo for locking the frequency of the diode laser [40]. Circuit reproduced with permission.

3.4 Optimisation and characterisation of the ECDL

This section describes optimisation of optical feedback alignment for the ECDL. After alignment optimisation the ECDL was characterised near 780 nm.

3.4.1 Feedback alignment and optimisation procedure

The operation of the ECDL requires excellent coupling of the external optical feedback into the diode laser cavity. This demands careful alignment of the first-order diffraction from the grating to the diode laser. Alignment ensures that lasing is controlled by the external cavity with grating and not by the free-running diode laser.

The diffraction grating was positioned in such a way that the output from the diode laser will hit the centre of the grating surface using the rough alignment screws. The grating was positioned at a distance of about 10 mm from the collimation tube to give an external cavity length of approximately 15 mm. By observing the output of the diode laser and rotating the diode the dominant polarisation of the diode laser output was orientated perpendicular to the grating rulings. This arrangement provided enough feedback for the ECDL to control the lasing. The preliminary alignment procedure was carried out as follows.

- (i) The current through the diode laser is adjusted to about 80 mA to ensure that the feedback intensity is relatively high in order to be seen by the infrared (IR) viewer (Electrophysics 7215).
- (ii) A vertical alignment screw is adjusted so that the grating is tilted upwards until the feedback spot is completely separated from the diode laser output and can be seen by an IR viewer on the diode laser housing, above the collimation lens.
- (iii) While the feedback spot is above the diode laser housing, the horizontal alignment screw is adjusted to ensure that the feedback spot aligns vertically with the centre of the diode laser output.

When the feedback beam falls on the output beam from the diode laser one cannot distinguish the two beams by the IR viewer. Although the beams can overlap this is not a guarantee that the diode

laser output is well coupled to the feedback; fine alignment is therefore required and was carried as follows.

- (i) The current through the diode laser was adjusted close to the lasing threshold (around 40 mA) since the laser is most sensitive to optical feedback at this value [32].
- (ii) The vertical alignment screw was adjusted to steer the feedback downwards towards the laser diode while monitoring the brightening of the ECDL output.

The brightest spot ensures that the feedback is well aligned. Good alignment was also confirmed by inspecting the laser spectrum using the spectrometer to compare the background noise and bandwidth.

3.4.2 Experimental characterisation of the ECDL

The experimental setup used to characterise the ECDL is shown in Figure 3.13. The investigation was carried out after feedback optimisation. The same spectrometer and power meter were used as described in Section 3.1. The turn-on characteristics was investigated at a fixed temperature of 20 °C at selected wavelengths within the tuning range. Each wavelength was selected by manually rotating the grating by small angles. Since the wavelength of the output changes with current, each wavelength was selected by fixing the current at 80 mA and observing the central wavelength of the output spectrum on a computer. The grating was rotated in both directions (clockwise and anticlockwise), to have a rough estimate of the tuning range. Results of the spectrum as the grating is rotated were recorded.

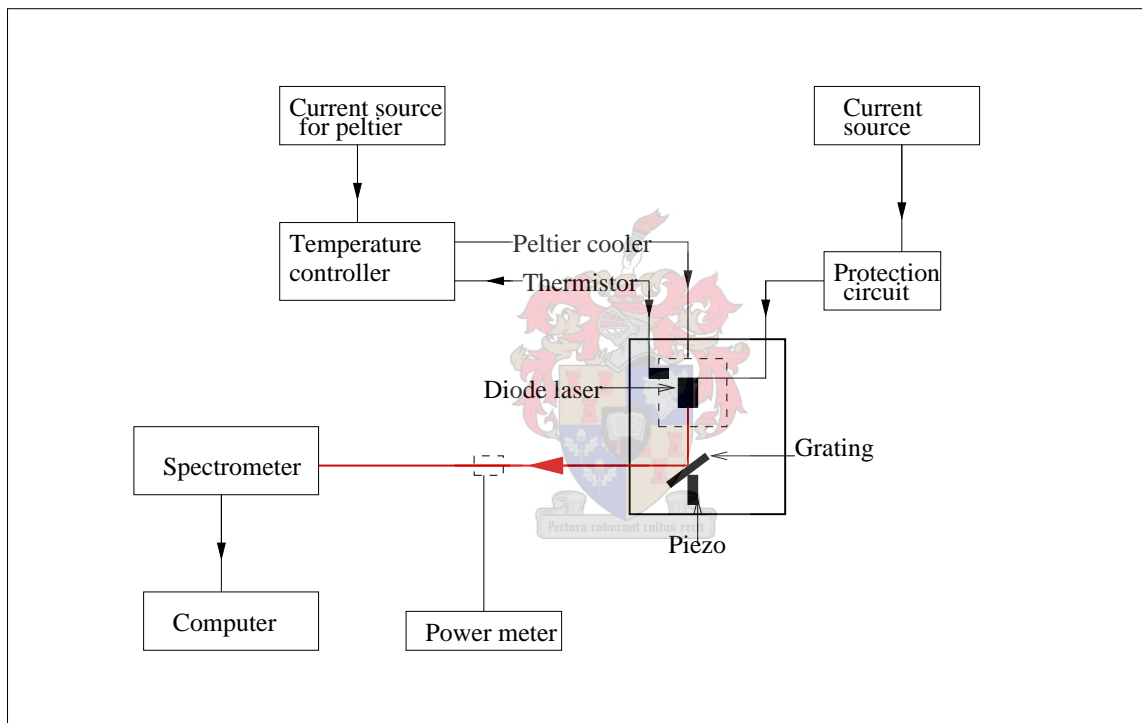
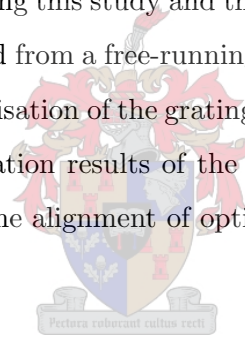


Figure 3.13: The experimental setup used for the characterisation of the ECDL.

Chapter 4

Results and discussion

The experimental results obtained during this study and their discussion and analysis are presented in this chapter. Firstly, results obtained from a free-running diode laser are presented and discussed in Section 4.1. Results on the characterisation of the grating and the ECDL are discussed in Sections 4.2 and 4.5 respectively. The optimisation results of the temperature controller are explained in Section 4.3. Results obtained during the alignment of optical feedback in the ECDL are discussed in Section 4.4.



4.1 Free-running diode laser

The aim was to investigate how the wavelength and power output of the laser diode varies with temperature and current in the absence of external optical feedback. Knowledge of the preliminary results of the free-running diode laser was useful in the experimental setup of the ECDL. The turn-on and tuning characteristics of the diode laser were investigated.

4.1.1 Turn-on characteristics

The results for the turn-on characteristics of the free-running diode laser (Hitachi HL7851G) are shown in Figure 4.1. The optical power output was measured as the injection current of the diode laser was varied at fixed temperatures. The fixed temperatures chosen were within the operating

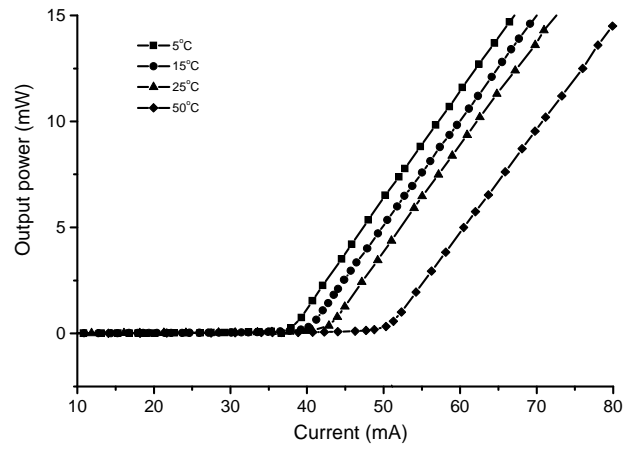


Figure 4.1: Graphical results of the turn-on characteristics of a free-running diode laser (Hitachi HL7851G) at different temperatures.

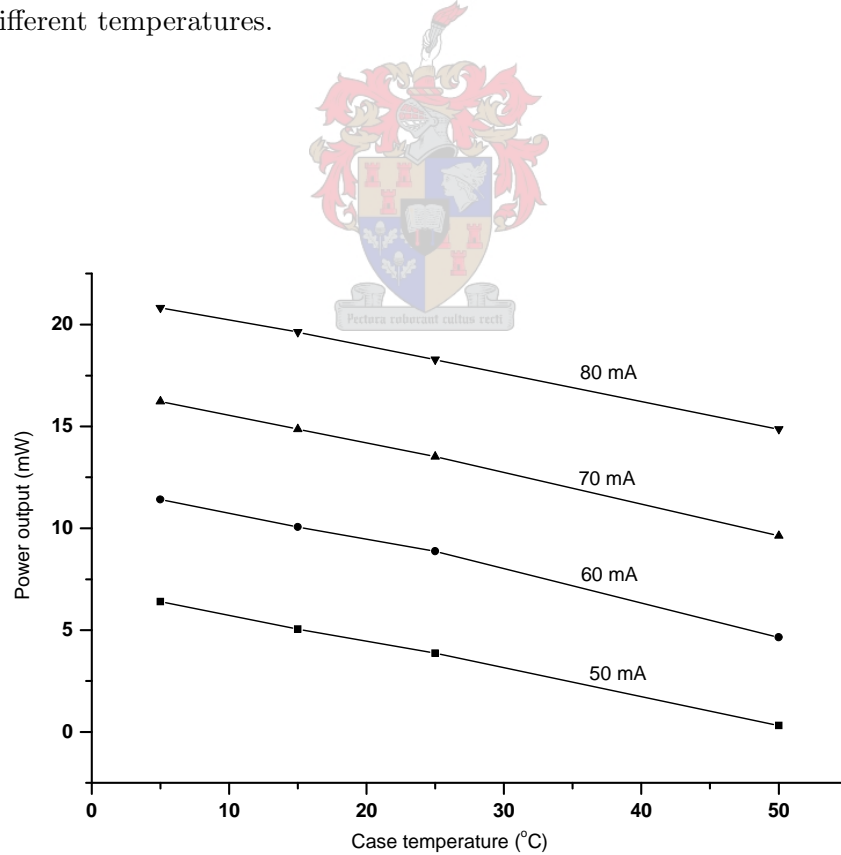


Figure 4.2: Graphical illustration of the temperature dependence of output power at fixed currents.

region of the diode laser.

Figure 4.1 shows that at low injection currents the optical power output is very low and approximately the same irrespective of the current and temperature of the diode laser. In this region there is no sufficient population inversion to compete with non-radiative recombination processes due to low pumping levels, therefore spontaneous emission dominates, to produce incoherent light. As the current is increased further there exists a threshold current where there is a sudden increase in optical power output and this marks the onset of laser action. Below threshold, the increase in injection current causes an increase of charge carrier density within the active region. Above threshold the charge carrier density remains constant and the increase in injection current only causes an increase of the optical power as a consequence of gain saturation. In this region the optical power output increases linearly with injection current as stimulated emission is increased by the increased rate of injection of charge carriers into the active region of the diode laser. The gradient of the lines above threshold, which gives the slope efficiencies of the diode laser, vary with temperature. The results shown in Figure 4.1 were analysed to yield results of the effect of

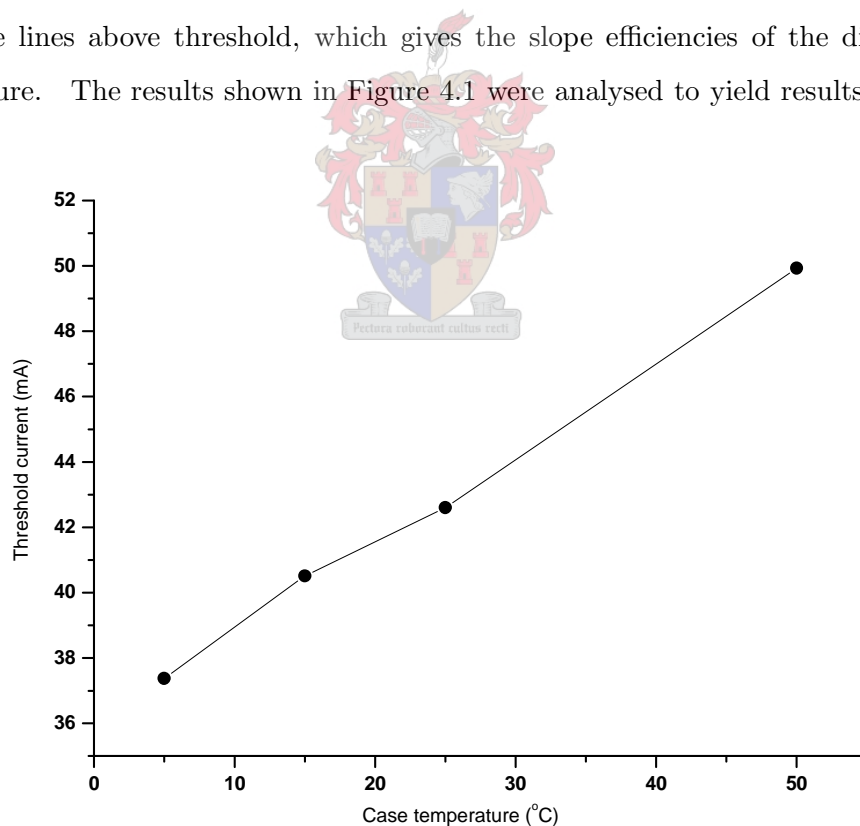


Figure 4.3: Illustration of the temperature dependence of threshold current derived from the turn-on curve, Figure 4.1.

temperature on the threshold current, slope efficiency and optical power output. Figure 4.2 shows

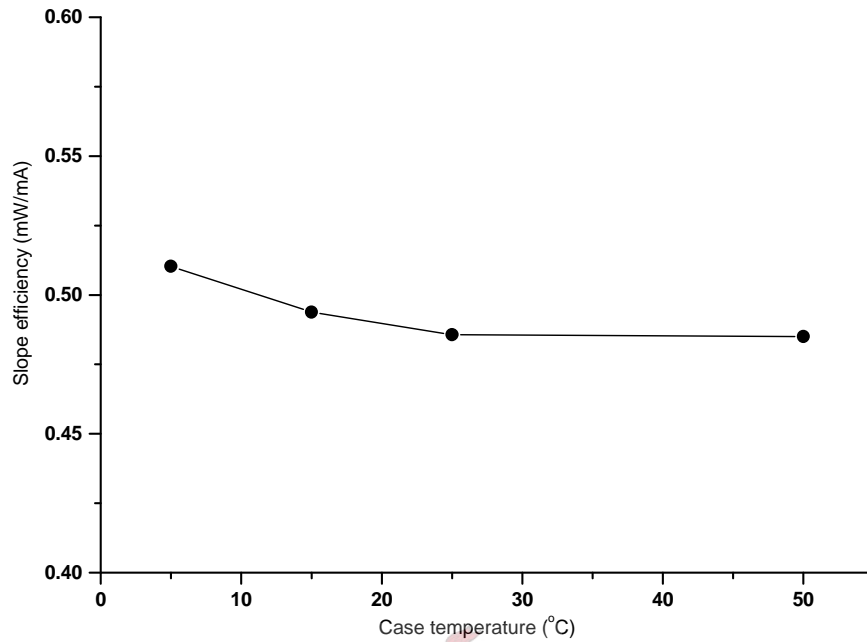


Figure 4.4: Graphical representation of temperature dependence of slope efficiency derived from Figure 4.1.

the dependence of optical power output on temperature at a fixed current. There is a decrease in optical power output as the temperature of the diode laser increases at specific currents. It is therefore advantageous to operate the diode laser at low temperatures when high optical powers are required. Figure 4.3 shows that as the temperature increases the threshold current of the diode laser increases. As the temperature of the diode laser increases the slope efficiency decreases, as shown in Figure 4.4. However the slope efficiencies are in the typical region of minimum 0.35 mW/mA to a maximum 0.70 mW/mA according to specification sheet [35]. It can be concluded that it is advantageous to operate the diode laser at low temperatures but above dew point.

4.1.2 Tuning characteristics

The effect of temperature and current on the output wavelength of the diode laser was investigated. The wavelength dependence on temperature at a fixed current of 122 mA is shown in Figure 4.5. At this current the diode laser is well above threshold therefore the laser diode is strongly lasing. The arrows indicate regions of discontinuity (mode-hops) in wavelength as the temperature increases,

as described in Section 2.8.1. The continuous segments correspond to tuning of a single mode due to changes in the cavity length caused by temperature changes. The mode-hops correspond to switching between different longitudinal cavity modes due to the shifting of the gain curve relative to the longitudinal modes. According to Weiman and Hollberg [17], for a GaAlAs diode laser, the gain curve shifts by 0.25 nm/K and cavity mode frequencies shift by about 0.06 nm/K. This is in agreement with the experimental results in Figure 4.5. The experimental values obtained are a gain curve shift of 0.23 nm/K and an average of about 0.045 nm/K in cavity mode frequency shift. The mode-hops are larger than an expected value of approximately 0.35 nm because of the low resolution of the spectrometer, or hops to another mode (at least one), other than the closest neighbour.

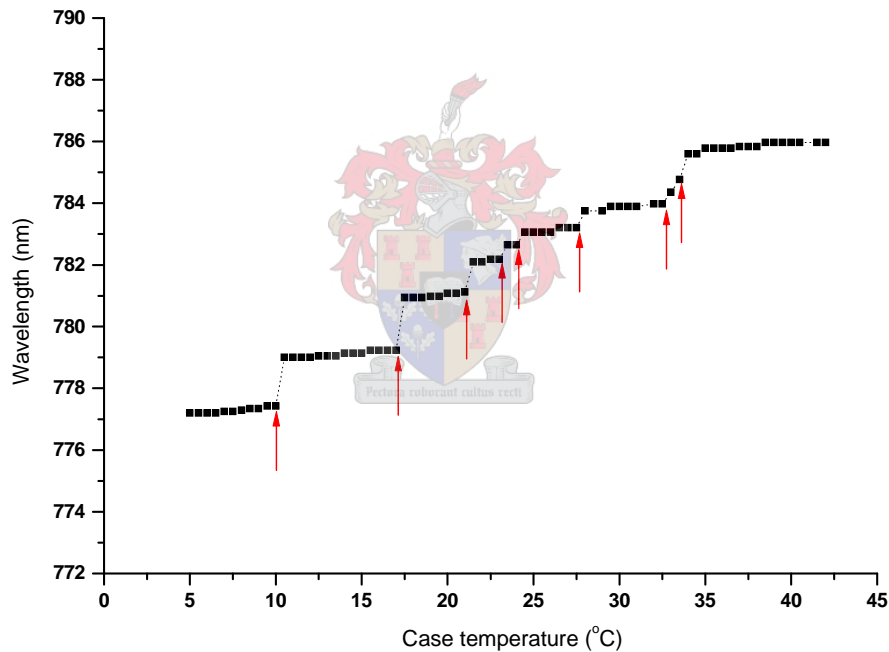


Figure 4.5: Graph showing the variation of wavelength with temperature at a fixed current of 122 mA. The arrows show regions of mode-hops.

The effect of current on wavelength was investigated at two fixed temperatures of 15 °C and 22 °C, as shown in Figure 4.6. Only currents above threshold could give a measurable spectrum. Mode-hops exist in the current-wavelength tuning curve as indicated by the arrows in Figure 4.6. The continuous segments in Figure 4.6 do not show any slope compared to those in Figure 4.5. The spectrometer cannot resolve the small changes in wavelength as the current is changed. For this

reason the current is used for fine wavelength tuning while temperature is used for rough tuning. The results show that an increase in temperature or current causes a red shift in the output

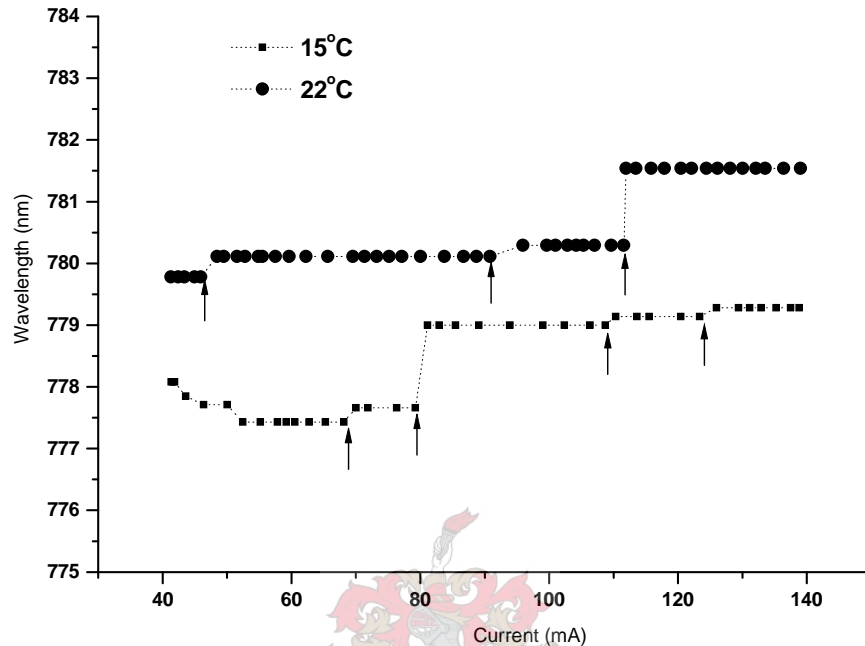


Figure 4.6: Graph showing the variation of wavelength with current at two fixed temperatures. Mode hops are indicated by small arrows.

wavelength of the diode laser.

4.2 Characterisation of the grating

The grating efficiency is a function of wavelength and polarisation of the incident light, and depends on the groove frequency, the shape of the grooves and the grating material. The grating was characterised for two different orientations of the dominant polarisation (horizontal and vertical) at different angles. The wavelength was approximately constant at 780 nm, achieved by fixing the temperature and current of the diode laser. The results for the characterisation of the grating are shown in Figures 4.7 and 4.8. Figure 4.7 shows the results when the incident beam is horizontally polarised (p-polarisation parallel to the plane of incidence of the grating but perpendicular to the grating rulings). Figure 4.8 shows the results when the incident beam is vertically polarised (s-polarisation perpendicular to the plane of incidence but parallel to the grating rulings). Each

figure shows the calculated fractional values, since the incident power is constant throughout the experiment. It follows that

- (i) The fraction of the first-order diffraction power that is coupled as feedback to the diode laser is given by

$$\text{Fraction in first order} = \frac{\text{first-order diffracted power}}{\text{Incident power}}$$

- (ii) The fraction of the zeroth-order diffraction power which is the output of the ECDL is given by

$$\text{Fraction in zero order} = \frac{\text{zeroth-order diffracted power}}{\text{Incident power}}$$

- (iii) The fractional losses at the grating as a result of scattering and diffraction into higher orders other than the zeroth and first orders is given by

$$\text{Fractional losses} = \frac{\text{Incident power} - (\text{first order power} + \text{zero order power})}{\text{Incident power}}$$

For angles below 30° the diffracted beam could not be measured because of low output powers and low intensity. Above 75° , the beam was clipping on the grating making measurements unreliable. In Figure 4.7, for polarisation perpendicular to grating rulings the first-order diffracted power, zero-order diffracted power and losses are relatively constant for angles between 30° and 60° , with the first order power ($\sim 55\%$) having higher values than the zero order power ($\sim 42\%$) and the losses ($\sim 0.4\%$). At higher angles both the diffracted and reflected power decrease as the losses increase. In Figure 4.8, for polarisation parallel to grating rulings the first order power increases at low angles up to a maximum ($\sim 15\%$) and zero order power decreases to about 60% , while the losses ($\sim 23\%$) are almost constant. At higher angles the zero order component power increases rapidly while the first order power and losses decrease.

The absolute grating efficiency is defined as the amount of the incident flux that is diffracted into a given diffraction order. Using this definition and by comparing the results of the two polarisations of the incident light on the grating it can be concluded that when the grating rulings are perpendicular to the polarisation of the incident light the grating diffracts more efficiently than when the polarisation is parallel to the grating rulings. Maximum efficiency of 60% was obtained when the polarisation is perpendicular to the grating rulings and 15% when polarisation of light is parallel to the grating rulings.

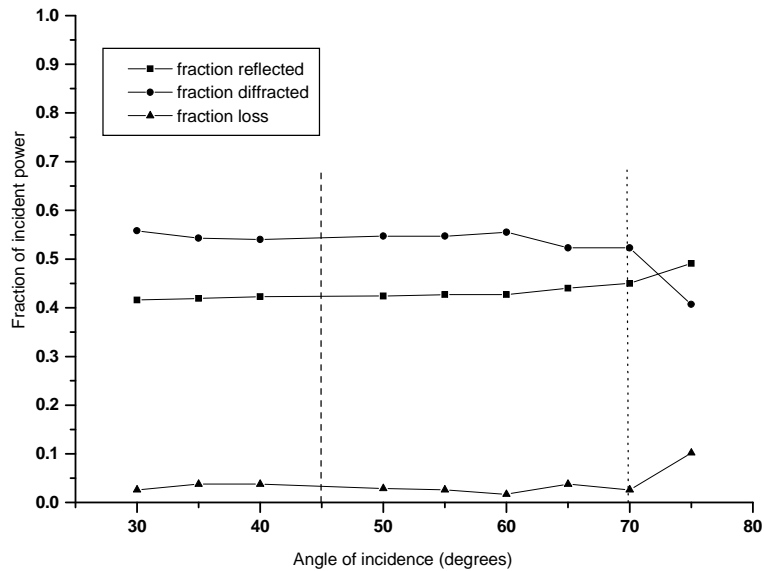


Figure 4.7: Characterisation of the grating for incident light polarised perpendicular (p-polarisation) to the grating rulings. The dashed line shows the Littrow angle, and a typical angle for the Littman-Metcalf angle is shown by the dotted line.

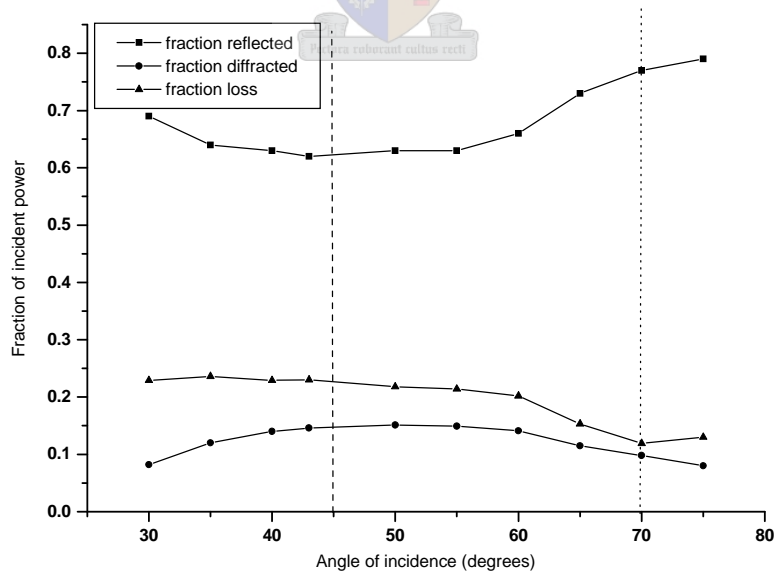


Figure 4.8: Characterisation of the grating for incident light polarised parallel (s-polarisation) to the grating rulings. The dashed line shows the Littrow angle, and a typical angle for the Littman-Metcalf angle is shown by the dotted line.

The two polarisation orientations to the grating can be used in an ECDL depending on the sensitivity of the diode laser to various feedback strengths. In the case where strong feedback should be coupled to the diode laser, horizontally polarised light is required, but the ECDL output will be much lower than 40% due to the orientation which favours more first-order diffracted power than zeroth-order diffracted power (output) in addition to losses in the cavity. In the case where more output is required and the diode laser being used is sensitive to weak feedback (15%) vertically polarised light is preferred. The zero order power can be as high as 75%, with low first order powers of about 10%.

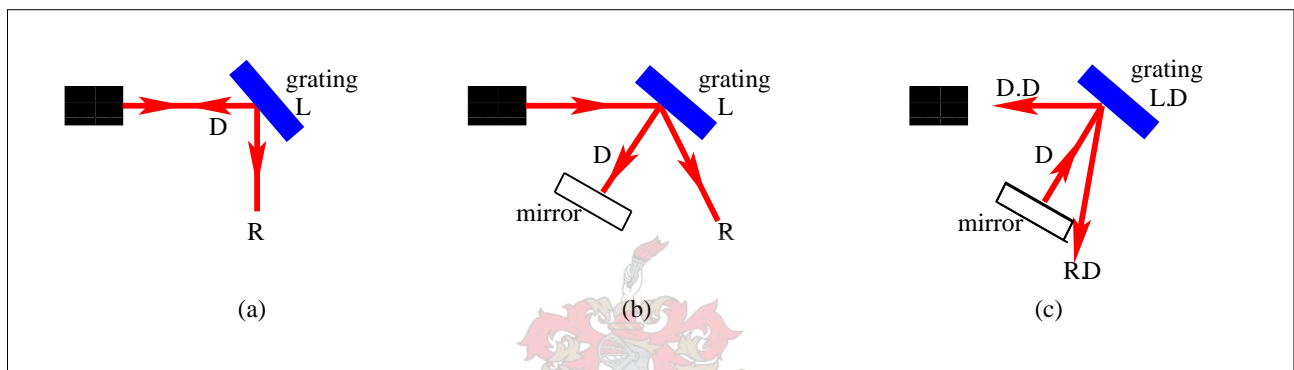


Figure 4.9: (a) The Littrow configuration showing the first-order diffraction (D) and zeroth-order diffraction (R) components with losses (L) at grating. (b) A sketch of Littman-Metcalf geometry before the diffracted light is reflected back by the mirror. (c) Littman-Metcalf configuration after mirror reflection.

A summary of the feedback, output and losses for two polarisations on the grating when used in the Littrow and Littman-Metcalf cavities is given in Tables 4.1, 4.2 and 4.3. To calculate these values Figures 4.9(a), (b) and (c) are used. Figure 4.9(a) represent the Littrow cavity. The first-order diffraction (D) is the optical feedback. The zeroth-order diffraction (R) is the output of the cavity and only the losses (L) at the grating are considered. At the Littrow angle of 45° , D, R and L are summarised in Table 4.1.

Polarisation	Feedback (%)	Output (%)	Losses (%)
Vertical	15	62	23
Horizontal	55	42	3

Table 4.1: A summary of the feedback, output and losses for a Littrow cavity at a Littrow angle of 45° for the two polarisation orientations.

In the Littman-Metcalf geometry the typical grazing incidence can be chosen as 70° , as shown by the dotted lines in Figures 4.7 and 4.8. Figure 4.9(b) shows the first-order diffraction (D) before reflection by the mirror and the summary is given in Table 4.2. After reflection from the mirror

Polarisation	Diffraction (%)	Output (%)	Losses (%)
Vertical	10	75	15
Horizontal	53	46	0.8

Table 4.2: Typical percentage values for the first order power, output power and losses at 70° for a Littman-Metcalf geometry before the diffracted beam is reflected by the mirror.

the first-order diffraction (D) is sent to the grating where it is diffracted again. The first order of the reflected component (D.D) is sent to the diode laser as optical feedback. The zeroth-order diffraction component of the diffracted part (R.D) is sent in the opposite direction of the initial R, hence it contributes to the losses of the cavity as shown in Figure 4.9(c). At the grating during the second diffraction the light experiences further losses (L.D). Neglecting any mirror losses, the total losses of the Littman-Metcalf cavity for the two polarisations can be approximated as $L + L.D + R.D$.

For vertical polarisation

$$\begin{aligned} \text{Feedback} &= D.D = 10\%.10\% \\ &= 1\% \end{aligned}$$

$$\begin{aligned} \text{Total losses} &= 15\% + 15\%.10\% + 75\%.10\% \\ &= 24\% \end{aligned} \tag{4.1}$$

For horizontal polarisation

$$\begin{aligned} \text{Feedback} &= D.D = 53\%.53\% \\ &= 28.1\% \end{aligned}$$

$$\begin{aligned} \text{Total losses} &= 0.8\% + 0.8\%.53\% + 46\%.53\% \\ &= 25.6\% \end{aligned} \tag{4.2}$$

Polarisation	Feedback (%)	Output (%)	Losses (%)
Vertical	1	75	24
Horizontal	28.1	46	25.6

Table 4.3: Typical percentage values for the feedback, output power and losses at 70° for a Littman-Metcalf geometry after a retroreflection of the beam by the mirror.

Although the incident angle of 70° chosen for the Littman-Metcalf geometry is arbitrary and can have a different value other than 70° the above calculations do illustrate that the Littman-Metcalf cavity has higher losses than the Littrow cavity when the same grating is used. In general, the Littman-Metcalf has higher losses due to losses at the mirror, and the fact that light is diffracted twice by the grating contributes significantly to the losses.

4.3 Optimisation of temperature controller

For too low Peltier current and PID gain no oscillations could be obtained by increasing R1. The error signal remained high, indicating that the cooling was not sufficient to reduce the temperature to that of the reference. After the maximum current was increased to 1.5 A, and increased by adjustments described in Section 3.3.3, both the error signal and current signal could be made to oscillate in a sinusoidal way around zero by increasing the value of R1. Any disturbance to the system, such as switching the reference temperature to a higher or lower value, would cause large transient oscillations that would clip at the maximum and minimum allowed values, but these will be damped and the error signal would return to stable oscillations or a constant value. The stable oscillations could be obtained for specific combinations of R1 values and the reference temperature.

For stable oscillations at a temperature of 17°C and R1 at $188\text{ k}\Omega$, the voltage across the Peltier cooler was 4.1 V. The period of oscillation was taken at different times and averaged, and the time was found to be 38 seconds. The time constant was set by inserting $5.8\ \mu\text{F}$ capacitors C_1 and C_2 .

The integrator and differentiator were switched on and the current and error signals were noted at different set temperatures to determine the operating region of the temperature controller. Figure 4.10 shows the magnitude of the error and current signals at different set temperatures. From Figure 4.10, the error signal is stabilised at zero between 8°C and 23°C . The temperature controller can be operated in this region without much deviation from the set temperatures. At temperatures far

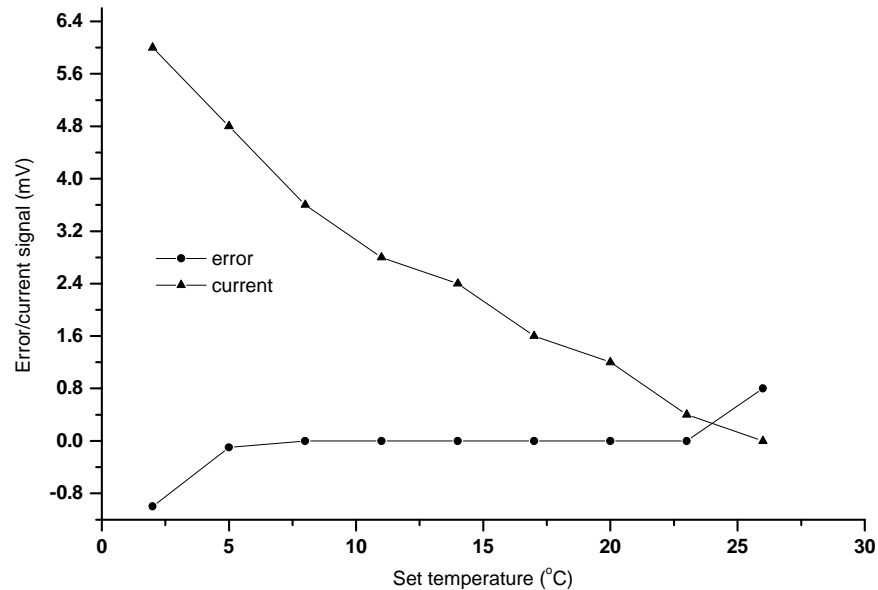


Figure 4.10: Results of the optimisation of the temperature controller indicating the region where the error signal is zero. The proportional current through the Peltier cooler is shown.

from 17 °C the error signal took a longer time to stabilise the temperature to the set value. At 2 °C and 27 °C the set temperature could not be reached and the error signal remained at a non-zero value. As the set temperature increases the current through the Peltier decreases. The current through the Peltier is high at low temperatures since more current is required for the Peltier cooler to work faster and more efficiently in order to reduce the temperature. Above room temperature the current signal is zero, indicating that the Peltier is not drawing any current as expected from the control circuit designed for cooling without provision of heating. Heating is done by ambient temperature, and can therefore not increase beyond room temperature.

4.4 Alignment of feedback

During the alignment process the output from the ECDL sometimes showed a multimode emission spectrum as shown in Figure 4.11. This was experienced when the feedback level coupled to the diode laser is changed due to alignment. According to Coldren and Corzine [19], different feedback levels can show different effects on the diode laser output such as multimode emission, linewidth broadening or narrowing, chaotic behaviour and coherence collapse. Hong [32] argues that the

multimode emission of the diode laser is as a result of poor feedback alignment and shows that the output of the ECDL is controlled by the gain peak of the semiconductor active region.

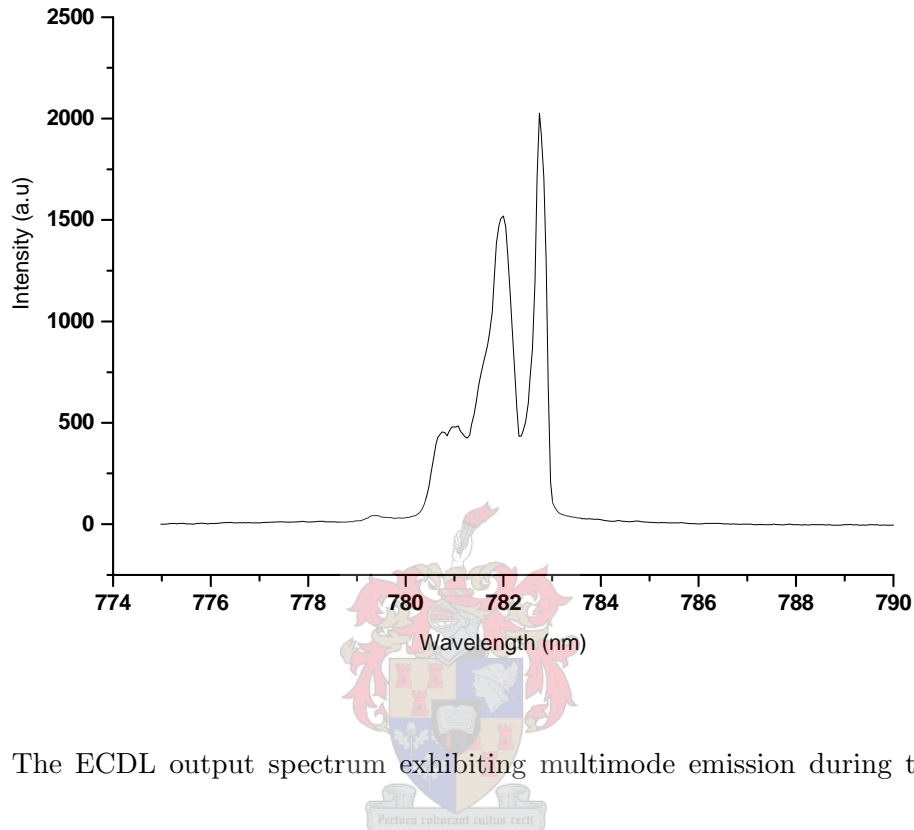


Figure 4.11: The ECDL output spectrum exhibiting multimode emission during the alignment process.

The preliminary alignment procedure carried out as described in Section 3.4.1 was complemented by inspecting the output spectrum displayed on a computer. This is useful when the feedback coincides with the diode laser output. The spectrum in Figure 4.12 distinguishes good alignment from bad alignment. The graphs were obtained at a relatively high current of 80 mA that gives strong lasing of the diode laser, while the temperature was fixed at 14 °C. The bad alignment was captured when the feedback was completely misaligned. Comparison of the two signals shows that the good alignment produces 20 times greater intensity at the lasing wavelength compared to the bad alignment. The spectrum of good alignment shows that lasing of the ECDL is strongly enhanced by the optical feedback, which is coupled to the diode laser. The ECDL is not fully controlling the lasing in bad alignment as most of the feedback is lost outside by poor coupling due to imperfect alignment.

To optimise the alignment, the diode laser's sensitivity to optical feedback at threshold is used as

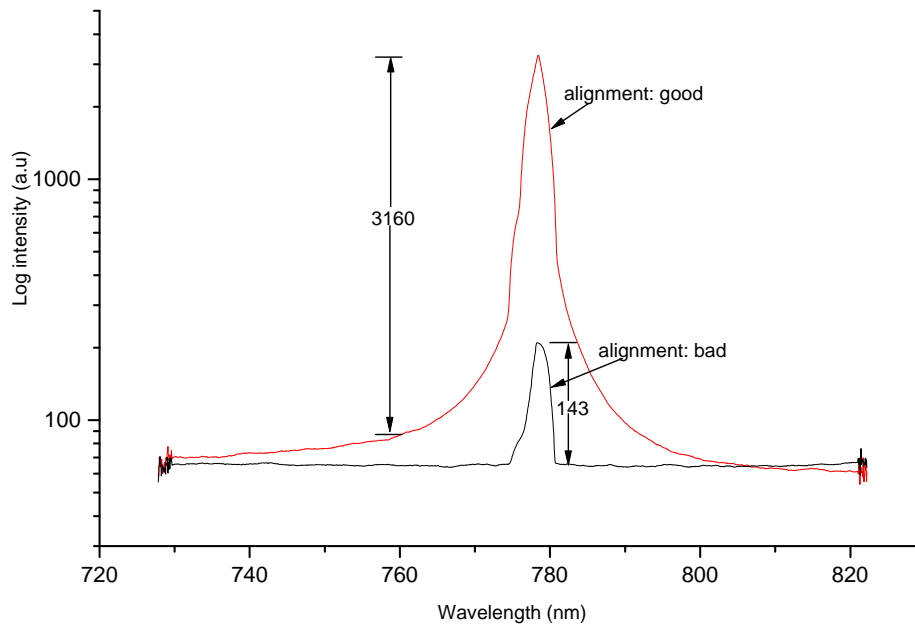


Figure 4.12: Captured spectrum results showing good and bad alignment, taken at a temperature of 14 °C and operating current of 80 mA.

described in Section 3.4.1. The optimal point is where the output from the ECDL is brightest as the grating is tilted around the point of rough alignment.

4.5 Characterisation of the ECDL

After the alignment of the optical feedback to the diode laser the ECDL was characterised near 780 nm. Characterisation was done when the dominant polarisation of the output of the diode laser was oriented horizontally, perpendicular to the grating rulings. This arrangement provided enough feedback for the external cavity to control the lasing. When the diode laser output dominant polarisation was oriented vertically (15%) the feedback from the grating was not enough to control the lasing. This is caused by the non-negligible reflection from the front facet of the diode laser that competes with the grating feedback. Therefore the grating feedback should be stronger than 15% in order to control lasing and the value is shown in Table 4.1.

The results of the turn-on characteristics are shown in Figure 4.13. The results were obtained at

given wavelengths within the tuning range. At each wavelength the turn-on curves qualitatively resemble that of the free-running diode laser. The absence of dips and kinks in the curves guarantees that the ECDL can be used within the tuning range.

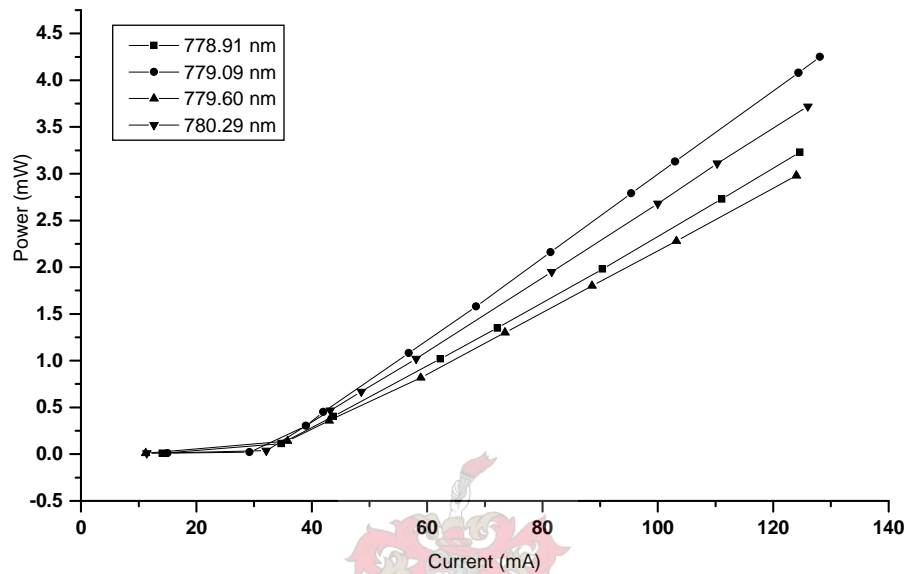


Figure 4.13: The turn-on characteristics of the ECDL at certain wavelengths within the tuning range.

Figure 4.14 is derived from the results of Figure 4.13. The power outputs versus wavelength at fixed currents were plotted. Generally, an increase in the injection current through the diode laser also increases the power output at each wavelength. The maximum power obtained in this alignment is about 4,5 mW at 130 mA, at a wavelength of 779 nm. The low output powers are largely due to the horizontally polarised output from the diode laser which provides more feedback from the grating than the output of the ECDL. Optimal results obtained with horizontal polarisation provide 10 mW of power at an operating current of 130 mA at 780 nm. The optimal power is sufficient for spectroscopy applications. According to Wieman et al. [5], 5 mW of power is suitable.

Figure 4.15 shows the results of the wavelengths attained when the grating is manually rotated. The graph shows that a tuning range of approximately 3.50 nm is possible around 780 nm for the developed ECDL. Mechanical tilting of the grating using a piezo allows fine frequency tuning of the diode laser.

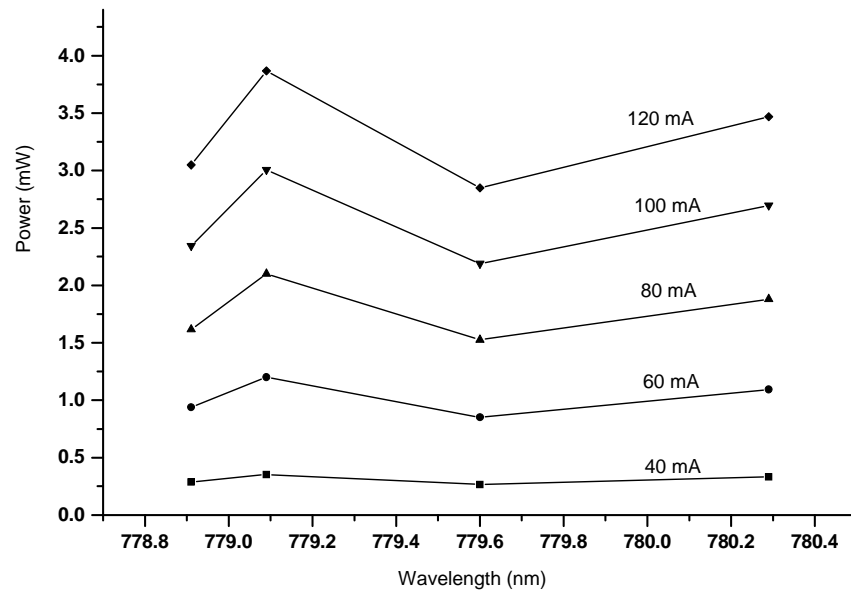


Figure 4.14: The ECDL's power versus wavelength at fixed currents based on results of Figure 4.13.

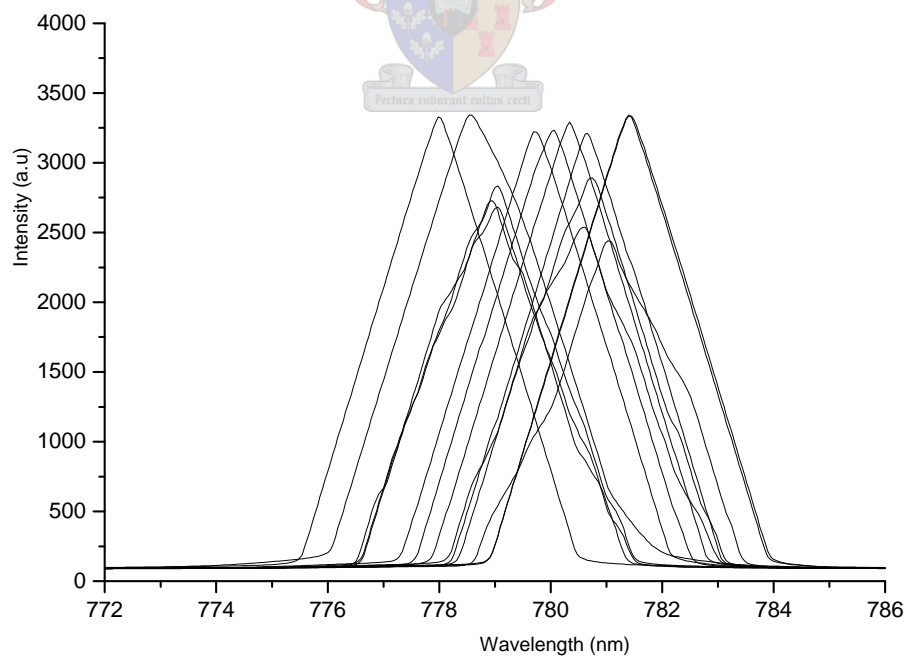


Figure 4.15: Results of the approximate tuning range showing the change in wavelength as the grating is manually rotated at a fixed current of 80 mA.

4.5.1 Comparison of the turn-on curves for a diode laser and ECDL

In Figure 4.16, the effect of an external cavity on the threshold and the slope efficiency of a diode laser is illustrated by comparing the turn-on curve of the free-running diode laser and the ECDL with an identical diode laser. The temperature was kept constant since it has an effect on the power output, threshold and slope efficiency. From Figure 4.16, the threshold current of a free-running

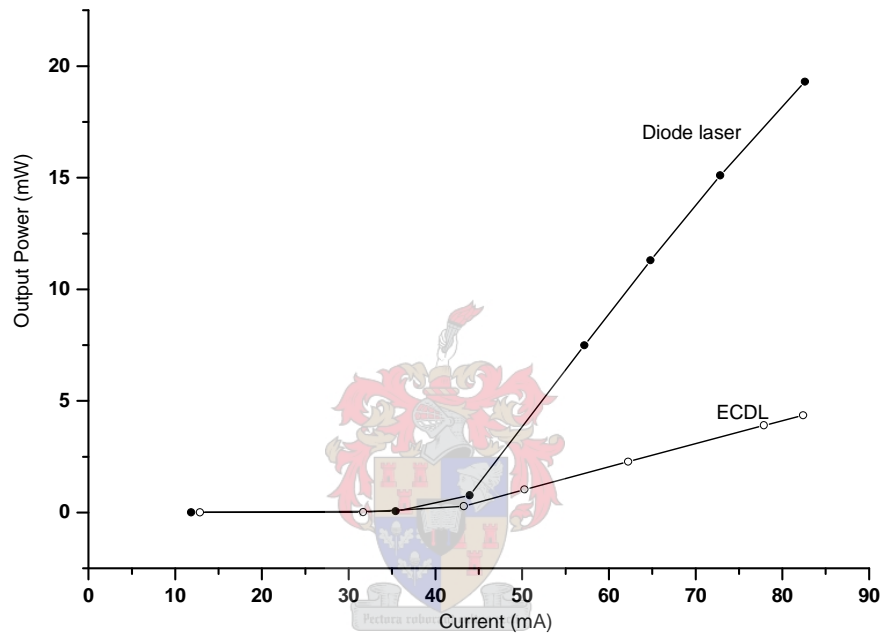


Figure 4.16: A comparison of the turn-on curves for the free-running diode laser and the ECDL at room temperature.

diode laser is 41.8 mA. This value is lower than the specified typical value of the diode laser of 45 mA [35], which might be due to a higher facet reflectivity than is typical for the diode laser [43]. The threshold current of the ECDL of 38.5 mA is about 3 mA lower than that of the free-running diode laser, as a result of external optical feedback.

The slope efficiency of a free-running diode laser is 0.48 mW/mA and is within the specified region of a minimum of 0.35 mW/mA to a maximum of 0.7 mW/mA, with a typical value of 0.55 mW/mA [35]. The slope efficiency of the ECDL curve of 0.04 mW/mA is about 92% lower than that of a free-running diode laser. The grating reduce the fraction coupled out of the combined cavity system. With the polarisation orientation of the diode laser output onto the grating the output is expected

to be about 40% of that of the free-running diode laser (see Section 4.2). The addition of the external cavity increases the total power losses.



Chapter 5

Summary and conclusions

The research focused on the experimental characterisation of the free-running diode laser, the design and development of an ECDL and the experimental characterisation of the ECDL using the same diode laser.

The experimental results obtained in the preliminary study of the free-running diode laser shows that both temperature and current have an effect on the output wavelength and output power of the diode laser. A decrease in the diode laser temperature and injection current causes a blue shift in the output wavelength, but at different rates. From a central wavelength of 785 nm at room temperature the output wavelength of 780 nm is obtained at temperatures in an approximate range of 15 – 20 °C depending on the injection current through the diode laser. Within a temperature range of about 5 – 50 °C wavelengths between 777 nm to 786 nm are accessible at injection currents of 100 mA or higher. Both temperature and current tuning of the diode laser output wavelength are characterised by mode-hops. The magnitude of the wavelength jump measured at a mode-hop is larger than the theoretical predictions for the wavelength difference between neighbouring modes, indicating hops of several mode spacings. It was found that temperature is suitable for coarse tuning of the output wavelength and current is suitable for fine wavelength tuning. It was evident that mode-hops do not occur at specific temperature and current combinations and therefore cannot be predicted. The output power decreased with an increase in temperature at fixed currents. The output power of the diode laser increases with increasing injection current above the threshold current. The results obtained in the preliminary study provided approximate temperature and

current combinations for which the ECDL is characterised.

The ECDL system based on a Littrow cavity was successfully designed and developed. The cavity geometry was designed to increase the mode-hop-free tuning range. The electronic components of the ECDL, that is, the current and temperature controller, and the protection circuit were developed and tested. The current controller was calibrated before being used to characterise the ECDL. The readout on the current source was found to be unreliable, but the current output was found to be stable and reproducible by independent measurements. The variation of power output of the diode laser with injection current using this current controller corresponded closely to specifications. It can be assumed that the current source together with the protection circuit eliminates transient spikes efficiently in the injection current supplied to the diode laser since the source has been used several times without damaging the diode laser.

Although some of the electronic components of the temperature controller were removed from the original design circuit, the constructed temperature controller has been shown to achieve temperature stability over several hours. The temperature controller was not designed to scan temperatures over a large range, but to stabilise the ECDL temperature at specific values below room temperature over a small range. The PID system of the controller worked efficiently after optimisation of the gain and setting of the time constants of the differentiator and integrator. While in use the automatic switching on and off of current through the Peltier cooler by the PID controller was good since this occurred on the onset of temperature deviation from the set value. The low thermal load of the geometry allows temperature stabilisation in the range 5 °C to a room temperature of 23 °C, although the current through the Peltier cooler was lower than the value for which the Peltier cooler is rated. The aluminium base plate provided sufficient thermal damping.

The developed ECDL was successfully characterised near 780 nm. The output powers obtained were approximately 20% of that of the free-running diode laser but sufficient for spectroscopy applications. It was observed that the output power of the ECDL was sensitive to alignment of the optical feedback from the grating with optimal alignment power as high as 10 mW was obtained. In some cases of alignment where there is poor coupling of the optical feedback into the diode laser the ECDL output showed multimode emission. It was found that lasing dominated by the external optical feedback from the grating could only be achieved when the dominant polarisation of the diode laser was orientated perpendicularly to the grating rulings, resulting in the first-order

diffraction intensity being 55% of the incident intensity in the Littrow configuration. With the dominant polarisation of the diode laser is orientated parallel to the grating rulings lasing dominated by the grating feedback could not be achieved. This is caused by the low feedback intensity (only 15% of the incident being diffracted into first-order) which is not sufficient to dominate over the non-negligible reflection from the front facet of the diode laser. In ECDL designs where higher output powers are required the orientation of dominant polarisation should be parallel to the grating rulings due to its orientation which favours more power in the zeroth-order diffraction than the first-order diffraction feedback. However, a diode laser with higher quality antireflection coatings on the front facet will be required for such ECDL designs.

A tuning range of about 3.5 nm was obtained around 780 nm by manually rotating the grating. However, as the grating is rotated the beam steers, as is typical for the Littrow cavity. Results obtained for the turn-on characteristics of the ECDL indicate a lower threshold current and smaller slope efficiency to that of a free running diode laser. The lower threshold is a feature of ECDLs caused by the presence of external optical feedback. The smaller slope efficiency is caused by higher losses in the extended cavity. Although the linewidth was not measured with the setup used in this study it is well documented by many authors [3, 22, 25, 27, 28, 34, 45] that due to the presence of a wavelength selective element the linewidth can be reduced significantly. In future the linewidth can be measured experimentally using the self-heterodyne technique, interferometric methods or spectroscopy methods using the absorption line of cooled rubidium atoms.

The experimental setup and theory to lock the diode laser frequency using a sidelock servo circuit was discussed in Section 3.3.4. The sidelock servo is still under construction. It will be used for future locking of the diode laser frequency to an atomic absorption line of rubidium.

In this study the design and development of an ECDL system was demonstrated. The mechanical and electronic components were successfully used together to provide a working ECDL with the desired output powers. In addition to the physics and technical knowledge gained in this study, the design provided a low cost system. All components and materials, and the manufacturing of the circuit boards for the ECDL, current controller and temperature controller, costs less than US\$ 2 500 compared to a commercially turn-key system which costs at least US\$ 10 000 (2006 prices). The ECDL was characterised near 780 nm. The characteristics found to date will make the developed ECDL a suitable candidate for spectroscopy and laser cooling of rubidium atoms.

The system can also be used for educational purposes for undergraduate students.

In future the ECDL system can be upgraded to a Littman-Metcalf cavity to avoid beam steering but is associated with low output powers due to higher losses, and makes alignment of the optical feedback to the diode laser difficult. Further work in the implementation of the servo circuit for frequency locking of the diode laser is necessary. Using the servo circuit the ECDL can be used for both ordinary and saturated absorption spectroscopy of rubidium atoms. Once this is achieved a further development to laser cooling and trapping of neutral rubidium atoms will be possible. The first prototype ECDL system developed can be used as a versatile laser source in different wavelengths regions by using different diode lasers with appropriate gratings in order to obtain specific wavelengths that can be used in spectroscopy of many atomic or molecular species that are relevant in gas analysis and environmental monitoring.



Appendix A

Diode laser (GaAlAs) mode spacing

Most diode lasers do not employ cavity mirrors because the refractive index of the semiconductor material is large enough to give considerable reflections at the semiconductor/air interfaces. Only modes which are integral multiples of the wavelength are supported in the cavity such that for an empty cavity the length of the cavity is $L = m\lambda/2$, and the allowed wavelengths in such a cavity are given by $\lambda = 2L/m$. The corresponding frequency mode is given by

$$\nu_m = \frac{mc}{2L} \quad (\text{A.1})$$

where m is the cavity mode number and c the speed of light in vacuum. For most semiconductors the active area fills the whole cavity, L is replaced by the optical path length $n(\nu)L$, where $n(\nu)$ is the refractive index of the material which depends on the frequency of the propagating light. Taking the refractive index into consideration equation A.1 becomes

$$\nu_m = \frac{mc}{2n(\nu)L} \quad (\text{A.2})$$

By including phase change at the end facets equation A.2 becomes equation 2.16, recalling

$$\nu_m = \frac{mc}{2n(\nu_m)L + \varphi/2\pi\nu_m} \quad (\text{A.3})$$

Assuming no phase change of light at the end facets then $\varphi = 0$, which is true when the travelling

light is normal to the end facets and the index of medium is higher than the index outside. Assuming also that the refractive index between adjacent frequencies is constant, that is, $n(\nu_{m+1}) = n(\nu_m) = n$, equation A.3 is reduced to

$$\nu_m = \frac{mc}{2nL} \quad (\text{A.4})$$

Using the value of $n = 3.65$ for a GaAlAs active layer as given by Genty [25]. From [16], a typical value of $L = 400 \mu\text{m}$ and the wavelength of operation is 780 nm, then the longitudinal modes are spaced by

$$\begin{aligned} \Delta\lambda &= \lambda_{m+1} - \lambda_m = \frac{2nL}{m+1} - \frac{2nL}{m} \\ &= \frac{2nL}{(m+1)m} \approx \frac{2nL}{m^2} = \frac{\lambda^2}{2nL} \\ &= \frac{(780 \times 10^{-9})^2}{2 \times 3.65 \times 400 \times 10^{-6}} \\ &\approx 0.228 \text{ nm} \end{aligned}$$

In terms of frequency

$$\begin{aligned} \Delta\nu &= \nu_{m+1} - \nu_m = \frac{(m+1)c}{2nL} - \frac{mc}{2nL} \\ &= \frac{c}{2nL} = \frac{c\Delta\lambda}{\lambda^2}, \quad \text{since } 2nL = \lambda^2/\Delta\lambda \\ &= \frac{3 \times 10^8 \times 0.228 \times 10^{-9}}{(780 \times 10^{-9})^2} \\ &\approx 99 \text{ GHz} \end{aligned}$$

Appendix B

Derivation of equations 2.25 and 2.31

Consider a working diode laser subjected to changes in ambient temperature and injection current. The changes in injection current cause a change in the internal temperature of the diode laser, particularly the active layer, as a result of Joule heating. Suppose that at a temperature T_1 , the geometrical length of a diode laser cavity is given by L_1 and the refractive index of the active material is given by n_1 . If the temperature is increased by ΔT to T_2 , the new length of the cavity is L_2 and the refractive index changes to n_2 , such that $\Delta T = T_2 - T_1$, $\Delta L = L_2 - L_1$ and $\Delta n = n_2 - n_1$. The change in mode frequency is

$$\Delta\nu_{mode} = (\nu_m)_{T_2} - (\nu_m)_{T_1} \quad (\text{B.1})$$

and, using equation A.1

$$\begin{aligned} \Delta\nu_{mode} &= \left(\frac{mc}{2n_2L_2} \right)_{T_2} - \left(\frac{mc}{2n_1L_1} \right)_{T_1} \\ &= \frac{mc}{2} \frac{n_2L_2 - n_1L_1}{n_1n_2L_1L_2} \end{aligned}$$

Assuming that the changes in refractive index and geometrical length of the active layer are small

so that $n_1 \approx n_2$ and $L_1 \approx L_2$ then

$$\Delta\nu_{mode} = \frac{mc}{2} \left(\frac{n_2L_2 - n_1L_1}{n^2L^2} \right) \quad (\text{B.2})$$

Modifying $n_2L_2 - n_1L_1$ as

$$\begin{aligned} 2(n_2L_2 - n_1L_1) &\approx n_2L_2 - n_1L_1 + n_2L_2 - n_1L_1 \\ &= n(L_2 - L_1) + L(n_2 - n_1) \\ &= n\Delta L + L\Delta n \end{aligned} \quad (\text{B.3})$$

substituting equation B.3 into B.2 will yield

$$\Delta\nu_{mode} = \frac{mc}{4n^2L^2} (n\Delta L + L\Delta n) \quad (\text{B.4})$$

But from equations 2.20, 2.21 and 2.24, Δn and ΔL can be substituted into B.4 so that

$$\Delta\nu_{mode} = \frac{mc}{4nL} (\beta_1 + \beta_2 + \beta_3\beta_4) \Delta T \quad (\text{B.5})$$

since $\nu_m = mc/2nL$, therefore equation B.5 becomes

$$\begin{aligned} \Delta\nu_{mode} &= \frac{\nu_m}{2} (\beta_1 + \beta_2 + \beta_3\beta_4) \Delta T \\ \Delta\nu_{mode} &= \phi_{mode} \Delta T \quad \text{where} \quad \phi_{mode} = \frac{\nu_m}{2} (\beta_1 + \beta_2 + \beta_3\beta_4) \end{aligned} \quad (\text{B.6})$$

The effects of current are derived in the same way since the temperature changes with current. An additional term is added as a result of changes in the density of charge carriers in the active layer which affects the refractive index of the material

$$\Delta\nu_{mode} = (\phi_{mode}\alpha_2 + \frac{\nu_m}{2L}\beta_3\alpha_1) \Delta I \quad (\text{B.7})$$

where ϕ_{mode} is the effective coefficient representing temperature changes, $\alpha_1 = \partial N/\partial I$ represents the coefficient of current effects to the refractive index and $\alpha_2 = \partial T/\partial I$ is the coefficient of current effects to temperature.

Appendix C

PID controller

A proportional-integral-derivative (PID) controller is a common feedback loop in many control systems such as temperature controllers. It is used to automatically adjust some variables to hold the measurement or process at the set point. The set point is where the measurement should be and the error is the difference between measurement and set point. The error signal, $e(t)$, is applied to a PID controller which uses the error signal to produce a control signal, $u(t)$, that manipulates the physical input to the process, causing a change in the regulated variable that will stably reduce the error [44], as illustrated in Figure C.1.

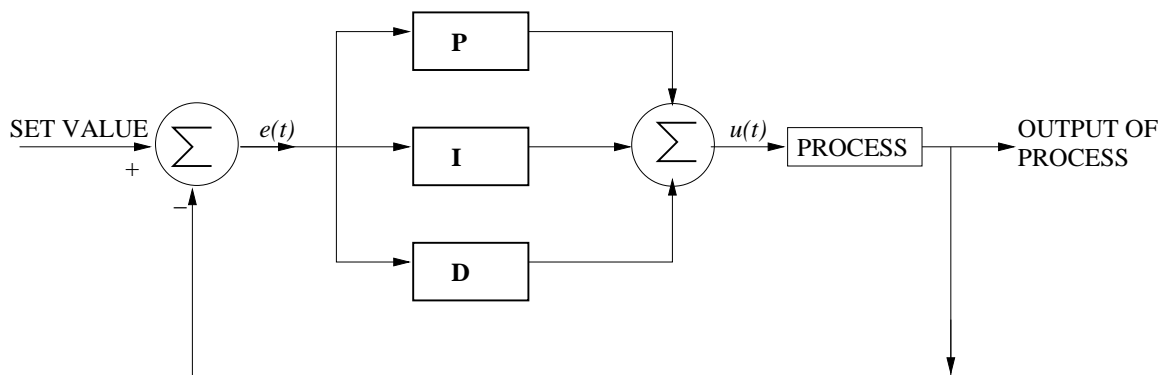


Figure C.1: A sketch diagram showing a control loop using PID control function [44]

The output of a PID can be written as

$$u(t) = P_{contribution} + I_{contribution} + D_{contribution}$$

where $P_{contribution}$, $I_{contribution}$ and $D_{contribution}$ are the feedback contributions from the PID components of the controller, defined as

$$P_{contribution} = K_p e(t) \quad (C.1)$$

$$I_{contribution} = K_i \int_{-\infty}^t e(t') dt' \quad (C.2)$$

$$D_{contribution} = K_d \frac{de(t)}{dt} \quad (C.3)$$

where K_p , K_i and K_d are constants that are used to tune the PID control loop.

Proportional control

This is the main drive in the control loop and applies a corrective term proportional to the error. The proportional gain K_p reduces the main part of the error. Large K_p means faster response to changes in set point and the final error is reduced but the system becomes less stable, resulting in overshoots, ringing, and undamped oscillations.

Integral control

The integral control reduces the final error in a system to zero since the proportional part does not reduce the error to zero. It sums up small errors over time to produce a drive signal large enough to move the system towards a small error. The higher the integral gain constant K_i the faster the error goes to zero. If K_i is too high it will cause instability and oscillations.

Derivative control

This is proportional to the time derivative or rate of change of the error signal. It counteracts the K_p and K_i terms when the output is unstable. The derivative control can improve the stability, reduce the overshoot that arises when proportional and integral terms are used at high gain, and improve response speed by anticipating changes in the error, but it does not have effect on the final error [44]. The gain K_d is the damping constant and is usually adjusted to achieve a critically damped response to changes in set point or the regulated variable.

Normally, in most tuning methods such as the Ziegler-Nichols procedure used in this study, the PID

is implemented with the K_p' gain applied to the $I_{contribution}$ and $D_{contribution}$ terms in the following form

$$u(t) = K_p' \left(e(t) + K_i' \int_{-\infty}^t e(t') dt' + K_d' \frac{de(t)}{dt} \right) \quad (C.4)$$

In this form the K_i' and K_d' gains relate only to dynamics of the process and the K_p' relates to the total gain of the process. However, the gain K_p' , has to be adjusted so that there is gain greater than one for frequencies smaller than the resonance frequency of the system but gain less than one for frequencies greater than the resonance frequency [41]. The system works fine for correcting the errors that fluctuate at frequencies lower than the resonance frequencies because the phase difference between $u(t)$ and output is less than 180° . Above the system resonance there is positive feedback due to 180° phase lag and the system is driven into undamped thermal oscillations if the gain is greater than one at such frequencies. The general method used was to turn up the gain until it just starts to oscillate at the 180° phase shift point and then reduce the gain to establish operating gain. The PID therefore increases the system stability, reduce overshoots and improves the transient response.



Bibliography

- [1] C. Ye; *Tunable External Cavity Diode Lasers*, World Scientific Publishing, First Edition, New Jersey, 2004.
- [2] M. Laschek, D. Wandt, A. Tünnermann and H. Welling; *Electro-optical frequency modulation of an external-cavity diode laser*, Optics communications 153, 59-62, 1998.
- [3] K.B. MacAdam, A. Steinbach, and C. Wieman; *A narrow-band tunable diode laser system with grating feedback, and a saturated absorption spectrometer for Cs and Rb*, American Journal of Physics 60 (12), 1098-1110, 1992.
- [4] M. Merimaa, H. Talvitie, P. Laakkonen, M. Kuittinen, I. Tittonen and E. Ikonen; *Compact external-cavity diode laser with a novel transmission geometry*, Elsevier, Optics communication, 175-180, 2000.
- [5] C. Wieman, G. Flowers and S. Gilbert; *Inexpensive laser cooling and trapping experiment for undergraduate laboratories*, American Journal of Physics, Vol 4, 1995.
- [6] K.C. Harvey and C.I. Myatt; *External-cavity diode laser using a grazing-incidence diffraction grating*, Optical society of America, Vol. 16, No. 12, 1991.
- [7] B.E.A. Saleh and M.C. Teich; *Fundamentals of Photonics*, Wiley Series in Pure and Applied Optics, A Wiley-Interscience Publication, New York, 1991.
- [8] D. Halliday and R. Resnick, *Fundamentals of Physics*; John Wiley and Sons; Extended third Edition; New York; 1988.
- [9] W.W. Chow, S.W. Koch and M Sargent; *Semiconductor-Laser Physics*, Springer-Verlag, New York, 1994.

- [10] G. Grosso and G.P. Parravicini; *Solid State Physics*, Academic press, London, 2000.
- [11] J.T. Verdeyen; *Laser Electronics*, Prentice Hall Series in Solid State Physical Electronics, Third Edition, London, 1995.
- [12] C.C. Davis; *Lasers and Electro-Optics, Fundamentals and Engineering*, Cambridge University Press, First Edition, Cambridge, 1996.
- [13] W.T. Silfvast; *Laser Fundamentals*, Cambridge University Press, First Edition, Cambridge, 1996.
- [14] H. Ghafouri-Shiraz; *Principles of Semiconductor Laser Diodes and Amplifiers: Analysis and Transmission Line Laser*, World scientific publishing, 2000.
- [15] J.H. Eberly and P.W. Millonni; *Lasers*, Wiley-Interscience Publication, New York, 1991.
- [16] <http://data.sacher-laser.com/techdocs/PoDL.pdf>; Sacher Lasertechnik Group: Technical Documentation.
- [17] C.E. Wieman and L. Hollberg; *Using a diode laser for atomic physics - review article*, Rev. Sci. Instrum.62(1), 1991.
- [18] H. R. Telle; *Stabilization and modulation schemes of laser diodes for applied spectroscopy*, Spectrochimica Acta Vol. 15, No. 5, 1993.
- [19] L.A. Coldren and S.W. Corzine; *Diode lasers and Photonic Integrated Circuits*, Wiley Series in Microwave and Optical Engineering, Wiley Interscience, 1995.
- [20] T.E. Barber, P. E. Walters, M. W. Wensing and J. D. Wineforder; *Topics in Laser Spectroscopy - Diode laser atomic absorption using a new reference method*, Pergamon Press, Spectrochimica Acta, Vol. 46B, pp. 1009-1014, 1991.
- [21] T.A. Heumier and J.L. Carlstein; *Mode hopping in semiconductor lasers*, ILX Lightwave Application Note, http://www.ilxlightwave.com/appnotes/mode_hopping_semiconductor_lasers.pdf.
- [22] D. Wandt, M. Laschek, K. Przyklenk, A. Tunnermann and H. Welling; *External cavity laser diode with 40 nm continuous tuning range around 825 nm*, Optics communications, 81-84, 1996.
- [23] K.S. Repasky, J. D. Williams and J.L. Carlsten ; *Tunable external-cavity diode laser based on integrated waveguide structures*, Optical Engineering, Vol.42 No. 8, 2229-2234, 2003.

- [24] R. Lang and K. Kobayashi; *External optical feedback effects on semiconductor injection laser properties*, IEEE Journal of Quantum Electron, vol.QE-16, pp.347-355, 1980.
- [25] G. Genty, A. Grohn, H. Talvitie, M. Kaivola, and H. Ludvigsen; *Analysis of the linewidth of a grating-feedback GaAlAs laser*, IEEE Journal of Quantum Electronics, vol. 36. No. 10. 2000.
- [26] R. Hjelme; *Semiconductor laser stabilisation by external optical feedback*, EEJ, Quantum Electron, Vol. 20 pp. 1023-1032, 1984.
- [27] L. Ricci, M. Weidemuller, T. Esslinger, A. Hemmerich, C. Zimmermann, V. Vuletic, W. Konig, and T.W. Hansch; *A compact grating-stabilised diode laser system for atomic physics*, Optics Communication 117, 541-549, Elsevier Science, 1995.
- [28] T. Erneux, A. Gavrielides, K. Green and B. Krauskopf; *Analytical theory of external cavity modes of a semiconductor laser with phase conjugate feedback*, The International Society for Optical Engineering, Proceedings of SPIE, Vol.5452, pp. 263-272, 2004.
- [29] L. Hilderbrandt, R. Knispel, S. Stry, J.R. Sacher and F. Schael; *Antireflection-coated blue GaN laser diodes in an external cavity and Doppler-free indium absorption spectroscopy*, Journal of Applied Optics, vol.42, No. 12, April 2003.
- [30] P. McNicholl and H.J. Metcalf; *Synchronous cavity mode and feedback wavelength scanning in dye laser oscillators with gratings*, Applied optics, Vol.24, No.17, 2757, 1985.
- [31] M.G. Littman and H.J. Metcalf; *Spectrally narrow pulsed dye laser without beam expander*, Applied optics, Vol. 17, 2224, 1978.
- [32] W. Hong and O.J. Painter; *Design and characterisation of a Littrow configuration external cavity diode laser*, <http://www.cee.org/rsi/docs/2004Papers/hong-wenxian-caltech-both.pdf>, California Institute of Technology.
- [33] W. Demtröder; *Laser spectroscopy: Basic concepts and instrumentation*, Springer-Verlag, New York, 3rd Edition, 2003.
- [34] T. Hof, D. Fick and H.J. Jansch; *Application of diode lasers as a spectroscopic tool at 670 nm*, Optics communications, Elsevier, 1995.
- [35] Thorlabs specification sheet of the diode laser HL7851G, <http://www.thorlabs.com>, June 2006.

- [36] H.M von Bergmann; *Laser techniques class notes*, University of Stellenbosch, 2005.
- [37] Thorlabs specification sheet of collimation tube C230TM, <http://www.thorlabs.com>, June 2006.
- [38] J. Hall and T. Brown; *Design QQ020*, JILA, University of Colorado in Boulder, Colorado, USA, 2004.
- [39] T. Brown and M. Whitmore; *Design QQ035A4PC*, JILA, University of Colorado in Boulder, Colorado, USA, 2004.
- [40] C.E. Wieman and JFAF; *Design QQ075A1*, JILA, University of Colorado in Boulder, Colorado, USA, 1998.
- [41] T. W. Hansch and M. Inguscio; *Frontiers in Laser Spectroscopy*, Proceedings of the International School of Physics, Italian Physical Society, 1994.
- [42] C.M. Steenkamp; *Postdoctoral research laboratory notes*, JILA, University of Colorado in Boulder, Colorado, USA, 2004.
- [43] C.M. Steenkamp, G.P. Nyamuda and E.G. Rohwer; *Design and development of an external cavity diode laser system for laser cooling and spectroscopy applications*, Poster presentation, 51st SAIP Annual Conference, 2006.
- [44] E. Neary; *Mixed-Signal Control Circuits Use Microcontroller for Flexibility in Implementing PID Algorithms*, Analogue Dialogue, Vol 38, No. 1, 3-5, 2004.
- [45] S. Stry, L. Hilderbrandt and J. Sacher; *Compact tunable diode laser with diffraction limited 1 Watt for atom cooling and trapping*, The International Society for Optical Engineering, Mark S. Proceedings of the SPIE, Volume 5336, pp. 17-25 (2004).
- [46] G. Kotze and P.E. Walters; *Evaluating absolute number densities in atom reservoirs using diode laser spectroscopy*, Thesis Project for Master of Science, University of Stellenbosch, 1995.
- [47] C.J. Hawthorn, K.P. Weber, and R.E. Scholten; *Littrow configuration tunable external cavity diode laser with fixed output beam*, American Institute of Physics, Vol. 72, 4477-4479, 2001.
- [48] Chip Structures; <http://www.opnext/products/details/InfoIndustryLD.cfm>.
- [49] M. Pan, B. Shi and G.R. Gray; *Semiconductor laser dynamics subject to strong optical feedback*, Optics letters, Vol. 22, No. 3, 1997.

- [50] S. Sivaprakasam, R. Saha, P. A. Lakshmi and R. Singh; *Mode hopping in external-cavity diode lasers*, Optics letters, Vol. 21, No. 6, 1996.
- [51] J. Hult, I.S. Burns and C.F. Kaminski; *New light sources- wide tuning range and rapid scanning blue extended cavity diode lasers*, Optical society of America, 2005.
- [52] H.J. Metcalf and P. van der Straten; *Laser cooling and Trapping*, Springer-Verlag, New York, 1999.
- [53] G.P. Nyamuda, C.M. Steenkamp and E.G. Rohwer; *Characterisation of an external cavity diode laser (ECDL) for laser cooling and spectroscopy applications*, 51st SAIP Annual Conference, Oral Presentation, 2006.
- [54] B. Sapoval and C. Hermann; *Physics of Semiconductors*, Springer-Verlag, New York, 1995.

